Application of Nano-Structured Silica Technology and Modified Starch Biopolymers into Highly Precipitated Calcium Carbonate Filled Mechanical Grade Paper

by

YIZHOU SANG

M.Sc., University of New Brunswick, Canada (2008)
M.Sc., Tianjin University of Science and Technology, China (2006)
B.Sc., Shaanxi University of Science and Technology, China (2003)

A THESIS SUBMITTED IN PARTIAL FULFILLMENT OF THE REQUIREMENTS FOR THE DEGREE OF

DOCTOR OF PHILOSOPHY

in

THE FACULTY OF GRADUATE STUDIES

(Chemical and Biological Engineering)

THE UNIVERSITY OF BRITISH COLUMBIA
(Vancouver)

September 2012

Abstract

Increasing loading level of precipitated calcium carbonate (PCC) in high value added communication-grade papers from bleached thermo-mechanical pulp (TMP) beyond the current level not only further reduces the production cost but also mitigates the shortage of good quality wood fibres. This thesis explores the possibility to retain increased amounts of PCC by taking advantage of the most recent developments in starch and nanoparticle technologies. Response surface methodology was used to optimize the addition strategy of chemicals and evaluate their effects in laboratory trials using mill samples. Empirical process models were also constructed to predict the retention and drainage results. It was found that linear high charge cationic starch S880 always resulted in highest retention for PCC preflocculation strategy and best drainage performance regardless of conventional chemical addition sequence or PCC preflocculation strategy. PCC preflocculation by starch resulted in higher breaking length and burst indices compared to the conventional chemical addition sequence.

The relationship among starch properties, process conditions, and floc properties was established through the investigation of PCC aggregation kinetic and floc structure evolution to allow the judicious selection of starch for PCC preflocculation. The population balance modelling approach was adopted to describe PCC flocculation. It was found that the linear high charge cationic starch S880 is associated with lower collision efficiency; lower restructure rate and higher energy dissipation rate to break up the flocs compared to the low charge cationic starch S858. The presence of NaCl was found to affect the high charge cationic starch S880 but had no influence on the low charge cationic starch S858. The collision efficiency decreases with the increase of the shear rate for both starches. The knowledge of the floc aggregation, breakage and restructure under various process conditions is expected to enable the manipulation of the floc with specified size, strength, and structure for better retention and drainage.

Preface

Four chapters of this thesis have been published in refereed journals as following:

1. Chapter 2: Sang, Y., McQuaid, M., Englezos, P. (2011). "Optimization of Chemical Use for Highly Filled Mechanical Grade Papers with Precipitated Calcium Carbonate." BioResources **6**(1): 656-671.

The authors for this paper are Sang, Y., McQuaid, M., and Englezos, P. Professor Peter Englezos is my research supervisor. Michael McQuaid represents Catalyst Paper Corporation. This company has sponsored the project through a Grant-In Aid to Professor Englezos and also supplied the materials for the experiments. NSERC co-sponsored the project with Catalyst through a Collaborative Research Grant. I planned, designed and performed all the experiments and analyzed the data under the supervision of Professor Peter Englezos. Michael McQuaid provided feedback and facilitated the transfer of the knowledge generated from this research for paper mill application.

2. Chapter 3: Sang, Y., McQuaid, M., Englezos, P. (2012). "Pre-Flocculation of Precipitated Calcium Carbonate Filler by Cationic Starch for Highly Filled Mechanical Grade Paper." BioResources, 7(1): 354-373.

The authors for this paper are Sang, Y., McQuaid, M., and Englezos, P. Professor Peter Englezos is my research supervisor. Michael McQuaid represents Catalyst Paper Corporation. This company has sponsored the project through a Grant-In Aid to Professor Englezos and also supplied the materials for the experiments. NSERC co-sponsored the project with Catalyst through a Collaborative Research Grant. I planned, designed and performed all the experiments and analyzed the data under the supervision of Professor Peter Englezos. Michael McQuaid provided feedback and facilitated the transfer of the knowledge generated from this research for paper mill application.

3. Chapter 4: Sang, Y., Englezos, P. (2012). "Flocculation of Precipitated Calcium

Carbonate (PCC) by Cationic Tapioca Starch with Different Charge Densities. I: Experimental." Colloids and Surfaces A: Physicochemical and Engineering Aspects. DOI: 10.1016/j.colsurfa.2012.07.019.

The authors for this paper are Sang, Y., Englezos, P. Professor Peter Englezos is my research supervisor. I planned, designed and performed all the experiments and analyzed the data under the supervision of Professor Peter Englezos.

4. Chapter 5: Sang, Y., Englezos, P. (2012). "Flocculation of Precipitated Calcium Carbonate (PCC) by Cationic Tapioca Starch with Different Charge Densities. II: Population Balance Modeling." Colloids and Surfaces A: Physicochemical and Engineering Aspects. DOI: 10.1016/j.colsurfa.2012.07.028.

The authors for this paper are Sang, Y., Englezos, P. Professor Peter Englezos is my research supervisor. I developed the model, performed the simulations and analyzed the results under the supervision of Professor Peter Englezos.

Table of Contents

List of Tables

List of Figures

Nomenclature

ANOVA	Analysis of variance
CCD	Central composite design
CE	Collision efficiency
CFD	Computational fluid dynamics
CMC	Carboxymethyl cellulose
CPAM	Cationic polyacrylamide
DCS	Dissolved and colloidal substances
DFR	Drainage, freeness, retention tester
DS	Degree of substitution
DTPA	Diethylene triamine pentaacetic acid
EDR	Energy dissipation rate
ES	Extremely significant
GCC	Ground calcium carbonate
LDS	Laser diffraction spectroscopy
MFD	Mass fractal dimension
MP	Microparticle
NP	Nanoparticle
ODE	Ordinary differential equations
PCC	Precipitated calcium carbonate
PCD	Particle charge detector
PDA	Photometric dispersion analysis
PSD	Particle size distribution
PEI	Polyethyleneimmine
PEO	Polyethylene oxide
Poly (DADMAC)	Polydiallyldimethylammonium chloride
PVC	Polyvinyl chloride
PVFA/NaAA	sodium polyvinylformamide-acrylic acid
PVSK	Poly(vinyl sulfate) potassium
RR	Restructure rate
RSM	Response surface methodology
S	Significant
SASLS	Small angle static light scattering
SEM	Scanning electron microscopy
TAPPI	Technical association of the pulp and paper industry
TMP	Thermo-mechanical pulp
VS	Very significant
V_B	PVSK volume consumed for the blank sample
V_S	PVSK volume consumed for the adsorption sample
M_F	Mass of dry cellulose fibres
M_P	Mass of starch
G	Shear rate
d_F	Mass fractal dimension
$d_{F,max}$	Maximum mass fractal dimension

$d_{4,3}$	Volume mean size
d_0	Characteristic diameter for the class i=0
V_0	Volume of primary particle
R_c	Effective capture radius
T	Absolute temperature
k_B	Boltzmann constant
V	Volume of the vessel
P	Power consumption
D_S	Stirrer diameter
g_c	Newton's law proportionality factor
$N_{Renynolds}$	Reynolds number
Q	Scattering vector
I(q)	Scattered light intensity
n	Refractive index of fluid
n(v), n(u), n(w)	Number concentrations of particles of volume u, v and w
b(υ/w)	Breakage probability density function of particles of volume w into particles of volume v
S(v)	Specific fragmentation rates for the particles with volume v
S(w)	Specific fragmentation rates for the particles with volume w
N_i	Number concentration of particles in section i
F_A	Net attractive force binding the particles
d	Floc size
Rci, Rcj	Effective collision radius
r_0	Primary particle radius
k_c	Unity
D_i	Characteristic floc diameter in interval i
S_j	Fragmentation rate

Greek letters

β_o	Intercept
β_i	Linear effect
β_{ij}	Interaction effect
β_{ii}	Quadratic effect
ω	Stirrer rotation speed
υ	Kinematic viscosity of the medium
ε	Average energy dissipation rate per unit mass
ε_{cj}	Critical energy dissipation rate
μ	Dynamic viscosity of the medium
ρ	Density of medium
$\beta_{i,j}$	Collision frequency for the particles in sections i and j
$\Gamma_{i,j}$	Breakage probability distribution function
ε_A	Floc porosity
α	Collision efficiency

γ	Restructure rate
ζ	Zeta potential
σ_z	Tensile strength
θ	Scattering angle
λ	Wavelength in vacuo of the laser light used

Subscripts

expt	Experimental
max	Maximum

Acknowledgements

I first would like to thank my supervisor Professor Peter Englezos for guiding me throughout my PhD work, for being very understanding, encouraging and supportive. I also appreciate the opportunities he gave me to conferences to present my work and to get exposed to new ideas in the field.

I would like to thank my research committee members, Prof. Savvas Hatzikiriakos, Prof. Mark Martinez and Prof. John F Kadla, for their helpful advice and suggestion.

I would like to gratefully acknowledge the advice, discussion and inputs from Michael E. McQuaid, Senior Corporate Specialist, Catalyst Paper Corporation for guiding this project in the right direction.

I would like to acknowledge the financial support from Natural Science and Engineering Research Council of Canada (NSERC) and Catalyst Paper Corporation for this project.

I wish to thank all friends and members of my research group: Dr. Praveen Linga, Dr. Nayef Al Saifi, Dr. Christos Stamboulides, Cef Haligva, Jeffry Yoslim, Nagu Daraboina, Alireza Bagherzadeh, Babak Amir-Sardary, Mehrnegar Mirvakili, Sima Motiee, Duo Sun and Soo Feng Ker.

Dedication

To my parents,
my wife L. Hao
and my daughter Sophie

Chapter 1 Introduction

In this chapter various approaches proposed to produce highly filled paper, the retention/drainage aid systems used in papermaking and the dry strength additives are presented. In addition, the flocculation of precipitated calcium carbonate and the use of population balance to model the flocculation are briefly discussed. The chapter concludes with the presentation of the research objectives.

1.1. Highly Filled Paper

1.1.1. Lumen loading

By beating a mixture of fibres and mineral filler zinc sulphide, Haslam and Steele [1] observed that part of the filler was present inside the lumen. This observation led Green et al. [2] to propose a novel approach ("lumen loading") for the manufacture of highly filled paper. This would be accomplished by immersing (impregnating) the pulp in an agitated, concentrated suspension of filler to allow the filler particles to enter the lumens via pit apertures. This would be followed by a washing step to remove the particles from the exterior surfaces of fibre. It was reported that lumen loading of TiO_2 was 0.125 g filler/g unbleached black spruce kraft pulp when impregnation was carried out in water without additives [3]. Okayama et al. [4] reported that the $CaCO_3$ lumen loading level depends on the particle size. A loading of 0.08 g filler/g fibre was achieved. The reason for the lower $CaCO_3$ loading is the size of $CaCO_3$ which is in general larger than that of TiO_2. A maximum loading level of 0.12 g filler/g fibre was achieved by pretreating the fibres with polyethylenimine when $CaCO_3$ filler with a particle size of 0.48 μm was used [5].

A pretreatment of the fibres with a cationic polyacrylamide followed by elevated temperature (75°C) during lumen loading enabled a loading of 0.30 g filler/g softwood bleached kraft fibre [5]. A prolonged agitation of fibres with a quantity of filler close to that finally required in the pulp was suggested by Middleton and Scallan [6]. It is noted

that the strength properties of paper with lumen loaded fibres are improved as the filler within the lumen will not interfere with fibre-fibre bonding [3, 5-7]. It was proposed that the fillers simply diffuse into the lumen via aperture instead of transferring through the lumen [8].

However, lumen loading has limitations. Because the filler particles must be small in size to flow through the pit apertures, lumen loading is appropriate for TiO_2 which is expensive filler. An excess amount of filler is required to enhance the kinetics of lumen loading and an additional process is required to recycle this excess filler. The lumen loading level depends on filler concentration, pulp consistency, impregnation time and level of agitation [2]. Even if these parameters are kept constant, the loading level may vary because the bond strength between the filler and the lumen surface varies [3]. Finally, it should be noted that lumen loaded fibres cannot be beaten [9].

1.1.2. Cell wall loading

Loading of the cell wall by mixing two salt solutions to precipitate an insoluble compound has been reported [9-12]. The pulp is then vigorously washed to remove the excess filler from the outer fibre surfaces [9]. The strength loss with cell wall loading was found to be comparable to that in lumen-loaded paper [11].

Klungens and coworkers [13, 14] mixed calcium oxide with dewatered bleached northern softwood kraft pulp to deposit calcium hydroxide on the cell wall. Pressurized refiner was used to mix CO_2 with the calcium hydroxide loaded pulp under high shear to form $CaCO_3$ filler. It was found that the $CaCO_3$ was distributed approximately equally in the lumen, within the cell walls and on the surface of the cellulose fibres. The handsheet from the pulp prepared in this way had higher strength compared to conventional filler addition but the optical properties deteriorated.

1.1.3. Fines-filler composites

A composite was produced by precipitating $CaCO_3$ on fibre fines. Cousin and Mora [15, 16] patented such a process. Miller and Paliwal [7] also precipitated the calcium carbonate on fines to produce paper. Gavelin [17] mixed filler and pulp containing a high proportion of fines with a retention aid to produce paper. However, the flocs were weak and easily broken down.

Silenius [18] introduced the so called "SuperFill" technology in which a fines-filler composite having a size range approximately the same as the diameter of the filler particle was produced by precipitating $CaCO_3$ exclusively on fines. Subramanian et al. [19], followed the approach of Silenius [18], prepared colloidal PCC (c-PCC), rhombohedral PCC (r-PCC) and scalenohedral PCC (s-PCC). They then used bleached kraft pine pulp fines to form a fine-filler composite. It was found that the paper properties depend on PCC morphology [19] and colloidal PCC has the highest first-pass retention. Colloidal PCC and rhombohedral PCCs added to paper showed minimum and maximum internal bond strength at all filler contents, respectively [19]. Subramanian et al. [20] used the microfines-filler composite for a new uncoated fine paper. The composite consisted of 60% or lower PCC, 15% to 30% cellulosic fines (80% of the fines had a diameter of 37 μm) and the balance were fibres. PCC filler was used for bulk, optical properties, porosity and shrinkage reduction. The cellulosic fines contribute to tensile strength and bending resistance whereas the fibres to tear. The concept of fines-pigment composite enabled the production of uncoated wood free paper with 50% - 60% filler.

1.1.4. Filler modification

Gill [21] reported cationic modification of ground and precipitated calcium carbonate by polymers with quaternary amine group. Alince [22, 23] demonstrated the potential of the cationic latex (sulfonium and quaternary ammonium type with a diameter of 110 nm) to produce handsheets containing up to 40% clay of low basis weight (50 g/m^2) with improved sizing efficiency attributed to the hydrophobic character of latex. Structured

fillers were produced in order to enhance the bonding with wood fibres by precipitation with starch [24, 25], complexation with starch and fatty acid [26], and regeneration with cellulose [27]. A clay-starch composite that was added in the pulp suspension enhanced the tensile strength of paper [25, 26]. However, washing and filtration were needed to remove the $(NH_4)_2SO_4$ solution that was used to precipitate the starch onto clay. Yoon and Deng [26] also used clay-starch-fatty acid composites to prepare handsheets with improved physical properties. It is noted that the fatty acid in the starch-fatty acid-clay composite also increases the hydrophobicity of the filler [26]. However, the increased hydrophobicity may interfere with hydrogen bonding between starch and fibres [26]. Yoon [27] also coated clay by cellulose from bleached kraft softwood pulp, unbleached kraft softwood pulp, and deinked news paper using the N-methylmorpholine-N-oxide dissolution technique. While the physical properties of handsheet filled with cellulose coated clay were significantly improved, the brightness and opacity were inferior to the handsheets filled with starch-clay composites [27].

1.1.5. Preflocculation of filler

The preflocculation of the mineral filler before adding it to a pulp suspension has received much attention. A macro filler floc was produced in a batch process and then sheared to smaller particle size flocs [28]. Batch processes are in general energy intensive and the product quality is inconsistent from batch-to-batch [28]. A continuous process to alleviate these concerns was also described [28]. Smith [29] also described a continuous method to provide preflocculated filler to a papermaking suspension. Preflocculated filler with starch phosphate and cationic polyacrylamide was prepared for higher filler loadings [30]. Brooks et al. [31] successfully incorporated a cold-water-soluble starch in the flocculant with the help of a third agent and such flocculant could be added in dry form directly to the filler slurry which greatly simplifies the preflocculation process. Palmer et al. [32] formed preflocculated filler composite by mixing filler particles with the raw starch granules with sizes between 40 and 70 μm. The paper produced with such filler was stronger than the paper produced conventionally with the same ash content. It is reported that the filler preflocculation by starch-based product increases filler content in

the sheet without strength reduction or inferior optical properties [33]. Preflocculation could provide approximately a 26% increase in first pass ash retention and a 13% increase in the tensile strength when same amount of filler was used from pilot plant trials [34]. Novak et al. [35] also studied the pretreatment of filler including kaolin and $CaCO_3$ with aluminum sulfate, cationic PAM, anionic PAM, and cationic starch in an effort to increase the filler content in paper while maintain the paper strength. However, for calcium carbonate, an increase in mechanical properties was achieved only with cationic additives [35]. Park and Shin [36] reported preflocculation of ground $CaCO_3$ and talc treated with high molecular weight cationic polyacrylamide (H-CPAM), low molecular cationic polyacrylamide (L-CPAM), and cationic starch. It was found that fillers treated with H-CPAM resulted in the largest and strongest flocs. Improved preflocculation technology by the use of dual polymers system to produce shear resistant filler flocs with a defined and controllable size distribution was also developed [37]. Filler flocs with a size distribution of 10-100 μm were prepared by first adding a polymer to the filler dispersion followed by addition of a second cationic polymer (copolymers of acrylamide with diethylaminoethyl acrylate) to initiate flocculation of the filler particles. Handsheets prepared with preflocculated and untreated PCC having equivalent ash content and basis weight showed increasing the floc size did not hurt brightness, but decreased the formation and opacity of the sheets slightly. The mechanical strength of the sheets increased significantly with increasing PCC floc size [37]. The increase in the strength of paper by the pretreatment of filler has been attributed to the reduction of the surface area of the filler. Therefore, disruption of fibre-fibre bonding from fillers becomes less frequent. It is noted however that the preflocculation reduces the number of individual filler particles, which decreases the opacity [37].

1.2. Retention/Drainage Aid System

The high molecular weight polymers used in papermaking to retain fibre fines, filler, and other fine materials also affect drainage [38] and filler Z-direction distribution [39]. The retention aid polymers function through the formation of bridges between particles [40] and usually create “hard flocs” which are able to resist hydrodynamic shear [41].

Microparticle and nanoparticle having a large surface area are used to deal with retention/drainage and formation challenges in wood containing furnish [42-45]. A comparison of the important characteristics of existing commercial microparticles and nanoparticle is shown in Table 1.1 [46, 47].

When flocculants are used to improve the retention of fines and fillers in paper, the increased retention often results in an impaired formation since retention aids also induce fibre flocculation [48-52]. Formation is a very important parameter since it affects the physical and optical characteristics of paper. In some cases, retention is sacrificed in order to achieve better formation. The uniformity of sheet formation depends mainly on fibre flocculation and shearing conditions in the forming section [53, 54]. The main factor affecting formation is the fibre floc strength. This in turn depends on the number of contacts between fibres in the headbox and the bond strength at each contact [55]. Retention aids are believed to increase the bond strength at the fibre-fibre contact points, which would lead to increased fibre flocculation and hence a poorer formation [56].

Table 1.1. Comparison of important characteristics of commercial microparticle (MP) and nanoparticle (NP) products

Product	Solid (%)	Surface area (m^2/g)	Degree of structure	Type of structure
Early NP silica	10-15	400-650	Very low	n/a
MP bentonite	85-93	700-800	n/a	n/a
Recent NP silica	7-11	650-900	Medium-high	Linear
Micropolymer	35	n/a	Very high	3D
On-site NP silica	1	1200-1400	Very high	3D
New NP silica	7	1100	Very high	Linear

Optical methods have been employed to study fibre flocculation [57-59]. Most studies report a quasi-linear relationship between flocculation and retention [60-62]. Krogerus [63] found that the formation varies significantly at a given retention, depending on the type of polyacrylamide (PAM) used for various types of retention systems consisting of PAM and bentonite. Albinsson et al. [60] report that a cationic starch/colloidal silica

system gives a slightly better formation than the PAM/bentonite one at the same retention level. Langley and Litchfield [64] employed a cationic polyacrylamide/anionic montmorillonite system. Huber et al. [53] used five retention systems in a pilot-scale flow loop with industrial type pulp furnishes and found that the cationic starch/silica system had the lowest tendency to flocculate fibres. It was also found that with an increased amount of filler formation improved probably because the polymer transferred from the fibre to the filler particles resulting in a reduction of fibre flocculation [42, 55, 65].

It is known that retention aids also can affect dewatering. In addition to higher retention and uniform formation, better drainage is also desired in papermaking. The most widely used low molecular mass, high charge density cationic polymers to improve drainage are polyethylenimine (PEI) and poly (DADMAC). High molecular mass, low charge density cationic polyacrylamide (CPAM) and cationic starches are components of microparticles also improve drainage [66, 67]. The flocculation of fines increases the permeability of the fibre web by reducing the plugging of the web pore structure.

1.3. Filler Effects on Paper Strength and Dry Strength Aids

The use of inexpensive mineral fillers has become more and more common in the TMP-based papers in order to lower the production cost of the paper and to improve its properties. However, the addition of the filler decreases the paper strength [67-69]. The type of the filler, filler particle size and size distribution, and particle shape are of great importance for the properties of the paper. Clay is less strength detrimental than precipitated calcium carbonate (PCC) or ground calcium carbonate (GCC). The prismatic PCC is less strength harmful than scalenohedral PCC [70, 71]. At constant total area of filler per mass of paper the burst strength was found to follow the trend: clay > talc > GCC $\cong$ PCC [72, 73]. Light scattering and abrasiveness also depend on particle size.

Fillers often form aggregates which may include fines before sheet formation [74]. Thus, it is likely that the size distribution within the sheet is not equal to the original size distribution in the filler dispersion. For a given filler type, the smaller fillers were found

to decrease paper strength more significantly possibly due to the higher total surface area [70, 75, 76]. A comparison of the strength of paper made with and without filler preflocculation showed that preflocculated fillers are less harmful to paper strength [77].

The filler particles on the surface of fibres are believed to affect sheet strength whereas the particles in voids did not influence fibre-fibre bonding and thus sheet strength [69]. It has also been reported that montmorillonite which has a platy hydrophilic surface has a small negative effect on paper strength [78]. Papermakers can add either fines [79] or dry strength aid polymers [24-26, 80] to compensate for the filler induced strength losses. It is believed that fines are large enough to increase the fibre-fibre and fibre-filler bonds. However, refining energy is required to produce fines. As another choice, water soluble polymers are used to increase fibre/fibre adhesion and fibre/PCC adhesion [81]. Zhang et al. [82] reported when compared at an equal mass content of polymer for strengthening, the difference in the cationic group content did not affect the paper tensile strength. The hydrophobicity-hydrophilicity property of polymer plays an important role in determining the dry strength of paper [81]. Cationic starch is the most widely used dry strength additive [83-86]. In addition to strength enhancement, starches also aid drainage, retention and formation [87, 88]. Significant synergism between silica and starch to improve PCC retention was reported [67, 89]. Also a properly selected starch does not necessitate the need for a fixation agent to deal with the DCS problem in some cases [90]. It should be noted that efficient adsorption of starch on the pulp furnish components is required to achieve the expected strength and also decrease the problems associated with the unretained starch. There are several types of starch and the papermaker needs a clear understanding of the interactions of starch with the other components of the pulp suspension in a particular paper machine system in order to make a judicious choice of the type of starch, starch dosage and feeding point.

Some other new approaches to improve paper dry strength have also been reported. Laine et al. [91, 92] have shown that the grafting of CMC onto a fibre surface through high temperature treatment yields very strong paper. The paper strength enhancement also depends on the location of adsorbed polymer [93]. Another area involves the application

of polyelectrolyte complex and polyelectrolyte multilayers, which results in significant paper strength enhancement [94, 95].

1.4. PCC Flocculation and Population Balance Modeling

Fillers usually form aggregates before their incorporation in the paper sheet [74]. The floc size, strength and structure have to be controlled and adjusted to an optimum value for the papermaking [96]. It has been suggested that filler aggregation can reduce the filler's negative effect on the paper strength because of the decrease of the filler surface area and smaller number of particles [97]. However, the filler aggregates are weak and can be broken by shear to smaller particles. Tang et al. [98] found the stronger the bonding between the particles the higher the floc strength. Similarly, the more compact the floc structure, the greater the number of interparticle bonds. This results in stronger flocs [99, 100]. The floc structure and strength of precipitated calcium carbonate (PCC) aggregates was studied using various polymers by static light scattering/diffraction (SLS), real time fluorescent video imaging, image analysis, photometric dispersion analysis (PDA) and scanning electron microscopy (SEM) [101]. It was found that PEO/cofactor induced PCC aggregates were weaker at high shear and less reversible than those induced by PVFA/NaAA or cationic starch. Flocs produced at low polymer dosages were smaller and weaker than those produced at higher dosages [101]. It is noted that it is difficult to develop a satisfactory technique to quantify floc strength due to the complexity in floc size and structure [102, 103].

Liimatainen et al. [104] found the stronger and denser flocs improve the dewaterability of pulp suspension. Hubbe [43] stated that compact structure formation could lead to expulsion of water from inside the flocs which could facilitate the drainage. Sang et al. [105] showed that the high charge density starch always resulted in the best drainage performance regardless of conventional chemical addition sequence or PCC preflocculaiton strategy probably because of the formation of more compact flocs. Gaudreault et al. [101] speculated that the open aggregates would be better for the optical properties because of the larger surface area to scatter more light. Hence, it is necessary

to control the floc properties through the manipulation of the process conditions. Knowledge of the rates of PCC floc formation (aggregation), breakage and restructure may enable the control of the floc size, strength, and structure. The population balance model which was first proposed by Smoluchowski [106] is widely used to describe the dynamics of particle or droplet size distributions and can be adopted to describe PCC flocculation [107-110]. A discretized population balance equation was developed to determine the growth and aggregation rates from experimental data [111]. In order to make the population balance model closer to the real systems, the fractal dimension has been incorporated into population balance equation to model the shear-induced flocculation of porous aggregates [112, 113]. Selomulya et al. [114] has demonstrated the importance of floc structure change during flocculation and introduced the restructure process to the population balance modeling which is responsible for the decrease in floc size and increase in floc compactness. Kusters et al. [115] proposed a model which correlates the collision efficiency with the dimensionless floc size. Heath and Koh [116] incorporated the population balance model to computational fluid dynamics (CFD) and found the combined population balance/CFD model gave the local aggregate size distribution which varies considerably across the vessel depending on the local conditions.

1.5. Summary

Although various approaches including lumen loading, cell wall loading, fine-filler composite, filler modification and filler preflocculation have been investigated to increase the filler content without compromising the paper properties, except for the filler preflocculation strategy, none of the above mentioned approaches has been successfully implemented to the existing production process for the highly filled paper manufacture. This is because additional processes are needed to remove the filler on the exterior fibre surface for lumen loading and cell wall loading which are far from common papermaking practice. Fine-filler composite approach needs to be further optimized on dewatering and printability because of the high ratio of fines in the composite. Slurry instability,

formation of agglomerates and more proneness to sedimentation are the drawbacks associated with the filler modification technology.

In this thesis, it is proposed to take advantage of the most recently developed cationic starch and nano-structured silica in order to further increase the filler content in paper beyond current levels by using existing paper machines. The thesis examines the performance of such starch and silica on the retention/drainage and the paper properties under the conventional chemical addition sequence and the PCC preflocculation strategy.

Extensive work has been done to investigate the kinetics of PCC flocculation by various flocculants used in papermaking. However, information on the floc structure and its evolution is sparsely available. Moreover, it is important to establish a relationship among floc properties and flocculant characteristics and process conditions. In this thesis the population balance model is employed to study the dynamics of PCC flocculation by starch and develop a relationship among collision efficiency, floc strength, restructure rate and process conditions (shear rate, ionic strength, temperature, polymer concentration, etc).

1.6. Research Objectives

Currently, the shortage of cheap and good quality fibre is perhaps the biggest challenge to the paper industry. This occurs due to the sawmill closure and the industry has shifted to producing high-value added communications grade paper from mechanical pulps instead of only newsprint papers. In view of the current fibre shortage, the papermaker reduces the fibre percentage in the feedstock by replacing it with mineral filler to produce high-brightness highly-filled opaque paper. Due to the lack of capital for the investment in new paper machine, judicious engineering solutions at the wet end of paper machine have to be introduced for the production of highly filled paper. The scope of the thesis is to determine how the PCC content in mechanical grade paper can be increased beyond the current levels by using existing paper machines in a manner that does not compromise the paper properties. The hypothesis is that optimal dosages and addition sequence of

starch, nano-particle silica and CPAM can be found to achieve higher PCC loading. The following specific objectives are identified:

1. Determine dosages of starch, CPAM and nano-structured silica for optimal retention and drainage in a TMP suspension.
2. Develop new retention aid program by taking advantage of the most recently developed nano-structured silica and starch and determine the addition sequence and feeding points for the production of highly PCC filled paper by using the existing paper machine.
3. Establish the relationship among starch properties, process conditions and floc properties that would allow the judicious selection of starch type for better retention and drainage in papermaking process.
4. Present a population balance model to describe the floc size evolution and compare it with the experimentally obtained PCC flocculation data. Establish relationships among collision efficiency, floc strength, restructure rate and the experimental conditions (shear rate, ionic strength, temperature, starch concentration).

1.7. Thesis Organization

Chapter 1 discusses the highly filled paper and the approaches proposed or used for its production. It also describes the retention/drainage aid system used in papermaking and the filler effect on the paper properties. The basic information about PCC flocculation and population balance modeling is provided in this chapter. The motivation of the present research is also discussed.

Chapter 2 presents the results for chemical additive optimization for highly PCC filled mechanical grade papers production. The material of this chapter has been published.

● Sang, Y., McQuaid, M., Englezos, P. (2011). "Optimization of Chemical use for Highly Filled Mechanical Grade Papers with Precipitated Calcium Carbonate." BioResources **6**(1): 656-671.

Chapter 3 presents the results for PCC pre-flocculation by cationic starch in an effort to increase the filler retention and reduce the negative effect of the filler on the paper strength. The material of this chapter has been published.

● Sang, Y., McQuaid, M., Englezos, P. (2012). "Pre-Flocculation of Precipitated Calcium Carbonate Filler by Cationic Starch for Highly Filled Mechanical Grade Paper." BioResources, 7(1): 354-373.

Chapter 4 studies the PCC aggregation kinetics and establishes the relationship among starch properties, process conditions and floc properties. Relevant electrokinetic and starch adsorption measurements are also presented. The material of this chapter has been published.

● Sang, Y., Englezos, P. (2012). "Flocculation of Precipitated Calcium Carbonate (PCC) by Cationic Tapioca Starch with Different Charge Densities. I: Experimental." Colloids and Surfaces A: Physicochemical and Engineering Aspects. DOI: 10.1016/j.colsurfa.2012.07.019

Chapter 5 presents a population balance model to describe the floc size evolution and compare it with the experimentally obtained PCC flocculation data. The relationships among collision efficiency, energy dissipation rate, restructure rate and the experimental conditions is also established. The material of this chapter has been published.

● Sang, Y., Englezos, P. (2012). "Flocculation of Precipitated Calcium Carbonate (PCC) by Cationic Tapioca Starch with Different Charge Densities. II: Population Balance Modeling." Colloids and Surfaces A: Physicochemical and Engineering Aspects. DOI: 10.1016/j.colsurfa.2012.07.028

The conclusions, contribution to knowledge from this work and recommendations for future work are presented in Chapter 6.

Chapter 2 Optimization of Chemical Use for Highly Precipitated Calcium Carbonate Filled Mechanical Grade Papers[1]

This conventional addition sequence of dry strength additive (starch) followed by the retention aid (flocculant/silica) to a pulp/filler suspension is evaluated in this chapter. Statistically designed laboratory trials were conducted. Retention and drainage were measured as well as handsheet breaking length, burst index, and ash content.

2.1. Introduction

Mechanical grade papers benefit from the use of calcium carbonate filler because of gains in brightness, a key quality determinant of the performance-to-cost ratio [68]. In general, paper produced with higher filler content has improved brightness and opacity. The replacement of wood fibres with less expensive mineral filler such as precipitated calcium carbonate (PCC) has an economic benefit, and it also mitigates to a certain extent the shortage of wood fibres. The paper industry has been able to manufacture paper with significant levels of filler loading with the use of existing machinery and relying on advances in wet end chemistry technology. However, the addition of increased amounts of filler reduces the strength and requires an effective retention system [69]. Starch is usually added to compensate for the strength loss [117]. The effective retention of starch in the paper sheet is a significant step to determine its performance. Cationic and amphoteric starches were found to be retained in the sheet primary through forming ionic bonds between cationic groups in the starch derivatives and carboxyl groups in pulp fibres or fines [118, 119]. In addition, a number of parameters also affect the starch performance in a papermaking system [80, 84, 120, 121]. Consequently, the papermaker needs to evaluate the performance of a starch product in order to make a judicious choice of the type of starch, starch dosage, and addition point. It should be noted that fibre fines

[1] A version of this chapter has been published: Sang, Y., McQuaid, M., Englezos, P. (2011). "Optimization of Chemical use for Highly Filled Mechanical Grade Papers with Precipitated Calcium Carbonate." BioResources **6**(1): 656-671.

are also effective as strengthening agents [79]. Fines have the ability to bridge the filler-induced voids present in the fibre/fibre binding domain. Subramanian et al. [20] explored the benefits from fibre fines and discussed a composite paper concept that contains up to 50-60 % PCC.

While starch is added primarily for the purpose of strength enhancement, it is also known that a properly selected starch can provide additional benefit of performing as a retention aid and in some cases does not necessitate the need for a fixation agent [89, 90]. Microparticle or nanoparticle retention aid systems have also been developed to help deal with retention, drainage and formation challenges related to increased amount of filler. There is extensive information on these retention systems in the literature [43, 122-126]. In the past decades, many variations of the microparticle systems have been developed to further improve their performance. These include modifications of the physical and chemical structure of silica particles.

It is of interest to explore whether it is possible to increase the level of loading beyond the current typical limit of about 25% by taking advantage of recent developments in starch and nanoparticle technologies. The objective of the present study was to evaluate the ability of three new starches to be used in conjunction with a new nanoparticle retention system to retain increased amount of PCC. In order to optimize the chemical dosages, "laboratory trials" were carried out in which mill wood fibre suspensions were utilized. Laboratory retention and drainage tests have been traditionally carried out on a trial and error basis using a conventional "change one factor at a time" approach. This experimentation method is time consuming and not capable of reaching the true optimum because interaction among variables is neglected [127]. To resolve this problem, response surface methodology (RSM) with a central composite design was employed to optimize the addition strategy of chemicals and evaluate their effects. An empirical process model was then constructed to predict the retention and drainage results. In addition, handsheets were prepared and their ash content, breaking length, and burst index were determined. Moreover, the partition behavior of starch between fibre and fines was also studied.

2.2. Experimental

2.2.1. Materials

The pulp used in the experiments was peroxide-bleached TMP that had a pH of 6.9 ± 0.2 and was supplied by a leading pulp and paper mill in British Columbia. It is a mixture of spruce, pine, and fir.

The PCC used for this work was an acid-tolerant PCC which was subjected to polyacrylate treatment and obtained at a solids content of 28 wt% from Specialty Minerals Inc (Bethlehem, PA, USA). This PCC has a negative zeta potential -15 ± 5 mV at 0.002 wt%. It is noted that pure PCC exhibits a positive zeta potential in the range +10 to +25 mV. The density of the PCC is 2.71 g/cm^3. The PCC has a scalenohedral structure and an average particle size of 2.71 ± 0.15 μm. Its particle size distriubtion (PSD) was obtained with a Malvern Mastersizer 2000. The hydrodynamic surface area 1.45 m^2/g was calculated from the measured PSD assuming that all the particles are spheres. This PCC had a brightness of 98% ISO and and a pH of 8.7 ± 0.1.

Cationic tapioca starches (CATO 304, Alias S304, 0.22-0.26% N, DS = 0.03, charge density = 0.24 meq/g; OptiPro 858, Alias S858, 0.55-0.60% N, DS = 0.07, charge density = 0.57 meq/g; OptiPro 880, Alias S880, 0.90-1.10% N, DS = 0.13, charge density = 1.08 meq/g) having 17% amylose and 83% amylopectin with different nitrogen contents were used in the experiments. These starches were supplied by National Starch ULC and had an average molecular weight of 3 million Da (Surrey, BC, Canada). The cationic substituent of the starches is quaternary ammonium. Prior to use, the starches were cooked following the procedure provided by National Starch ULC.

Cationic polyacrylamide (CPAM, average molecular weight is 10 million Da) supplied by Eka Chemicals (Magog, QC, Canada) was used as flocculant. It had a branched structure and a charge density of 2.1 meq/g as determined by polyelectrolyte titration using 0.001N anionic PVSK.

Silica with a mean size of 5 nm was supplied by Eka Chemicals (Magog, QC, Canada) as an 8.1 wt% suspension. Distilled and deionized water was used for the preparation of the polymer solutions.

Back titration was used to determine the starch partition behavior between fibre and fines using poly (vinyl sulfate) potassium (PVSK), which was received as a 0.001 N solution from BTG Americas (Pointe-Claire, QC, Canada).

Process water was the water obtained by centrifuging the pulp collected from the storage chest following the bleach tower. The pulp was placed in a screen bag and uniformly loaded into the centrifuge (Bock, Toledo, USA). During the centrifugation process, the water from the outlet was collected, while the pulp left in the screen bag was discarded. It was expected that the process water contained dissolved and colloidal substances. The average particle size of materials suspended in process water was found to be 388 μm as determined by the Malvern Mastersizer 2000. In addition, the zeta potential and the cationic demand were found to be equal to -16.5 mV and 2.2 μeq/g, respectively. This process water was used for the dilution of the pulp to simulate the papermaking process as much as possible [125].

2.2.2. Starch cooking procedure

Starch suspension (1.67 wt %) in a jar was placed in a boiling water bath, ensuring that the level of the bath water exceeded the level of the slurry in the jar. For the first few minutes, the starch slurry was continuously stirred until reaching the gel point. Once the gel point was reached, a rolling boil was sustained in the bath for a total of 30 minutes. Care was taken to top up the jar to avoid the net evaporation of water during the cook cycle. The suspension was stirred approximately every 10 minutes to help break down any un-burst grains until the 30 minutes cook cycle was reached. After the starch was cooked, it was cooled down to room temperature. Cooked starch prepared according to this procedure was used within 24 hours.

2.2.3. Retention and drainage experimental procedure

Retention and drainage experiments were performed using the DFR-04 device from BTG Americas Inc. (Pointe-Claire, QC, Canada). The main components of the DFR-04 device are the dosing unit, stirring chamber, wire screen, and the balance. In addition, for retention measurements there is a two-way outlet valve with the RET 20 Lab sensor. For drainage measurements, there is a filtrate outlet. The dosing unit allows for the automatic addition of various chemicals to the pulp suspension. The sequence of addition, the timing of such additions, and data collection were programmed in advance using the accompanying software.

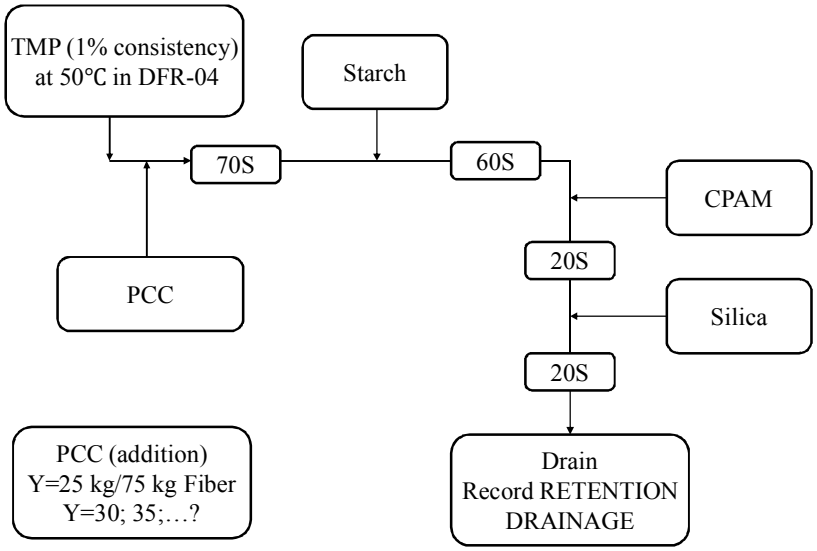

Fig. 2.1. Block flow diagram for retention and drainage experiments

A 50 mesh (200 μm hole) screen was used for the retention and drainage measurements, which were carried out following the procedure shown in Fig. 2.1. Y is the ratio between the weight of PCC and the weight of fibres. For retention measurements, the DFR-04 was first calibrated using a 1% TMP suspension loaded with PCC. The water in the filtrate was first removed through the vacuum filtration, and the fibre/fines left on the filter paper were collected. Then the fibre/fines were placed in a 100 ºC oven for two hours to

determine their dry weight. Then the solids were ashed using a 575 ºC furnace for 12 hours. Details on the use of DFR-04 can be found in literature [89, 90].

During retention experiments, 1 kg of TMP pulp at 1% consistency and at 50 ^{o}C was first placed inside the stirring chamber. The additives were then added to the pulp suspension and allowed to mix (see Fig. 2.1). Retention was measured according to the TAPPI Standard Method T261 cm-94. Each run was repeated three times, and the average total retention and filler retention are reported. For the drainage measurements, a sample of 1 kg of TMP pulp at 1% consistency and at 50 ^{o}C was filtered through a screen, and the filtrate weight was determined gravimetrically. The drainage weights reported were the weight of filtrate collected over 60 seconds.

2.2.4. Retention and drainage experimental design

Response surface methodology using the central composite design (CCD) was used to study the effects of the PCC loading levels, dosages of starch, CPAM, and silica for higher PCC content in the final paper product. The experimental design and the analysis of the results were performed by using JMP IN 4.0 (SAS Institute Inc., Cary, North Carolina). Analysis of variance (ANOVA) was carried out to study the effect of each factor and construct the prediction model. The simplified prediction model was obtained based on the P value (probability) with 95% confidence level.

According to the design, the total number of experiments is $2^n + 2n + n_0$, where n is the number of independent variables (n = 4) and n_0 is the number of experiments at the central point (n_0 = 6). Totally 30 experiments with five coded levels were conducted [127]. The levels of the factors studied are shown in Table 2.1. The minimum and maximum ranges of chemicals were chosen on the basis of papermaking practice. The design is shown in Table 2.2.

The responses (total retention, filler retention and drainage) from the 30 experiments are used to fit an empirical model that describes the significant linear, interaction and second

order effects. The following quadratic model for the prediction of the total retention, filler retention and drainage was employed [127],

$$Y = \beta_0 + \sum_{i=1}^{n} \beta_i X_i + \sum_{i=1}^{n-1} \sum_{j=2, j\neq i}^{n} \beta_{ij} X_i X_j + \sum_{i=1}^{n} \beta_{ii} X_i^2 \qquad (2\text{-}1)$$

where β_o is the intercept. The coefficients β_i, β_{ij}, and β_{ii} represent the linear, interaction, and quadratic effects, respectively. This model was validated by comparing calculated values against experimental data from a set of independent conditions (other than those from the 30 experiments used in the ANOVA).

Table 2.1. Levels of the factors for experimental design

Factor	Components	Levels of factor				
		a (-2)	-1	0	+1	A (2)
X_1	PCC (%)	25	30	35	40	45
X_2	Starch (kg/t)	8	9	10	11	12
X_3	CPAM (kg/t)	0.1	0.2	0.3	0.4	0.5
X_4	Silica (kg/t)	0.2	0.3	0.4	0.5	0.6

2.2.5. Pulp separation for starch adsorption experiment

The Bauer-McNett classifier was used to separate the fibre and fibre fines, following TAPPI Standard T 233 cm-95, 1995. The pulp component that passed through the 200 mesh was taken as the fibre fines. The other component was identified as fibres.

Table 2.2. Full experimental design for the retention/drainage experiment

Sample ID	Pattern	PCC (%)	Starch (kg/t)	CPAM (kg/t)	Silica (kg/t)
1	a000	25	10	0.3	0.4
2	----	30	9	0.2	0.3
3	---+	30	9	0.2	0.5
4	--+-	30	9	0.4	0.3
5	--++	30	9	0.4	0.5
6	-+--	30	11	0.2	0.3
7	-+-+	30	11	0.2	0.5
8	-++-	30	11	0.4	0.3
9	-+++	30	11	0.4	0.5
10	0a00	35	8	0.3	0.4
11	00a0	35	10	0.1	0.4
12	000a	35	10	0.3	0.2
13-1	0000	35	10	0.3	0.4
13-2	0000	35	10	0.3	0.4
13-3	0000	35	10	0.3	0.4
13-4	0000	35	10	0.3	0.4
13-5	0000	35	10	0.3	0.4
13-6	0000	35	10	0.3	0.4
14	000A	35	10	0.3	0.6
15	00A0	35	10	0.5	0.4
16	0A00	35	12	0.3	0.4
17	+---	40	9	0.2	0.3
18	+--+	40	9	0.2	0.5
19	+-+-	40	9	0.4	0.3
20	+-++	40	9	0.4	0.5
21	++--	40	11	0.2	0.3
22	++-+	40	11	0.2	0.5
23	+++-	40	11	0.4	0.3
24	++++	40	11	0.4	0.5
25	A000	45	10	0.3	0.4

2.2.6. Diethylene triamine pentaacetic acid (DTPA) chelation stage

Wood fibres have very strong ion exchange properties with metal ions, which mostly are bonded tightly with the pulp fibres. The metal ions have negative effects during chemical adsorption process on the fibres. Chelation was achieved with DTPA at an addition level of 0.5% DTPA on oven dry pulp at a pulp consistency of 10%, and a temperature of 50^{o}C for 30 minutes before the adsorption experiments in an effort to remove most of the bonded metal ions from the fibre surface [128]. The pulps were then washed with deionized distilled water to remove the metal ions and unreacted DTPA.

2.2.7. Starch partition between fibre and fines

Adsorption experiments of cationic starches on cellulose fibres/fines were carried out at 50^{o}C and without further adjustment of the pH value of the pulp during the experiment. The consistency of the pulp suspension used was 0.1%. The fibres were left in contact with the starch solutions for five minutes under constant stirring at 200 rpm. This time was found in our laboratory [129] to be adequate for starch to reach the steady state adsorption on fibres and agrees with literature [84]. After centrifuge, the equilibrium concentration of cationic starch was determined by colloidal back titration PVSK solution, using the particle charge detector (PCD, Mütek, Herrsching, Germany) [130]. The blank experiment (no fibre) was also carried out following the above procedure. The amount (A) of adsorbed starch in mg/g was calculated with Eq. (2-2),

$$A = \frac{(V_B - V_S)}{V_B} \times \frac{M_P}{M_F} \qquad (2\text{-}2)$$

where V_B is the PVSK volume consumed for the blank sample, V_S is the PVSK volume consumed for the adsorption sample, M_F is the mass of dry cellulose fibres, and M_P is the mass of starch added to the pulp suspension.

2.2.8. Handsheet making apparatus

A modified handsheet former was employed to prepare handsheets [131]. The handsheet making procedure was the same as the standard, except for the application of vacuum to simulate the actual papermaking process. A vacuum of five inches of mercury was used during the handsheet making. This was done to study how the pulp suspension and filler distribution were affected when the forming fabric passes over a suction box. Briefly, the apparatus is constructed of a 3" diameter clear acrylic circular cylinder below a forming fabric. Another circular cylinder is attached above the forming fabric, and a gasket is placed around the outside to provide an airtight seal. A vacuum chamber is connected to the bottom of the test chamber by a ¾" PVC pipe and electrically actuated solenoid valve. The vacuum chamber pressure can be adjusted to the desired pressure by an attached vacuum pump [131].

2.2.9. Handsheet properties measurement

Typically in the pulp and paper industry the TAPPI T 494 om-96 method is employed to determine the tensile properties of paper. The standard sample length for the TAPPI method is 100 mm. The handsheet made from the apparatus in the present study had a diameter of around 3" (76 mm). Therefore, it was impossible to follow the TAPPI method. The COM-TEN Universal tester is another laboratory-scale apparatus used for performing tensile strength. The advantage is that it can be used for smaller length samples. Tensile tests of two office printing paper samples were carried out on both the L&W tensile tester and the COM-TEN Universal tester to check the reliability of the COM-TEN Universal tester. The tensile strength for paper sample 1 was 23.02 $\pm$ 0.43 MPa, as measured by L&W tensile tester. The corresponding tensile strength was 25.35 $\pm$ 0.79 MPa, as measured by the COM-TEN Universal tester. The tensile strength for paper sample 2 was 41.21 $\pm$ 0.63 MPa, as measured by L&W tensile tester. The corresponding tensile strength was 39.58 $\pm$ 0.89 MPa, as measured by COM-TEN Universal tester. It was concluded that the Com-Ten instrument was adequate to perform the tensile testing.

In this paper, breaking length, burst index, and ash content of the handsheet are reported. Breaking length, a measurement of tensile strength of paper, is the length beyond which a strip of paper of uniform width would break under its own weight if suspended from one end. Burst index is the quotient of the bursting strength of a paper and its grammage in the conditioned state as defined in the standard method of test. The burst index of the handsheets was determined according to TAPPI T 403 om-02. Ash is the residue left after complete combustion of paper at 575 ^{o}C. It is generally expressed as percent of original test sample and represents filler content in the paper. The ash content of the handsheets was determined according to TAPPI T211 om-93.

2.3. Results and Discussion

A total of 30 experiments for each one of the three starches (S304, S858, and S880) were conducted. In addition, another 30 experiments were also carried out to determine the corresponding drainage values for each starch. Figs. 2.2 to 2.4 show the retention and drainage results. As seen, the retention aid program using S858 gave the highest retention, whereas the S880 retention system gave best drainage performance. Not surprisingly, the maximum retention and drainage values were obtained at the highest dosages of starch, CPAM, and silica for all these three starches.

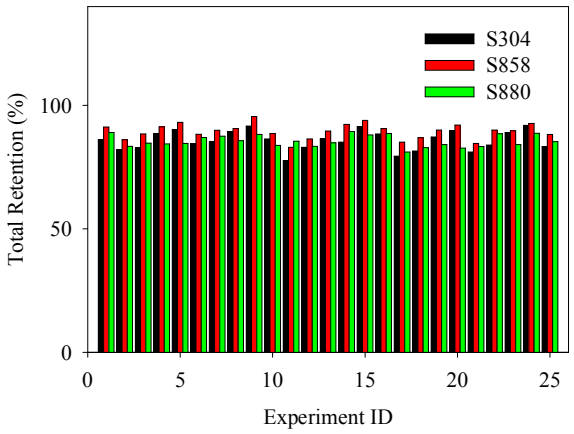

Fig. 2.2. Total retention for S304, S858 and S880 system

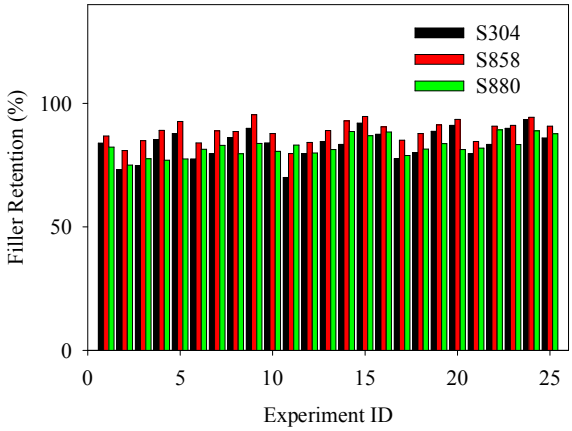

Fig. 2.3. Filler retention for S304, S858 and S880 system

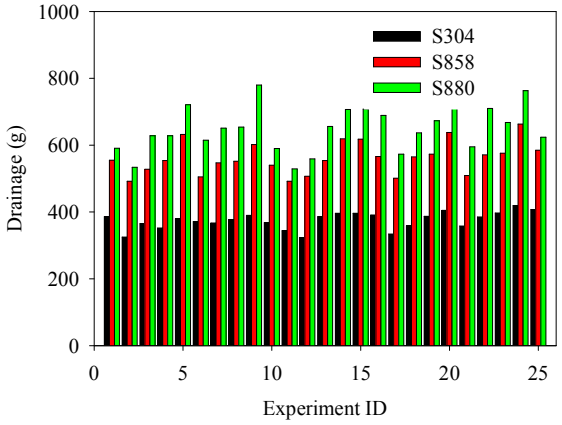

Fig. 2.4. Drainage for S304, S858 and S880 system

In the following part, the significant factors based on the analysis of variance (ANOVA) are presented for S858 system and S880 system separately in order to distinguish the effect of each factor and their interactions. Based on the ANOVA results, the regression models were also constructed.

2.3.1. ANOVA for S858 system

Table 2.3 (Refer to Appendix A for ANOVA details) shows the significant factors based on the analysis of variance results for S858 system. All the main effect were found to be extremely significant for all these three responses. The three interaction effects involving starch S858 were found to be statistically significant in filler retention. A very significant

synergism between starch S858 and silica was responsible for the total and filler retention improvement. The interactions between PCC and silica, as well as CPAM and silica were found to play a significant role in improving the drainage performance.

Table 2.3. Significant factors for S858 system

Factor	Total Retention	Filler Retention	Drainage
PCC	ES	ES	ES
Starch	ES	ES	S
CPAM	ES	ES	ES
Silica	ES	ES	ES
PCC*Starch	---	S	---
PCC*Silica	---	---	S
Starch*CPAM	---	S	---
Starch*Silica	VS	VS	---
CPAM*Silica	---	---	S
PCC*PCC	---	---	S
CPAM*CPAM	---	S	---

ES=extremely significant; VS=very significant; S=significant; ----: not significant

Khosrevani et al. [132] studied the effect of the cationic starch-anionic nanosilica system on the retention and drainage using a 85% bleached chemical eucalyptus/15% bleached chemical softwood pulp system. Their observations indicated that the nanosilica performance relied on the introduction of nanoparticles into the cationic starch-fines-fibres network, converting the fibre mat on the forming wire into a porous structure that is responsive to retention and drainage. In the present study, when the silica was added in the TMP suspension with starch and CPAM, the interaction mechanism became more complicated. This happens probably because the microflocculation of fines and fillers, which converts the fibre network to an open structure similar to the fines-free ones, took place with the help of the cationic polyelectrolyte and nano-particles.

The quadratic model that was fitted to the data for S858 system is shown in Table 2.5 and its validation is presented later. The model was employed to generate the prediction profiles for retention shown in Fig. 2.5 and the prediction profiles for drainage shown in Fig. 2.6. The 95% confidence intervals for the predicted values are also shown by error bars above and below each marker. As seen, the PCC had a negative effect on the total retention, while for the filler retention and drainage, the effect was positive. The positive effect of the increased PCC on the drainage is because PCC is easier to dehydrate than the fibre. CPAM and silica played more significant roles than starch, based on the steepness of the three prediction curves for the chemicals. It is also noted that CPAM and silica improved the responses throughout the entire experimental dosage range.

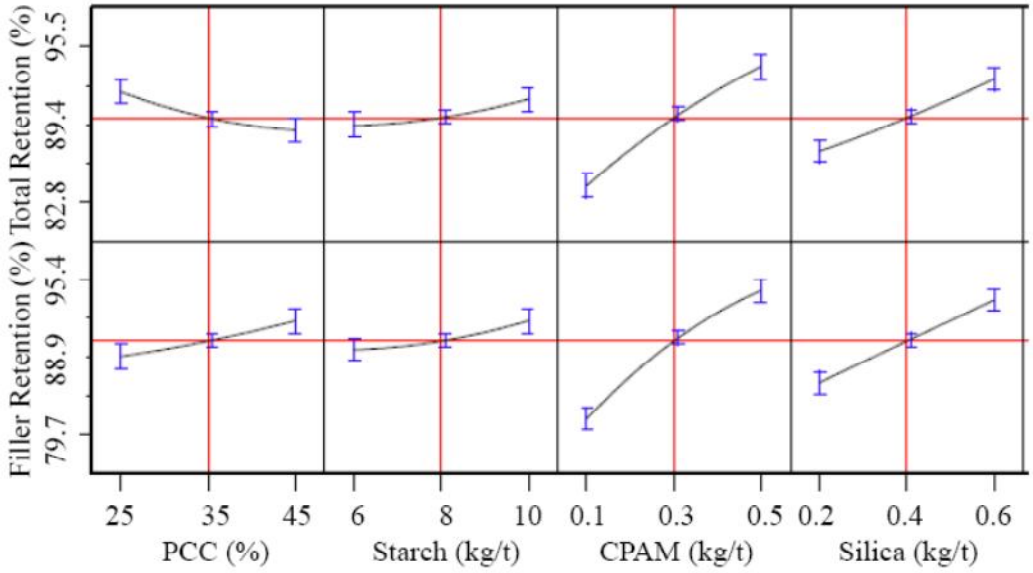

Fig. 2.5. Prediction profiles for retention for S858 system

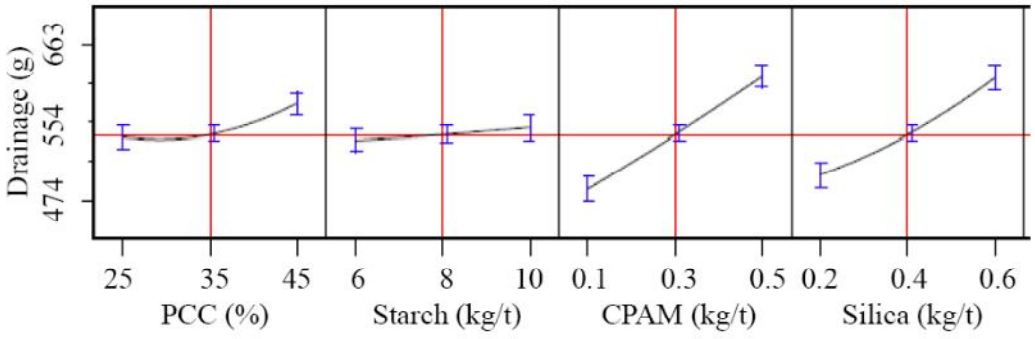

Fig. 2.6. Prediction profiles for drainage for S858 system

2.3.2. ANOVA for S880 system

The significant factors based on the analysis of variance for S880 system appear in Table 2.4 (Refer to Appendix A for ANOVA details).

Table 2.4. Significant factors for S880 system

Factor	Total Retention	Filler Retention	Drainage
PCC	VS	ES	S
Starch	ES	ES	ES
CPAM	---	---	ES
Silica	ES	ES	ES
Starch*Silica	S	S	---

ES=extremely significant; VS=very significant; S=significant; ----: not significant

For the total retention and filler retention responses, the change of CPAM dosages did not have any statistically significant effect, which is different from its behavior in the retention system with starch S858. This may be attributed to starch S880 having a much higher charge density than S858. In addition to functioning as strength agent for final paper and fixing agent for dissolved and colloidal substances, starch S880 also replaces the function played by the CPAM in retention. A significant interaction effect between starch S880 and silica was found, which may contribute to improve the total and filler retention. This interaction effect was also found for S858 and silica. All main effect terms were extremely significant for the drainage.

The quadratic model that was fitted to the data for the S880 system is also shown in Table 2.5 and its validation is presented later. The model was employed to generate the prediction profiles for retention shown in Fig. 2.7 and the prediction profiles for drainage shown in Fig. 2.8. As seen, the slope of S880 is much greater than that of S858. This may be attributed to starch S880 having a much higher charge density than S858; more cationic charge was introduced to the flocculation system for the same starch dosage increment. More significant flocculation would occur, resulting in improved retention

under the same starch dosage increment. The slope of CPAM was much smaller than those in the retention system using starch S858 for the total retention and filler retention response.

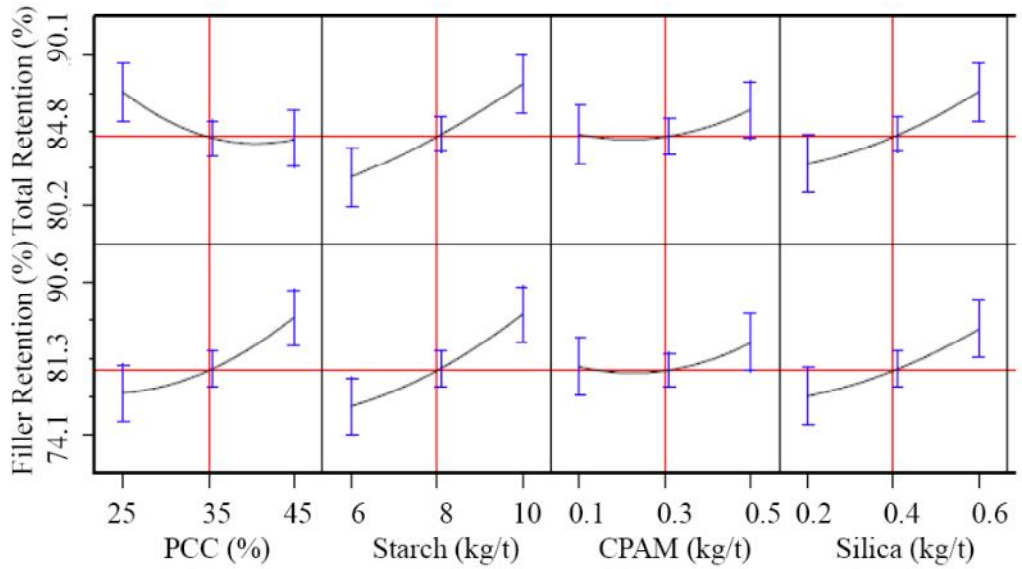

Fig. 2.7. Prediction profiles for retention for S880 system

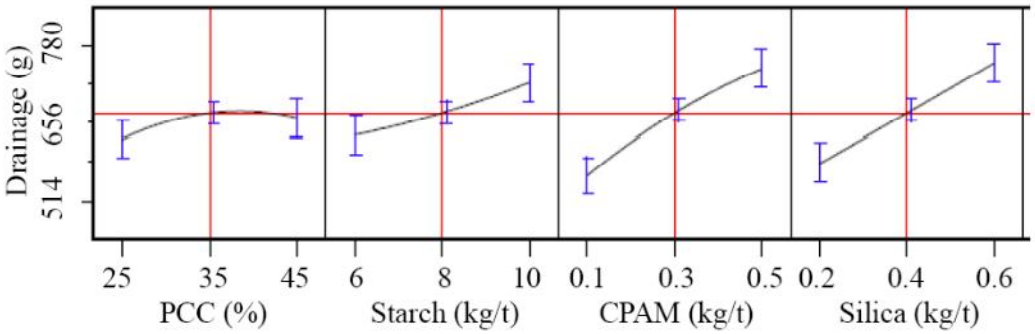

Fig. 2.8. Prediction profiles for drainage for S880 system

2.3.3. Model construction and validation

Based on the ANOVA, a regression model was constructed to predict the actual operating system. The estimated parameters for all main and crossed effects are reflected in equations shown in Table 2.5 for the retention system using S858 and S880. X_1, X_2, X_3 and X_4 are defined in Table 2.1.

To validate the accuracy of regression model, six additional experiments at the patterns (Table 2.6) other than those shown in Table 2.2 were performed, and the results were compared with the model predicted value. The experiment IDs in Fig. 2.9 correspond to those in Table 2.6. As seen from Fig. 2.9, the agreement was very good.

Table 2.5. Regression model for S858 and S880 system

	S858 Prediction Equation	S880 Prediction Equation
Total Retention	$Y=89.4-0.763X_1+0.529X_2+2.39X_3+1.44X_4+0.438X_2X_4$	$Y=84.8-0.729X_1+1.45X_2+1.11X_4+0.681X_2X_4$
Filler Retention	$Y=88.9+0.919X_1+0.748X_2+3.29X_4+2.13X_4-0.378X_1X_2-0.416X_2X_3+0.553X_2X_4-0.335X_3^2$	$Y=81.3+1.86X_1+2.26X_2+1.65X_4+0.969X_2X_4$
Drainage	$Y=554+10.2X_1+3.92X_2+34.3X_3+29.5X_4+4.50X_1X_4+4.75X_3X_4+4.45X_1^2$	$Y=656+8.50X_1+21.3X_2+43.0X_3+40.7X_4$

Table 2.6. Experimental conditions for model validation

Expt ID	Pattern	PCC (%)	Starch (kg/t)	CPAM (kg/t)	Silica (kg/t)
1	-0++	30	10	0.4	0.5
2	-+0+	30	11	0.3	0.5
3	00++	35	10	0.4	0.5
4	0+0+	35	11	0.3	0.5
5	+0++	40	10	0.4	0.5
6	++0+	40	11	0.3	0.5

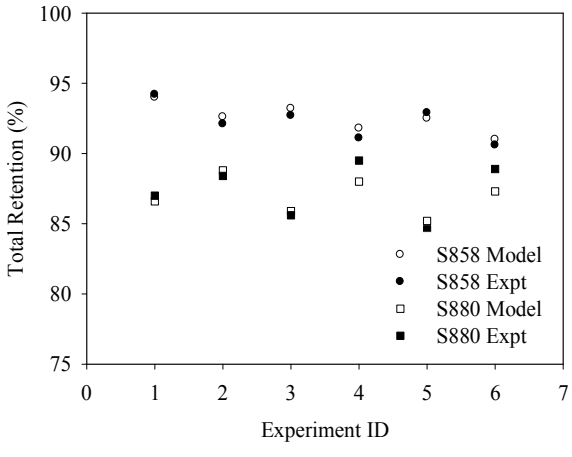

(a)

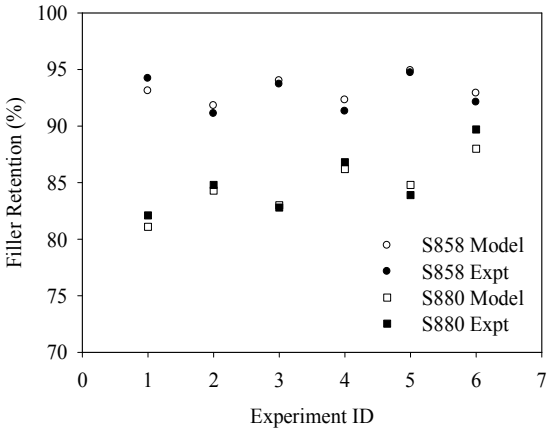

(b)

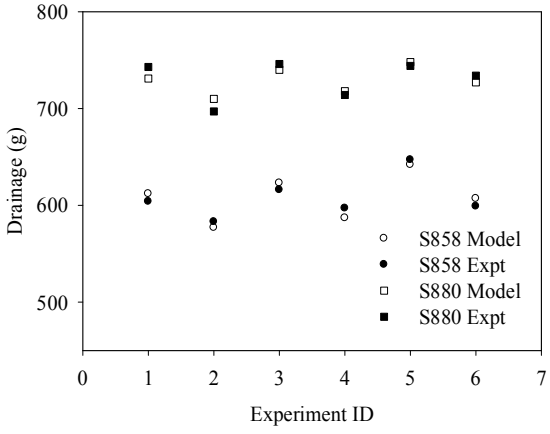

(c)

Fig. 2.9. Experimental and predicted values for (a) total retention, (b) filler retention, (c) drainage

2.3.4. Starch adsorption and partition

The results for starch adsorption on washed hydrogen peroxide bleached pulp show that S880 gave the highest adsorption amount (29.6 mg/g fibre) on fibre surface, followed by the S304 (13.0 mg/g fibre) and S858 (6.5 mg/g fibre). For S304 and S858, the starch adsorption amount was inversely proportional to its nitrogen content. This is in accordance with previous work [121]. The theoretical adsorption amount of cationic S880 starch on the pulp surface should be at about 3.2 mg/g pulp based on the charge neutralization theory [121]. The experimental result shows the actual adsorption amount of S880 on the pulp surface reached 29.6 mg/g, which was much higher than the theoretical value. This is because in the other two cases (starches S858 and S304) the interaction of cationic groups with the hydroxyl groups of the fibre surface was too weak and the starch was desorbed very easily. The higher adsorption amount may also be explained by the higher tendency of starch S880 to form clusters because of hydrogen bonding between hydroxyl group and polymer entanglement [133].

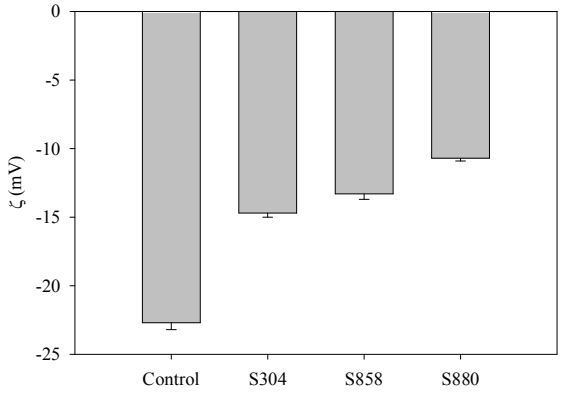

Fig. 2.10. Pulp zeta potential after starch adsorption

The pulp zeta potential after starch adsorption is shown in Fig. 2.10. As seen, the higher the charge density, the less negative the zeta potential, indicating more charge was introduced to the fibres by the high charge density starch and its high affinity to the pulp.
Fig. 2.11 shows the starch partition behavior between fibre and fines. The adsorbed amount of these three starches was found to increase linearly with the increase of fines

ratio in the pulp. This is due to the higher surface area of fines than that of fibre. The very high affinity of starch S880 with fibre and fines can improve the permeability of the pulp. This is supported by the fact that the best drainage performance was achieved with the retention system using S880, as shown in Fig. 2.4.

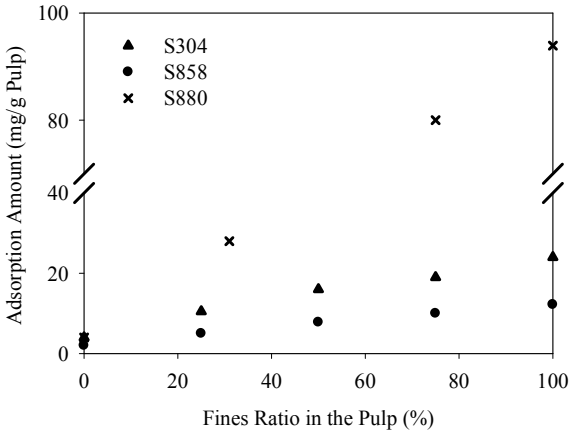

Fig. 2.11. Starch partition on fibre and fines

2.3.5. Handsheet properties

The handsheets were prepared using a modified handsheet former with vacuum suction based on the PCC content and chemical dosage as shown in Table 2.2. The ash content, breaking length, and burst indices of the handsheets are shown in Figs. 2.12 and 2.13. The sample IDs in Figs. 2.12 and 2.13 correspond to those in Table 2.2. With the help of the retention chemicals, the ash content of the handsheet could be pushed up to 40% for S858 and S880 retention systems. The S858 retention system always gave slight higher ash content than the S880 retention system. This is in accordance with the Mütek DFR-04 retention results, as shown in Fig. 2.3. The S880 resulted in higher breaking length and burst indices. One possible reason is the slightly lower ash content of the handsheet obtained with the S880 retention system. The other one, which is maybe more important, is the different adsorption behaviors of these two starches. S880 had a much higher affinity to fibres and fines than S858, as shown in Fig. 2.11. The high starch affinity with fibres will directly promote interfibre bonding [93] and thus the paper strength. This is supported by the paper physical properties as shown here.

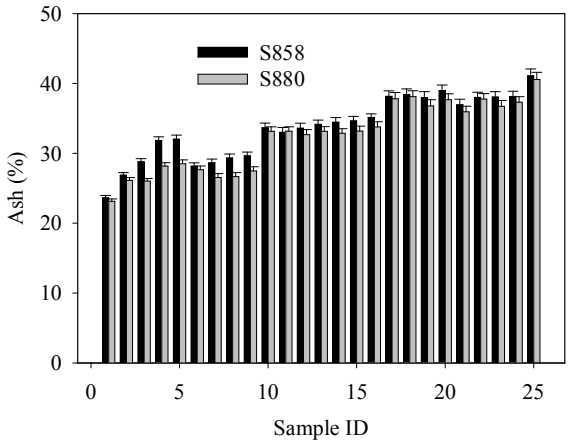

Fig. 2.12. Ash content of the handsheet made from S858 and S880

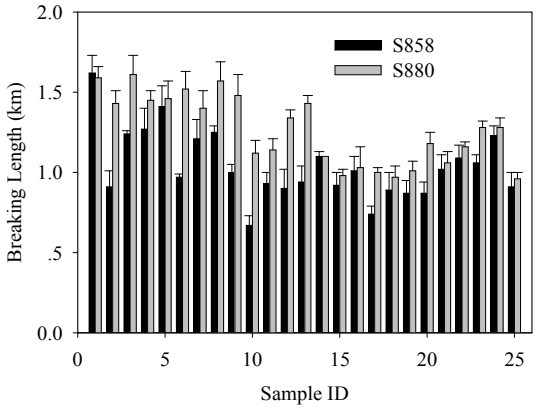

(a)

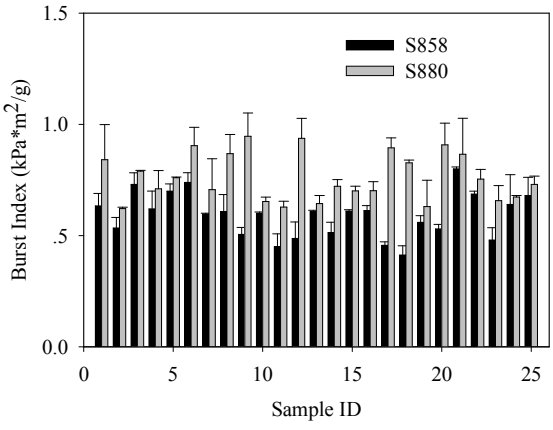

(b)

Fig. 2.13. Comparison of (a) breaking length (b) burst index of S858 and S880 retention system

2.4. Conclusions

The retention aid program using starch S858 gave the highest retention and slightly higher ash content, whereas the starch S880 resulted in the fastest drainage. A significant synergism was found between starch (S858 and S880) and silica, which improves the retention. Empirical models constructed in this work can accurately predict the retention and drainage under various conditions. The starch adsorption amount was inversely proportional to its nitrogen content of S304 and S858. The S880 system resulted in the higher breaking length and burst indices, possibly because it has a higher affinity for fibres and fines than S858 system. The work shows that a suitable choice of starch can be made depending of the objectives and priorities set by the papermaker.

Chapter 3 Pre-Flocculation of Precipitated Calcium Carbonate Filler by Cationic Starch for Highly Filled Mechanical Grade Paper[2]

An alternative addition sequence was investigated. Part of the dry strength additive (starch) was added to the filler (filler preflocculation) and the balance was added to the pulp/filler suspension after the CPAM. Statistically designed laboratory trials were conducted. Retention and drainage were measured as well as handhseet breaking length, burst index, and ash content.

3.1. Introduction

It is well known that an increase of filler content in paper can mitigate the shortage of good quality fibres, reduce production cost, and improve optical properties. However, increased filler also tends to decrease paper strength and may create linting/dusting problems. To incorporate more filler into paper without negatively impacting the papermaking operations and sacrificing the paper properties, various methods have been explored, including lumen loading [2, 134], cell wall loading [9], fines-filler composites [18], filler modification [11, 24], and fibre engineering [135, 136]. Due to the additional processes required and the unstable level of filler loading, lumen loading and cell loading have received little attention. The concept of fines-pigment composites enabled the production of uncoated wood free paper with 50% - 60% filler [20]. However, the process needs to be further optimized with respect to dewatering and printability because of the high ratio of microfines in the composite.

[2] A version of this chapter has been published: Sang, Y., McQuaid, M., Englezos, P. (2012). "Pre-flocculation of precipitated calcium carbonate filler by cationic starch for highly filled mechanical grade paper." BioResources, 7(1): 354-373

Cationic modification of fillers to increase filler loading in paper has also been considered, but the cationically modified filler tends to form agglomerates that result in sedimentation [136]. Moreover, paper made with such fillers may be prone to dusting.

Recently, a method for the PCC modification with coated starch gel was reported [25] . The results indicated that the PCC-filled sheet strength can be significantly improved when the filler surface is coated with starch.

Filler pre-flocculation prior to its addition to the paper stock has been studied in the past. Novak et al. [35] showed that pretreatment of filler with aluminum sulfate, cationic polyacrylamide (CPAM), anionic polyacrylamide (APAM), and/or cationic starch increased the filler content in paper without reducing paper strength. Park and Shin [36] showed that fillers that had been pre-flocculated with high molecular weight CPAM had the largest and strongest floc compared to low molecular weight CPAM and cationic starch but resulted in the poorest opacity.

Filler pre-flocculation may lead to larger aggregates, facilitate retention and, if properly manipulated, could improve paper formation and strength [34]. Palmer et al. [32] formed pre-flocculated filler composite by mixing filler particles with the raw starch granules. The paper produced with such pre-flocculated filler was much stronger than the conventional paper products with the same ash content. Mabee and Harvey [33] demonstrated that the filler pre-flocculation by starch could provide a significant increase in sheet filler content without loss in strength, optical properties, or runnability parameters. Moreover, filler pre-flocculation with starch was reported to be able to reduce linting and dusting problems [90]. A dual polymer system was also employed to

pre-flocculate the PCC, and it was found that the mechanical strength of the sheets increased significantly with larger flocs and higher median PCC floc size [37].

The mechanism to increase the strength of paper by the filler pre-flocculation has been attributed to the reduction of the surface area of filler and thus less disruption of fibre-fibre bonding from fillers. However, filler flocs formed through pre-flocculation with polymers tend to break down under high shear rate. The creation of shear-resistant filler flocs with narrow particle size distribution is perhaps the biggest challenge faced by the paper industry. The charge density and molecular weight of starch was found to play an important role on PCC filler flocculation kinetics and floc properties. With continuous advances in starch technology, high charge density (up to 0.90 to 1.10 percent nitrogen) and cross-linked starch have been introduced for the production of mechanical grade paper. Therefore, it is of interest to assess the performance of these most recently developed starches in the production of highly filled paper that uses mechanical pulp.

The objective of the present study was to evaluate the benefits from using three new starches for the pre-flocculation of the precipitated calcium carbonate filler in highly filled mechanical grade paper. A portion of starch was used for PCC pre-flocculation and the rest was added after the CPAM and prior to silica for strength compensation. It is also noted that the addition sequence of starch, CPAM, and silica was different from the conventional one that reported in Chapter 2 [67]. In order to optimize the chemical dosages, “laboratory trials” were carried out in which wood fibre suspensions and process water from a paper mill were utilized. A response surface statistical experimental design methodology (RSM) with a central composite design was used. An empirical process model was then constructed to predict the retention and drainage results based on the analysis of variance (ANOVA). In addition, handsheets were prepared and their ash

content, breaking length, and burst index were determined. The partition behavior of starch between fibre and fines was also studied.

3.2. Experimental

3.2.1. Materials

Peroxide-bleached TMP, process water, acid-tolerant PCC, CPAM, silica and potassium polyvinyl sulphate (PVSK) all are the same as those described in Section 2.2.1 of Chapter 2. X-Link 880 (Alias X880, 0.90-1.10% N, DS = 0.13, charge density = 1.08 meq/g), which has same charge as S880 but slightly "cross-linked" was used with the starch S858 and S880. Starch was cooked prior to use by following the procedure as described in Section 2.2.2 of Chapter 2.

3.2.2. Retention and drainage experiment

Retention and drainage experiments were performed using the DFR-04 device from BTG Americas Inc. (Pointe-Claire, QC, Canada), following the procedure in Fig. 3.1. The PCC was first pre-flocculated by the addition of 2 kg/t of 1.67 wt% cationic starch to a 26% PCC suspension at 50 ^{o}C in a glass beaker mixed at a speed of 550 rpm for 3 minutes. The pre-flocculated PCC was then added to the 1% consistency TMP pulp at 50 ^{o}C. The rest of the starch was added after the CPAM. It is noted that under the conventional papermaking practice, the starch is added first. The addition sequence for CPAM and silica is shown in Fig. 3.1. The experimental design was prepared by using JMP IN 4.0 (SAS Institute Inc., Cary, North Carolina) at five levels given in Table 3.1. The addition dosage of starch, CPAM, and silica was based on the oven-dried pulp. The design is shown in Table 3.2.

The following model was used for the prediction of the retention and drainage [67],

$$Y = \beta_0 + \sum_{i=1}^{n} \beta_i X_i + \sum_{i=1}^{n-1} \sum_{j=2, j\neq i}^{n} \beta_{ij} X_i X_j + \sum_{i=1}^{n} \beta_{ii} X_i^2 \qquad (3\text{-}1)$$

where n is the number of independent variables (n=4), X_i, (i=1, 2, …n) are the factors considered and β_o is the intercept. The coefficients β_i, β_{ij}, and β_{ii} represent the linear, interaction, and quadratic effects, respectively. This model was validated by comparing calculated values against experimental data from a set of independent conditions.

Table 3.1. Levels of the factors for experimental design

Factor	Components	Levels of factor studied				
		a (-2)	-1	0	+1	A (2)
X_1	PCC (%)	25	30	35	40	45
X_2	Starch (kg/t)	6	7	8	9	10
X_3	CPAM (kg/t)	0.1	0.2	0.3	0.4	0.5
X_4	Silica (kg/t)	0.2	0.3	0.4	0.5	0.6

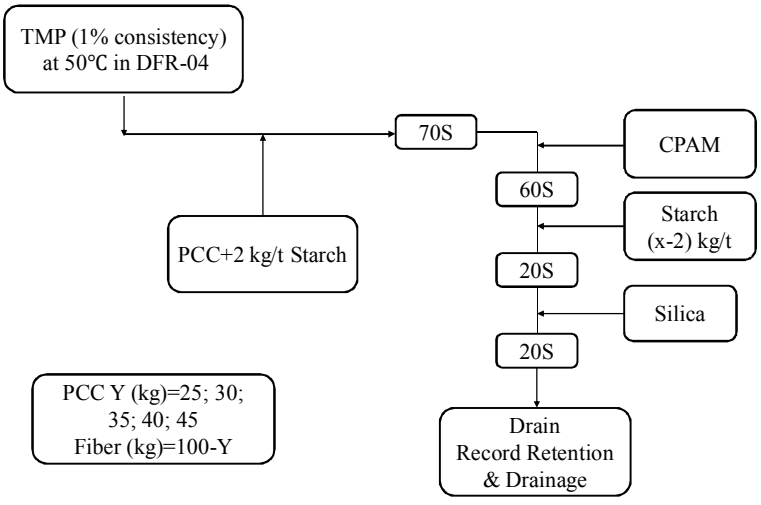

Fig. 3.1. Block flow diagram for experiments with PCC preflocculation

Table 3.2. Full experimental design for retention/drainage experiment

ID	Pattern	PCC (%)	Starch (kg/t)	CPAM (kg/t)	Silica (kg/t)
1	a000	25	8	0.3	0.4
2	----	30	7	0.2	0.3
3	---+	30	7	0.2	0.5
4	--+-	30	7	0.4	0.3
5	--++	30	7	0.4	0.5
6	-+--	30	9	0.2	0.3
7	-+-+	30	9	0.2	0.5
8	-++-	30	9	0.4	0.3
9	-+++	30	9	0.4	0.5
10	0a00	35	6	0.3	0.4
11	00a0	35	8	0.1	0.4
12	000a	35	8	0.3	0.2
13-1	0000	35	8	0.3	0.4
13-2	0000	35	8	0.3	0.4
13-3	0000	35	8	0.3	0.4
13-4	0000	35	8	0.3	0.4
13-5	0000	35	8	0.3	0.4
13-6	0000	35	8	0.3	0.4
14	000A	35	8	0.3	0.6
15	00A0	35	8	0.5	0.4
16	0A00	35	10	0.3	0.4
17	+---	40	7	0.2	0.3
18	+--+	40	7	0.2	0.5
19	+-+-	40	7	0.4	0.3
20	+-++	40	7	0.4	0.5
21	++--	40	9	0.2	0.3
22	++-+	40	9	0.2	0.5
23	+++-	40	9	0.4	0.3
24	++++	40	9	0.4	0.5
25	A000	45	8	0.3	0.4

3.2.3. Pulp separation for starch adsorption experiment

The Bauer-McNett classifier was used to separate the fibre and fibre fines following the procedure described in Section 2.2.5 of Chapter 2.

3.2.4. DTPA chelation stage

A DTPA chelation stage was performed to remove the metals present in the fibres as described in Section 2.2.6 of Chapter 2.

3.2.5. Starch partition between fibres and fines

The starch partition behavior between fibres and fines was studied by following the procedure as in Section 2.2.7 of Chapter 2.

3.2.6. Handsheet preparation and test

Procedure described in Section 2.2.8 of Chapter 2 was followed for the handsheet preparation and test.

3.3. Results and Discussion

A total of 30 experiments for each one of the three starches (S858, S880, X880) were conducted. In addition, another 30 experiments were also carried out to determine the corresponding drainage values for each starch. Figs. 3.2 to 3.4 show the retention and drainage results. As seen from the measurements, the S880 system gave the highest retention and drainage.

Not surprisingly, the maximum retention and drainage values were obtained at the highest dosages of starch, CPAM, and silica for all these three starches. Differences in the retention and drainage are likely influenced by the differences in floc size, floc compactness, and the interfloc voidage. The highest retention level and best drainage performance of S880 may be attributed to the larger and stronger flocs induced by this starch [137, 138]. Larger flocs are easier to be mechanically captured in the forming section. Stronger flocs can withstand the high shear force during the retention. More compact flocs are responsible for the better drainage of S880 system and this explanation is consistent with previous work [43, 104].

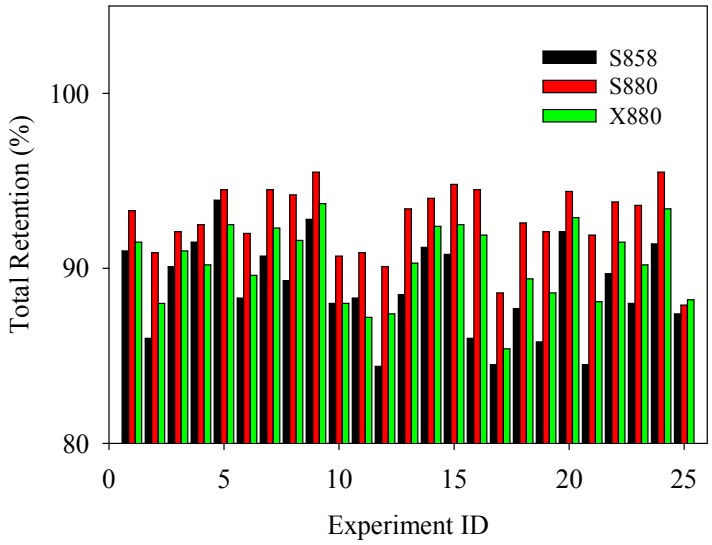

Fig. 3.2. Total retention for S858, S880 and X880 system

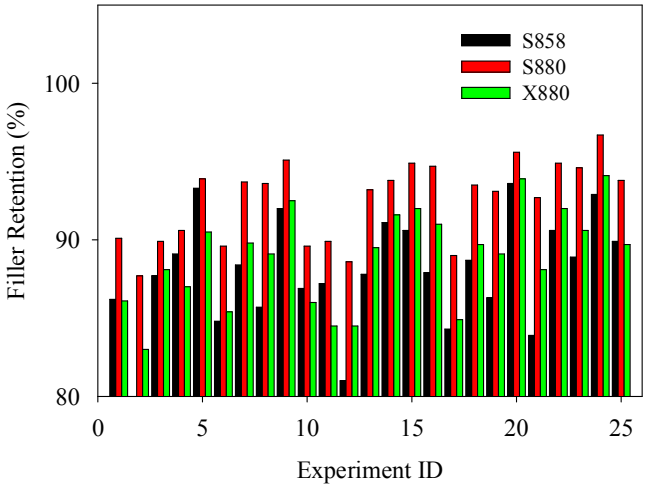

Fig. 3.3. Filler retention for S858, S880 and X880 system

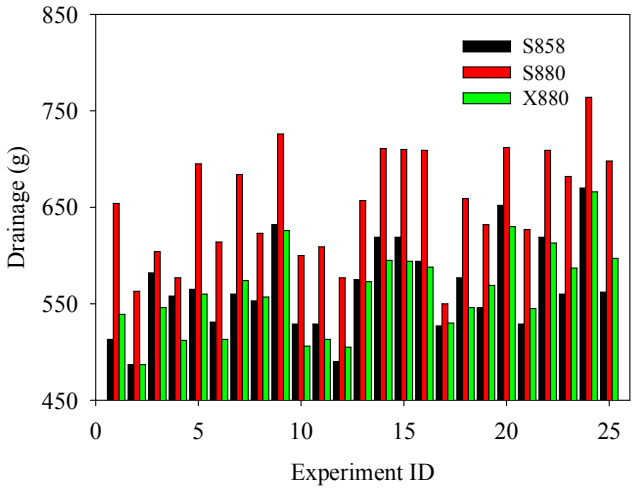

Fig. 3.4. Drainage for S858, S880 and X880 system

3.3.1. ANOVA for total retention

Table 3.3 (Refer to Appendix B for ANOVA details) shows the significant factors for total retention for the three systems using different charge density starches. All the main effect except for starch S858 was found to be extremely significant (ES) for total

retention. The interaction between PCC and silica was found to be significant for total retention only when the X880 starch was used.

The prediction profiles and the 95% confidence intervals for the predicted total retention are shown in Fig. 3.5. As seen, the PCC had a negative effect on the total retention for all the three retention systems. The slopes of the prediction curves for S880 and X880 were much greater than that of S858. This may be attributed to starch S880 and X880 having much higher charge densities than S858. More cationic charge was introduced and resulted in significant PCC flocculation that enhanced retention. S880 and X880 had similar slopes of the prediction curves probably because of the same charge density of these two starches. S880 and X880 improved the total retention through the entire dosage range. CPAM and silica played significant roles in total retention as seen from the steepness of the prediction curves. The CPAM and silica also improved the total retention throughout the entire dosage range for all the three retention systems.

Table 3.3. Significant factors for total retention

Factor	S858	S880	X880
PCC	ES	VS	ES
Starch	----	ES	ES
CPAM	ES	ES	ES
Silica	ES	ES	ES
PCC*Silica	----	----	S
PCC*PCC	----	VS	----

ES=extremely significant; VS=very significant; S=significant; ----: not significant

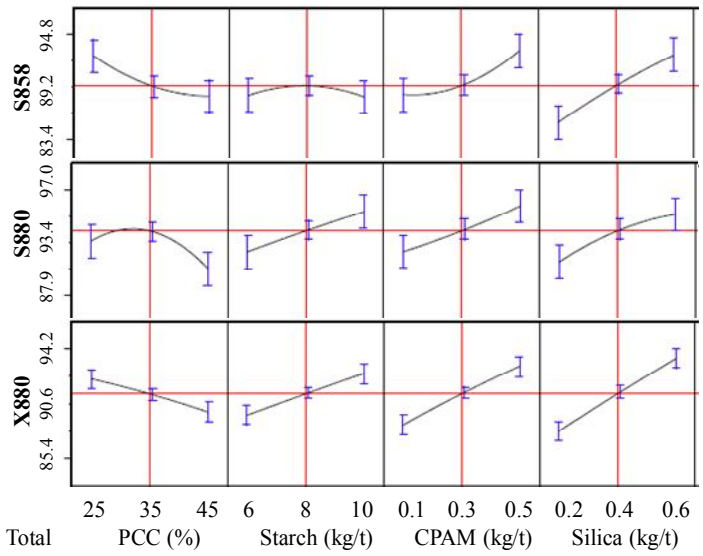

Fig. 3.5. Prediction profiles for total retention

3.3.2. ANOVA for filler retention

Table 3.4 (Refer to Appendix B for ANOVA details) shows the significant factors for filler retention for the three retention systems with different charge density starches. All the main effect was found to be extremely significant (ES) for filler retention with S880 and X880. The interaction between starch and CPAM was found to be significant (S) for filler retention only for the retention system using S880.

Fig. 3.6 shows the prediction profiles and the 95% confidence intervals for filler retention. As expected, the PCC had a positive effect on the filler retention for all the retention systems. The higher the loading level in the pulp suspension, the more filler would be retained in the final paper. As it was seen for total retention, the slopes of the prediction curves for S880 and X880 were much greater than that of S858 and correlate with the charge density of the starches. S880, X880, CPAM, and silica played significant

(S) role in filler retention as seen from the steepness of the prediction curves and improved filler retention.

Table 3.4. Significant factors for filler retention

Factor	S858	S880	X880
PCC	S	ES	ES
Starch	----	ES	ES
CPAM	ES	ES	ES
Silica	ES	ES	ES
Starch*CPAM	----	S	----
Silica*Silica	----	ES	----

ES=extremely significant; VS=very significant; S=significant; ----: not significant

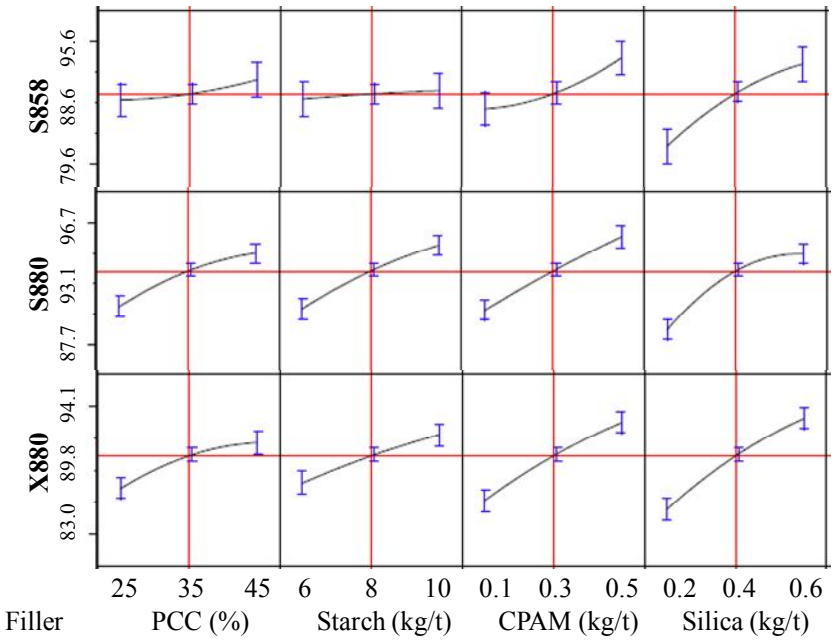

Fig. 3.6. Prediction profiles for filler retention

3.3.3. ANOVA for drainage

Table 3.5 (Refer to Appendix B for ANOVA details) shows the significant factors for drainage for the three retention systems using different charge density starches. All the main effect was found to be extremely significant for drainage. The interaction effect between PCC and silica was found to be significant when starch S858 was used. The interaction between starch and silica was found to be significant for drainage for the X880 starch.

Table 3.5. Significant factors for drainage

Factor	S858	S880	X880
PCC	ES	ES	ES
Starch	VS	ES	ES
CPAM	ES	ES	ES
Silica	ES	ES	ES
PCC*Silica	S	----	----
Starch*Silica	----	----	S
PCC*PCC	S	----	----
Starch*Starch	----	----	S

ES=extremely significant; VS=very significant; S=significant; ----: not significant

The prediction profiles and the 95% confidence intervals for the predicted drainage are shown in Fig. 3.7. The positive effect of increased PCC amount on the drainage is because the water is easier to be removed from the PCC than the fibre. All the three starches, the CPAM, and the silica played significant roles in drainage as seen from the steepness of the prediction curves and improved the drainage through the entire dosage range.

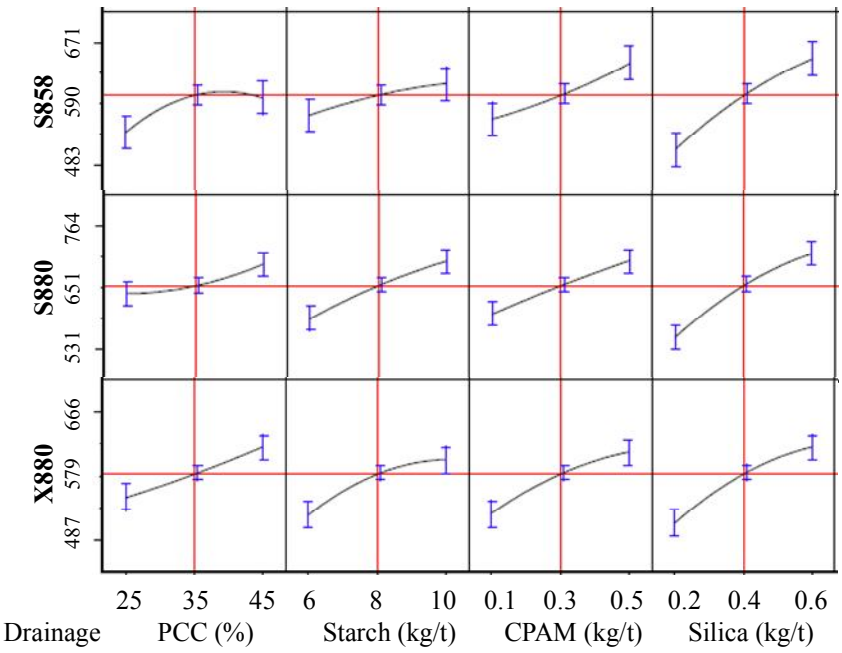

Fig. 3.7. Prediction profiles for drainage

3.3.4. Model construction and validation

The model equations are given in Table 3.6. The variables X_1, X_2, X_3 and X_4 are defined in Table 3.1. In order to evaluate the accuracy of regression model, six additional experiments were carried out to compare the results with model predictions. The experimental conditions are shown in Table 3.7. The data were found to be in very good agreement with the model predictions as seen in Fig. 3.8. The experiment IDs in Fig. 3.8 correspond to those in Table 3.7.

Table 3.6. Regression model for S858, S880 and X880 system

S858 Prediction Equation	
Total Retention	$Y_{858\ Total}=88.6-1.09X_1+1.18X_3+1.83X_4$
Filler Retention	$Y_{858\ Filler}=87.9+0.66X_1+1.66X_3+2.70X_4$
Drainage	$Y_{858\ Drainage}=577+12.9X_1+12.1X_2+21.0X_3+34.3X_4+9.13X_1X_4-7.52X_1^2$
S880 Prediction Equation	
Total Retention	$Y_{880\ Total}=93.4-0.60X_1+0.87X_2+0.99X_3+1.04X_4-0.52X_1^2$
Filler Retention	$Y_{880\ Filler}=93.2+0.98X_1+1.16X_2+1.35X_3+1.39X_4-0.26X_2X_3-0.38X_4^2$
Drainage	$Y_{880\ Drainage}=658+14.0X_1+27.3X_2+25.1X_3+39.7X_4$
X880 Prediction Equation	
Total Retention	$Y_{X880\ Total}=90.4-0.67X_1+0.84X_2+1.18X_3+1.46X_4+0.30X_1X_4$
Filler Retention	$Y_{X880\ Filler}=89.5+1.01X_1+1.06X_2+1.70X_3+1.98X_4$
Drainage	$Y_{X880\ Drainage}=573+17.8X_1+19.4X_2+21.5X_3+26.7X_4+5.81X_2X_4-4.55X_2^2$

Table 3.7. Experimental conditions for model validation

Expt ID	Pattern	PCC (%)	Starch (kg/t)	CPAM (kg/t)	Silica (kg/t)
1	-0++	30	10	0.4	0.5
2	-+0+	30	11	0.3	0.5
3	00++	35	10	0.4	0.5
4	0+0+	35	11	0.3	0.5
5	+0++	40	10	0.4	0.5
6	++0+	40	11	0.3	0.5

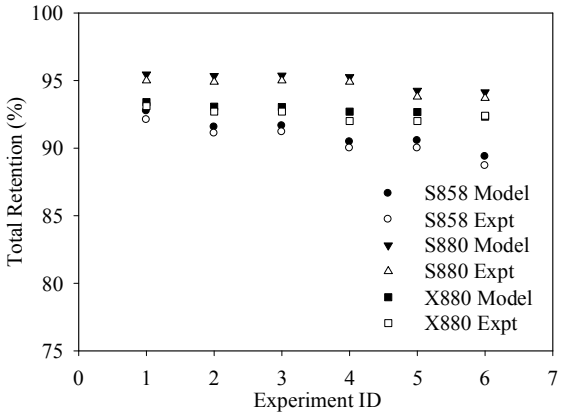

(a)

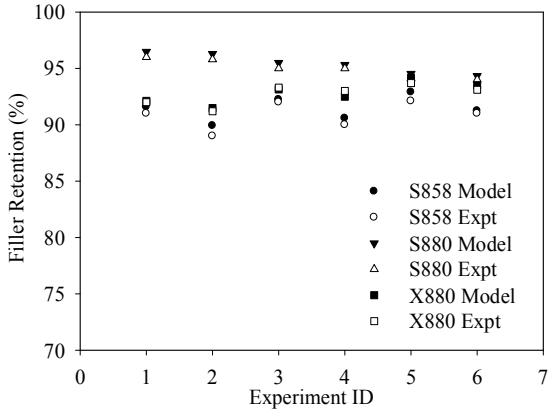

(b)

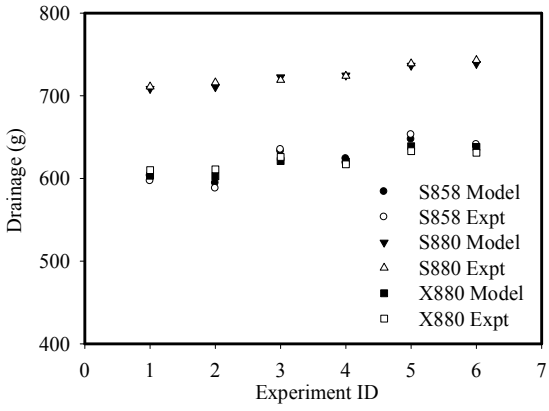

(c)

Fig. 3.8. Experimental and predicted values (a) total retention, (b) filler retention, (c) drainage

3.3.5. Comparison of retention and drainage at different starch addition strategies

The retention and drainage results for PCC pre-flocculation (this study) were compared with those obtained from the authors' previous investigation with the conventional chemical addition sequence shown in Chapter 2 [67]. As seen from the Fig. 3.9, the S858 retention system did not benefit from PCC pre-flocculation strategy. On the other hand, the high charge density starch S880 system with filler pre-flocculation gave higher total/filler retention and comparable drainage results compared to the conventional starch addition sequence as seen from Fig. 3.10. Thus, the PCC pre-flocculation by higher charge density starch may offer the opportunity to further enhance the retention, and this is due to the fact that the higher charge density starch produces larger, stronger and more compact flocs.

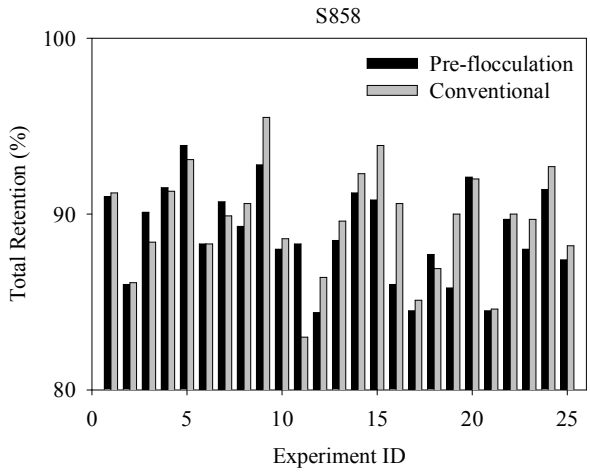

(a)

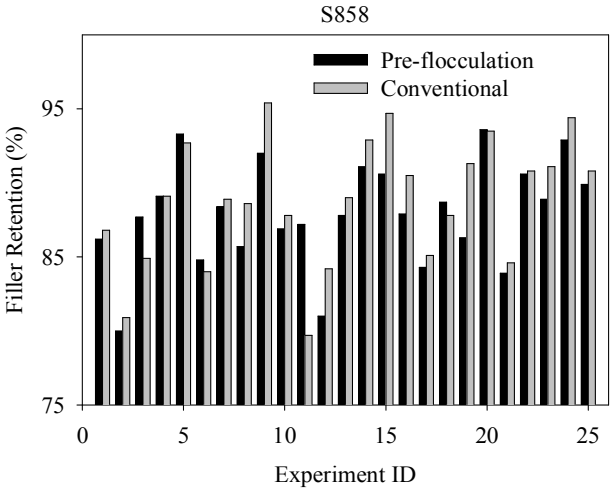

(b)

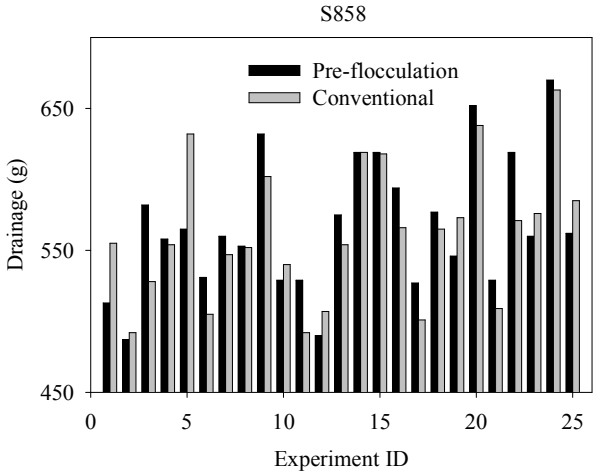

(c)

Fig. 3.9. (a) Total retention, (b) filler retention and (c) drainage at different chemical addition strategies with S858

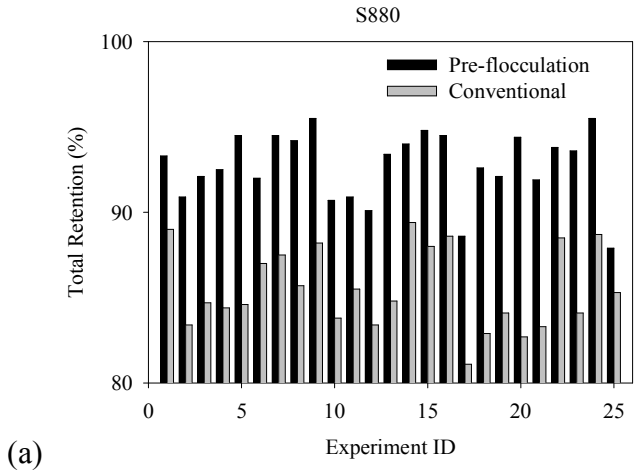

(a)

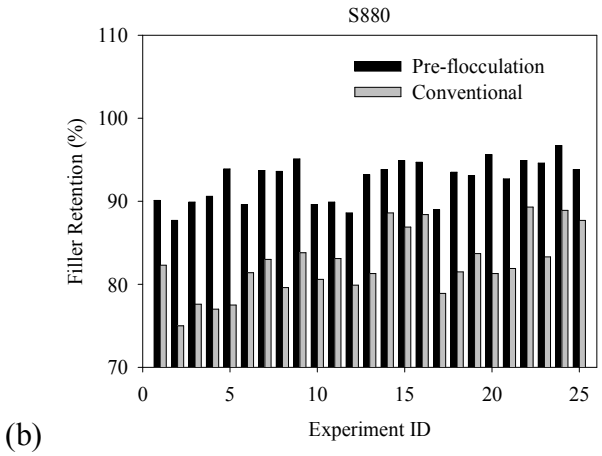

(b)

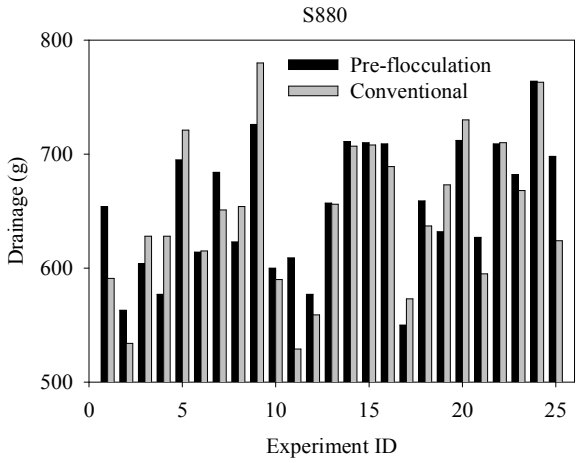

(c)

Fig. 3.10. (a) Total retention, (b) filler retention and (c) drainage at different chemical addition strategies for S880 system

3.3.6. Starch adsorption and partition

The results for starch adsorption on washed hydrogen peroxide bleached pulp show that S880 gave the highest adsorption amount (29.6 mg/g fibre) on fibre surface, S858 had the lowest adsorption amount (6.5 mg/g fibre). S880 (29.6 mg/g fibre) and X880 (26.0 mg/g fibre) had similar adsorption amount on fibre. The much higher adsorption amount of S880 and X880 than S858 on the pulp surface may most likely be attributed to the interaction of cationic groups with the hydroxyl groups of the fibre surface, which is stronger for the higher charge density starch. Fig. 3.11 shows how starch partitions between fibre and fines. The adsorbed amount of the three starches was found to increase linearly with the increase of the fines ratio in the pulp. This is due to the higher surface area of fines than that of fibre. Hydrodynamic specific surface area of the mechanical pulp fiber is 1.12 ± 0.15 m^2/g whereas for mechanical pulp fine is 23.20 ± 0.63 m^2/g. That means the fiber fines have 21 times as much surface area per unit mass, compared to the fibers. As shown in Fig. 3.11, the starch adsorption amount on fibers is 4 mg/g and on fines is 89 mg/g. The ratio is 22 which is comparable to the surface area ratio of fines to fibers.

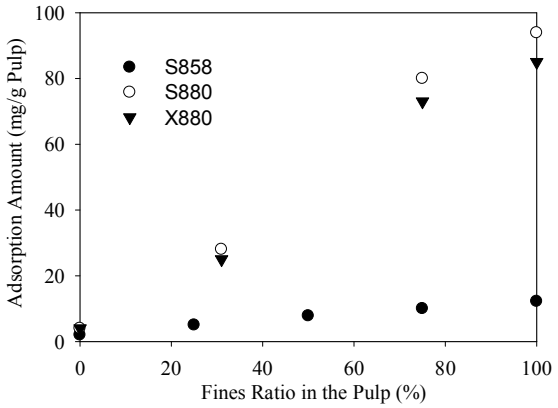

Fig. 3.11. Starch partition on fibre and fines

Fig. 3.12 shows the pulp zeta potential after starch addition. As seen, the higher the starch charge density, the less negative the pulp zeta potential, indicating more charge was introduced to the pulp suspension. As expected, S880 and X880 resulted in similar pulp zeta potential since they have similar charge densities.

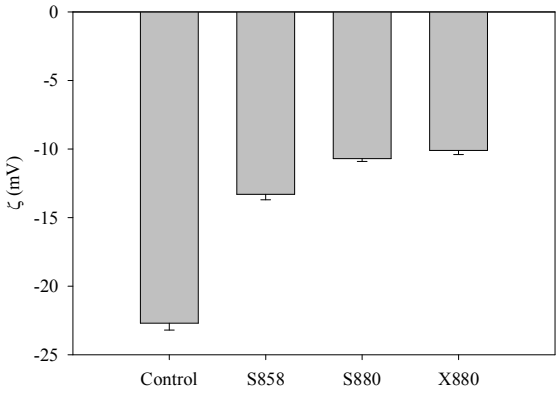

Fig. 3.12. Pulp zeta potential after starch adsorption

3.3.7. Paper ash content and physical properties

The ash content, breaking length, and burst indices of the handsheets are shown in Figs. 3.13 and 3.14. The sample IDs in Figs. 3.13 and 3.14 correspond to those in Table 3.2. With the use of the retention chemicals, the ash content of the handsheet could be raised to 40% with the S858 and S880 retention systems. The S880 resulted in higher breaking length and burst indices. This is because when fillers are preflocculated by S880, larger and fewer particles entities were induced compared to the S858 system. Larger and fewer aggregates do not interfere with the fibre-fibre bonding to the same extent as the non-flocculated filler does and thus paper strength is preserved. Also, S880 had a much higher affinity to fibres and fines than S858, as shown in Fig. 3.11. The high starch affinity with fibres promotes fibre-fibre bonding [93] and thus favors paper strength.

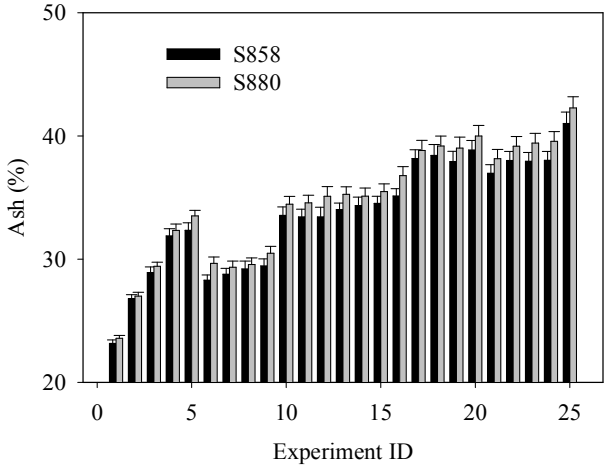

Fig. 3.13. Ash content of the handsheet made from S858 and S880 system

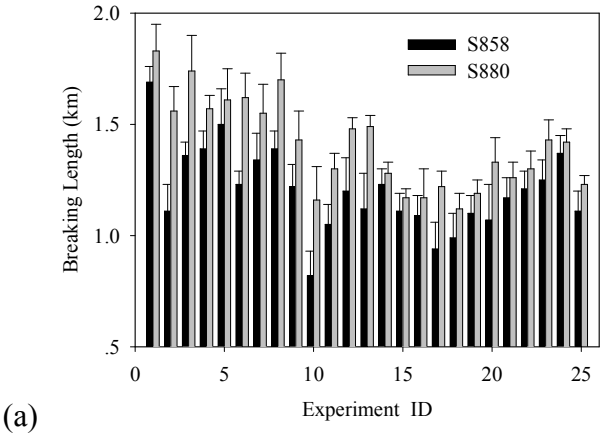

(a)

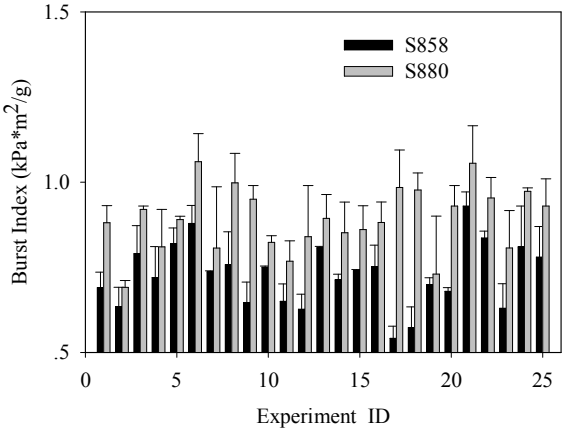

(b)

Fig. 3.14. Comparison of (a) breaking length (b) burst index of S858 and S880 system

It is important to point out that compared to the conventional starch addition strategy [67], filler preflocculated by starch resulted in improved paper physical properties no matter what kind of starch was used.

3.4. Conclusions

Statistically designed laboratory trials were carried out in order to evaluate the use of three commercial cationic starches along with precipitated calcium carbonate (PCC) filler in mechanical papermaking. The filler was pre-flocculated by a portion of the starch (2kg starch/t PCC). The retention program with the linear high charge cationic starch S880 with a molecular mass of 3 million Da resulted in highest retention and best drainage. Empirical models constructed in this work can predict the retention and drainage under various conditions. Same charge density cationic starch S880 (linear) and X880 (cross-linked) had similar adsorption amount on pulp and are much higher than the low charge cationic starch S858. The linear high charge cationic starch S880 retention system resulted in higher breaking length and burst indices, possibly because it has a higher affinity to fibres and fines than low charge cationic starch S858. Filler pre-flocculation by starch resulted in higher breaking length and burst indices compared to the conventional chemical addition sequence for both high charge and low charge cationic starches.

Chapter 4 Flocculation of Precipitated Calcium Carbonate (PCC) by Cationic Tapioca Starch with Different Charge Densities. I: Experimental[3]

Given the importance of PCC filler flocculation with starch, in this chapter the results from a set of statistically designed PCC flocculation experiments are presented along with relevant electrokinetic and starch adsorption measurements. The relationship among starch properties, process conditions and floc properties is discussed.

4.1. Introduction

The pre-flocculation of precipitated calcium carbonate (PCC) before adding it to a wood fibre suspension in the papermaking process improves the retention of the PCC and thus contribute towards manufacturing highly filled paper. Highly filled paper is a more profitable and more sustainable papermaking practice [34, 36, 105]. The PCC floc size and its structure and strength are important process parameters. Gaudreault et al. [101] employed static light scattering/diffraction, photometric dispersion analysis and microscopy imaging to study the structure and strength of PCC flocs formed by four polymers including cationic potato starch. Cationic potato starch was found to flocculate PCC fast and create PCC aggregates with size less sensitive to dosage at dosages less than 0.5 mg/g of PCC. Particles size equals to 18 microns was reached at a starch dosage of 7 mg/g. Modgi et al. [139] reported that the adsorption of a potato starch with a degree of substitution (DS) of 0.034 on PCC was greater than that of a potato starch with DS=0.1.

[3] A version of this chapter has been published online: Sang, Y., Englezos, P. (2012). "Flocculation of Precipitated Calcium Carbonate (PCC) by Cationic Tapioca Starch with Different Charge Densities. I: Experimental." Colloids and Surfaces A: Physicochemical and Engineering Aspects. DOI: 10.1016/j.colsurfa.2012.07.019

The investigation of PCC flocculation induced by a series of cationic polyacrylamide in distilled water shows that high charge density cationic polyacrylamide yielded stronger flocs which can be resistant to the higher shear [140]. The addition of inorganic salts to the flocculation system may improve the flocculation efficiency at low concentrations while higher concentrations (> 0.01 mol/L) impair the flocculation process [141]. Liimatainen et al. [104] found the stronger and denser fibre flocs improve the dewaterability of pulp suspension as the stronger flocs increased the ability of filter cake to resist compression and pore collapse and therefore reduced the sealing of the fluid passageways. Hubbe [43] stated that the process of compact structure formation could expel water from flocs which facilitates drainage.

Mineral filler flocs formed through pre-flocculation with polymers tend to break down under high shear rate. Thus, to understand the process conditions on the flocculation kinetics and flocs properties with an aim to produce shear resistant and compact filler flocs is a considerable engineering challenge in the practice of papermaking. Meanwhile, in order to minimize the yellowing of wood fibres in conventional groundwood papermaking, the PCC is usually subjected to acid-tolerant treatment using polyacrylate which not only renders the PCC surface negatively charged but also make PCC pre-flocculation even more complicated. Our previous work demonstrated that the pre-flocculation of PCC by high charge density cationic tapioca starch improved retention and drainage compared to the low charge cationic tapioca starch [105]. One might assume that larger, stronger and more compact flocs were formed by the high charge cationic tapioca starch but direct evidence is difficult to obtain, especially for the floc structure and its evolution with time.

The aim of the present research is to study the evolution of the PCC floc size and structure induced by the addition of starches with different charge densities. The floc structure is observed through the mass fractal dimension. The adsorption isotherm of starch on PCC

was also determined to provide information on the degree of surface coverage which affects the flocculation efficiency of the PCC dispersion.

4.2. Materials and Methods

4.2.1. Materials

Cationic tapioca starches S858 and S880 were used for PCC flocculation. The background electrolyte was analytical grade NaCl. The informaiton for the S858, S880 and PCC can be found in section 2.2.1 of Chapter 2.

4.2.2. Flocculation

The apparatus used for this study has been described in detail by Pang and Englezos [142]. Briefly, flocculation experiments were conducted in a 600 mL water-jacket plexiglass vessel in which water from a water bath flows through the water-jacket of the vessel to maintain a constant temperature. During the experiment, 1.63 g 18.45 wt% PCC (dry PCC = 0.30 g) was added to 600 mL water to get 0.05 wt% PCC suspension. The 0.05 wt% PCC suspension was continuously circulated through a 4 mm inner diameter plastic tube to the Mastersizer 2000 (Malvern Instruments Inc, Malvern, UK) for volume median diameter $d_{4,3}$ on-line analysis by small angle static light scattering (SASLS). The flow rate of the suspension from the vessel to the particle size analyzer was maintained at 100 mL/min with a peristaltic pump. In order to reduce the pump stress on the flocs, the pump was placed downstream of the Mastersizer 2000 [108].

Response surface methodology involving the central composite design was used to design the experiments by JMP IN 4.0 (SAS institute Inc., Cary, NC). The total number of

experiments was $2^n + 2n + n_0$, where n (n=4) is the number of independent variables and n_0 (n_0=6) is the number of repetition of experiments at the central point. Each factor was studied at five different levels (a, -1, 0, +1, A) as shown in Table 4.1. Analysis of variance (ANOVA) was performed to evaluate the effects of the factors. The shear rate *G* is calculated by an iterative procedure that is described in the next section. Shear rate for various components of paper machine are typically ranging from 200 s^{-1} to 4000 s^{-1} [143]. The experimental design is shown in Table 4.2.

Table 4.1. Experimental levels of the independent factors

	Factor	Levels of factor studied				
		a (-2)	-1	0	+1	A (2)
x_1	Temperature, T (ºC)	30	40	50	60	70
x_2	NaCl (mN)	0	10	20	30	40
x_3	Shear rate, *G* (s^{-1})	300	400	500	600	700
x_4	Starch dosage (mg/g)	10	20	30	40	50

4.2.3. Shear rate *G* (s^{-1})

The shear rate of the system is calculated using Eq. (4-1) [144, 145]:

$$G = \sqrt{\frac{\varepsilon}{\nu}} \qquad (4\text{-}1)$$

where ν (m^2/s) is the kinematic viscosity of water and ε (m^2/s^3) is the average energy dissipation rate per unit mass which was calculated as follows [146]:

$$\varepsilon = \frac{P}{\rho V} \qquad (4\text{-}2)$$

where V (m^3) is the volume of the vessel, and P (watts) is the power consumption. Compared to the large volume (600 mL) of water, the amount of starch added for PCC

flocculation (3 mg for 10 mg/g PCC, 6 mg for 20 mg/g PCC, 9 mg for 30 mg/g PCC, 12 mg for 40 mg/g PCC, 15 mg for 50 mg/g PCC) did not significantly affect the solution density and viscosity. Thus, the density ρ (kg/m^3) and the dynamic viscosity μ (N s/m^2) of the medium were assumed to be those of water.

Table 4.2. Experimental design for the flocculation experiment

ID	Pattern	T (℃)	NaCl (mN)	G (s^{-1})	Starch (mg/g)
1	a000	30	20	500	30
2	----	40	10	400	20
3	---+	40	10	400	40
4	--+-	40	10	600	20
5	--++	40	10	600	40
6	-+--	40	30	400	20
7	-+-+	40	30	400	40
8	-++-	40	30	600	20
9	-+++	40	30	600	40
10	0a00	50	0	500	30
11	00a0	50	20	300	30
12	000a	50	20	500	10
13	0000	50	20	500	30
14	000A	50	20	500	50
15	00A0	50	20	700	30
16	0A00	50	40	500	30
17	+---	60	10	400	20
18	+--+	60	10	400	40
19	+-+-	60	10	600	20
20	+-++	60	10	600	40
21	++--	60	30	400	20
22	++-+	60	30	400	40
23	+++-	60	30	600	20
24	++++	60	30	600	40
25	A000	70	20	500	30

Eq. (4-3) was used to calculate the power consumption *P*.

$$P = N_P \rho \omega^3 D_s^5 \qquad (4\text{-}3)$$

where D_S (m) is the diameter of the stirrer, N_P is the power number at the corresponding N_{Reynolds} (obtained from the power number versus N_{Reynolds} chart) [147].

Eq. (4-4) was used to calculate the Reynolds number.

$$N_{\text{Re}ynolds} = \frac{\omega D_S^2 \rho}{\mu} \qquad (4\text{-}4)$$

where ω (rad/s) is the rotation speed.

As seen in Table 4.1, factor x_3 is the shear rate *G*. The desired shear rate *G* is set through the setting of the stirrer rotation speed ω at a certain level. When the calculated value of *G* converges to the desired value, the iteration stops. If not, then a new value for ω is assumed and the calculations are repeated.

4.2.4. Mass fractal dimension

The mass fractal dimension (MFD) of flocs was calculated based on the scattered light density obtained from the Malvern Mastersizer 2000 [148]. In the static light scattering experiment, a beam of light is directed onto a sample and the scattered light intensity is measured as a function of the magnitude of the scattering vector Q given by Eq. (4-5):

$$Q = \frac{\pi n \sin(\theta / 2)}{\lambda} \qquad (4\text{-}5)$$

where *n* is the refractive index of the fluid, λ is the wavelength in vacuum of the laser light used, and θ is the scattering angle. The mass fractal dimension was obtained from the

negative slope of the linear region of the log-log plot of scattered light intensity I(q) versus scattering vector Q [149].

4.2.5. Adsorption of starch on PCC

The adsorption of starch on PCC was determined at various shear rates, electrolyte concentrations, temperatures and starch dosages. The experimental setup consists of a 800 mL batch reactor, equipped with a variable speed agitator and a water bath. The PCC suspension was mixed for a few minutes before adding the starch into the reactor. The setup consists of 0.30 g PCC in 600 mL water resulting in 0.05 wt% PCC suspension. Distilled deionized water was used in all experiments except for the study of the electrolyte effect. Five minutes after the starch addition to the PCC suspension, a sample of about 30 mL PCC dispersion was taken and subjected to centrifuge at 5000 rpm for 15 minutes. After centrifugation, the supernatant was used to detect unadsorbed starch by colloidal back titration with PVSK solution. For this purpose the particle charge detector (PCD, Mütek, Herrsching, Germany) was used [130]. The blank experiment (no PCC) was also carried out following the above procedure. The starch adsorption amount A in mg/g was calculated with Eq. (4-6),

$$A = \frac{(V_B - V_S)}{V_B} \times \frac{M_s}{M_{PCC}} \qquad (4\text{-}6)$$

where V_B is the PVSK volume consumed for the blank sample, V_S is the PVSK volume consumed for the adsorption sample, M_{PCC} is the mass of dry PCC, and M_S is the mass of starch added to the PCC suspension.

4.2.6. PCC surface zeta potential

One minute after the starch addition to the PCC suspension, the PCC suspension was subjected to zeta potential measurements using the Malvern Zetasizer (Malvern Instruments, UK) following the standard procedure. The contact time between PCC and starch has a significant impact on zeta potential and thus this effect is also evaluated.

4.3. Results and Discussion

4.3.1. Floc size and structure

The steady state floc size and mass fractal dimension (correlates with floc structure) under various experimental conditions are shown in Figs. 4.1 and 4.2, respectively. The experiment IDs in Figs. 4.1 and 4.2 correspond to those in Table 4.2. As seen the high charge density starch S880 resulted in larger and more compact (larger mass fractal dimension) flocs. This is because the bridges between PCC particles formed with the S880 are stronger. The high charge density starch S880 can also bring the PCC particles even closer and induce more compact flocs [85].

4.3.2. Evolution of floc size and structure

Fig. 4.3 (Refer to Appendix D for the rest of the flocculation kinetics, Appendix E and Appendix F for particle size distribution at condition “a000”) shows a typical flocculation kinetics induced by both starches. The PCC floc size quickly reaches a maximum value and then decays to a steady state. The maximum size is about 210 microns and 125 microns for S880 and S858, respectively. Initially, PCC floc growth is dominant and the size quickly reaches a maximum value. Subsequently, the size decays to a steady state

due to floc breakage and restructure under shear. Also, The initial flocculation rate is higher for S880. Interestingly, the rate of decay after 2 minutes is approximately equal for the two starch systems.

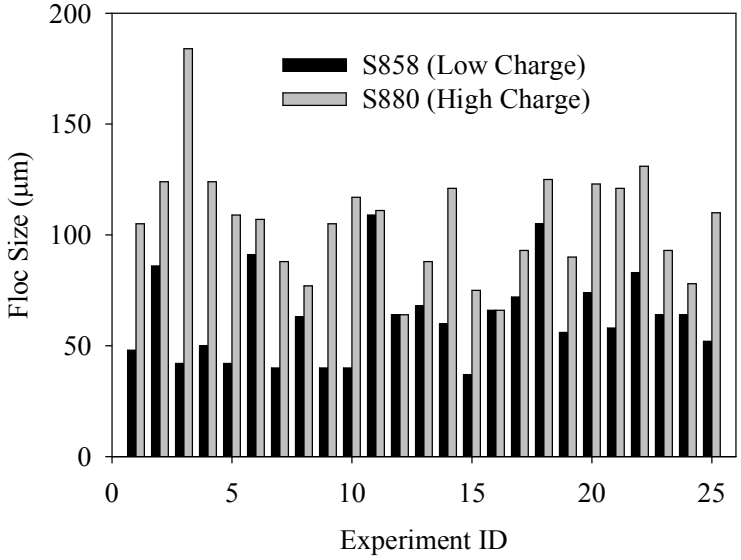

Fig. 4.1. Steady state floc size induced by S858 and S880 flocculation system

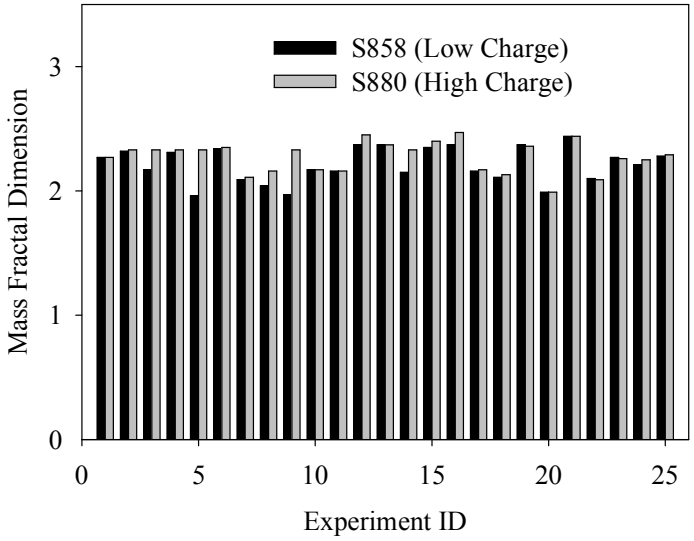

Fig. 4.2. Steady state mass fractal dimension induced by S858 and S880 flocculation system

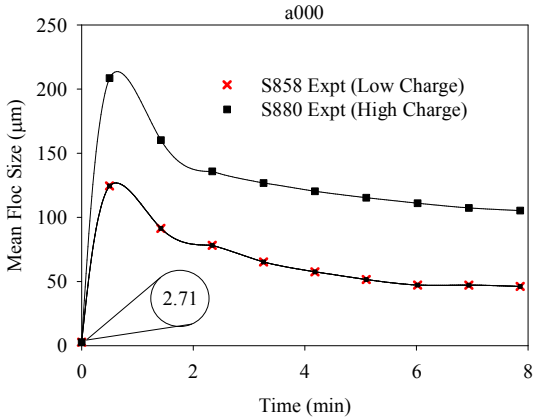

Fig. 4.3. Flocculation kinetics induced by S858 and S880. Experimental conditions: T = 30 ^{o}C; NaCl = 20 mN; Shear rate = 500 s^{-1}; Starch = 30 mg/g; Surface coverage θ = 0.68 for S858; Surface coverage θ = 0.44 for S880

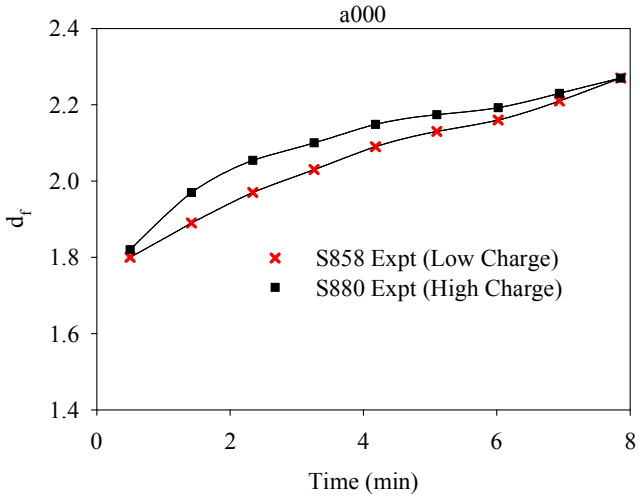

Fig. 4.4. Mass fractal dimension evolution of flocs induced S858 and S880. Experimental conditions: T = 30 ^{o}C; NaCl = 20 mN; Shear rate = 500 s^{-1}; Starch = 30 mg/g; Surface coverage θ = 0.68 for S858; Surface coverage θ = 0.44 for S880

As seen in Fig. 4.4 (Refer to Appendix G for the rest of the mass fractal dimension evolution), the mass fractal dimension of flocs increases steadily during the flocculation process indicating progressive formation of more compact flocs. It is possible that as the flocculation proceeds, fluid shear stresses break the PCC particle-starch bonds and as a

result the efficiency of subsequent collisions is reduced [150]. A reduction in the collision efficiency produces more compact, smaller flocs compared to the flocs formed at higher collision efficiency [151, 152]. As seen from Figs. 4.3 and 4.4, the mass fractal dimension continues increasing as the floc size reaches steady state. Shear-induced flocculation without restructuring produces flocs with a mass fractal dimension of 1.8 [153]. The mass fractal dimension shift from 1.8 to the higher value of 2.3 that was observed in this work is possibly due to shear-induced intensive restructuring.

4.3.3. Analysis of variance

The significant factors and interaction among factors based on the analysis of variance (ANOVA) are presented in Table 4.3 (Refer to Appendix C for ANOVA details). Based on the ANOVA, steady state models for floc size and mass fractal dimension are constructed and shown in Table 4.4.

Table 4.3. Significant factors for the flocculation induced by starch

Factor	Floc size		Mass Fractal Dimension	
	S858	S880	S858	S880
NaCl	---	VS	---	---
Shear Rate	ES	VS	---	---
Starch	---	VS	VS	S
T*NaCl	---	S	---	---
T*Starch	VS	---	---	---
T*T	---	S	---	---

ES=extremely significant; VS=very significant; S=significant; ----: not significant

Table 4.4. Steady state floc size and mass fractal dimension prediction model

	S858 Flocculation System	S880 Flocculation System
Floc Size	$d_{4,3-S858} = 67.7 - 11.1x_3 + 12.7x_1x_4$	$d_{4,3-S880} = 88.4 - 11.4x_2 - 10.3x_3 + 9.4x_4 + 9.8x_1x_2 + 7.3x_1^2$
Mass Fractal Dimension	$d_{f-S858} = 2.37 - 0.09x_4$	$d_{f-S880} = 2.37 - 0.05x_4$

Note: x_1, x_2, x_3 and x_4 correspond to temperature, NaCl concentration, shear rate and starch dosage, respectively.

As seen from Table 4.3, the floc size depends on shear rate and the interaction of temperature with the starch dosage for S858. On the other hand, more factors are influential when the high charge density starch S880 is used. In both cases the mass fractal dimension and consequently the compactness of the flocs is influenced by the starch dosage only. The prediction profiles in Figs. 4.5 and 4.6 show the effect (or lack of the effect) of each individual factor.

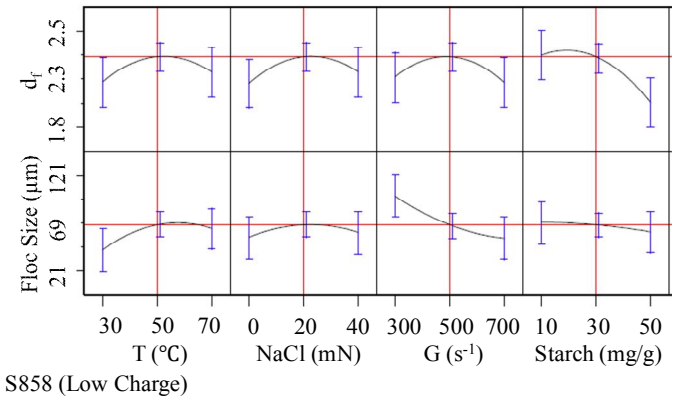

Fig. 4.5. Prediction profiles for S858 flocculation system

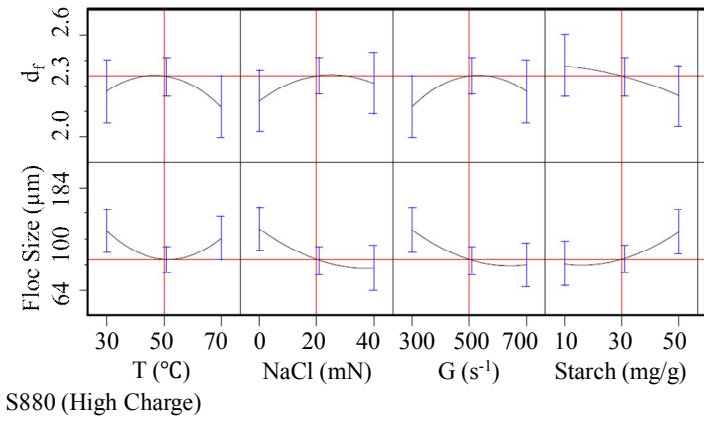

Fig. 4.6. Prediction profiles for S880 flocculation system

As seen from Fig. 4.6, the higher the NaCl concentration, the smaller the floc size for the high charge starch S880 flocculation system. As it will be seen later, the NaCl addition lowers the starch adsorption amount on PCC for both starches and the effect is more pronounced with S880. It is conceivable that Na ions interact with negative sites on PCC, which would otherwise interact with starch [154]. Thus, starch displacement occurs as a result of NaCl addition.

As seen from Table 4.3, the shear rate was found to have extremely significant effect on floc size for the S858 system and very significant effect for the S880 system, respectively. It is also seen from the prediction profiles in Figs. 4.5 and 4.6 that the larger the shear rate, the smaller the floc size for both systems. As the shear rate increases, the collision frequency between particles increases. On the other hand, as it will be shown later in Fig. 4.10, with the increase of the shear rate, less starch was adsorbed and more bridges may be broken. The effect is more pronounced for S858. The bridging between PCC particles is thus reduced and results in smaller floc size. As seen from Fig. 4.5, the increase of starch S858 dosage from 10 mg/g to 50 mg/g PCC did not increase the floc size further. Whereas

for S880, the floc size increased steadily for the dosage range investigated as shown in Fig. 4.6. The different effects observed may be explained by the different surface coverage as the bridging efficiency E is a function of surface coverage which can be calculated by Eq. (4-7) [155, 156]:

$$E = 2\theta(1-\theta) \qquad (4\text{-}7)$$

where θ is the degree of surface coverage of PCC surfaces by starch (see Table 4.5).

Table 4.5. PCC surface coverage and bridging efficiency by S858 and S880

Starch Dosage (mg/g PCC)	S858			S880		
	Adsorption amount Γ (mg/g PCC)	θ	E	Adsorption amount Γ (mg/g PCC)	θ	E
10	7	0.32	0.44	5	0.34	0.45
20	12	0.55	0.50	6	0.41	0.48
30	15	0.68	0.44	6.5	0.44	0.49
40	16.5	0.75	0.38	7.3	0.50	0.50
50	18	0.82	0.30	8	0.54	0.50

Note: $\Gamma_{max\ S858}$=22.0 mg/g PCC, $\Gamma_{max\ S880}$=14.7 mg/g PCC, $\theta=\Gamma/\Gamma_{max}$

As seen from Table 4.5, upon S858 adsorption on PCC, the surface coverage increased from 32% to 82% and the bridging efficiency decreased. PCC surface coverage beyond 50% may have prevented further aggregation [96]. On the other hand, with the increase of starch S880 dosage, the PCC surface coverage increased to 54% and the bridging efficiency increased to 0.50. Finally, it is noted that the increase of shear rate did not affect the floc structure. This means even the lowest shear rate can break the flocs and result in comparable steady state mass fractal dimension under investigated different shear rates.

4.3.4. Starch adsorption on PCC

Fig. 4.7 shows the adsorption isotherms of the two cationic tapioca starches on the negatively charged PCC in the absence of electrolyte. The maximum adsorption amount for S858 was about 22.0 mg/g PCC whereas for S880 the value was about 14.7 mg/g PCC. Thus, the maximum adsorption amount for S858 and S880 is roughly inversely proportional to their degree of substitution. Modgi et al. [139] also reported a greater amount of adsorption for a lower DS (DS = 0.034) potato starch compared to that of a potato starch with DS equals to 0.1 on PCC. The observed amount for S858 is in the same range as the values obtained by Modgi et al. [139] for the potato starch with DS of 0.1 and a tapioca starch with DS of 0.1. Gaudreault et al. [96] reported a maximum adsorption of 7 mg of potato starch per gram of PCC.

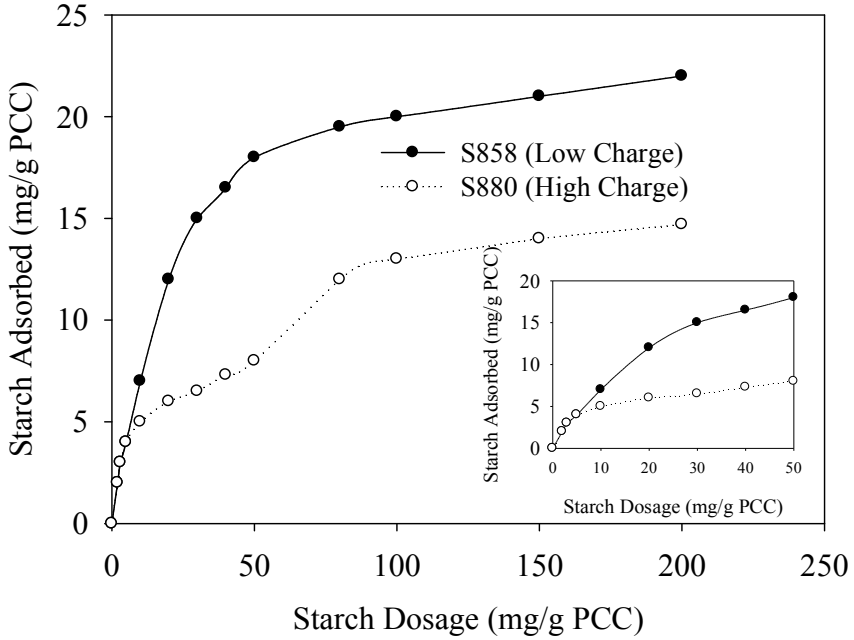

Fig. 4.7. Adsorption isotherm of S858 and S880 on PCC surface. Experiment conditions: T=50 ^{o}C; Shear rate = 300 s^{-1}; No electrolyte added

In order to clarify the effects of temperature, ionic strength, shear rate and starch dosage on PCC flocculation, the adsorption of starch on PCC surface was investigated in terms of these factors. Fig. 4.8 shows that the adsorption capacities for both starches increase with increasing temperature, suggesting that the adsorption is endothermic in nature.

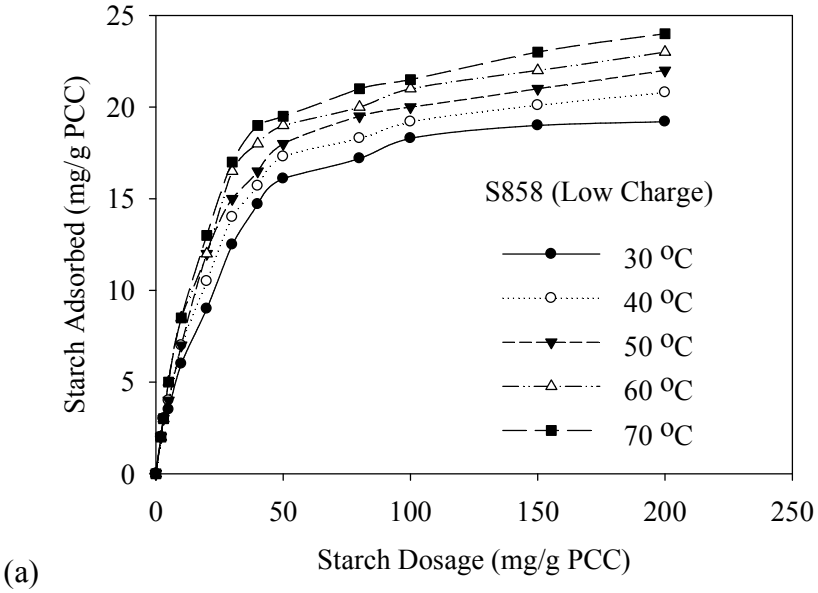

(a)

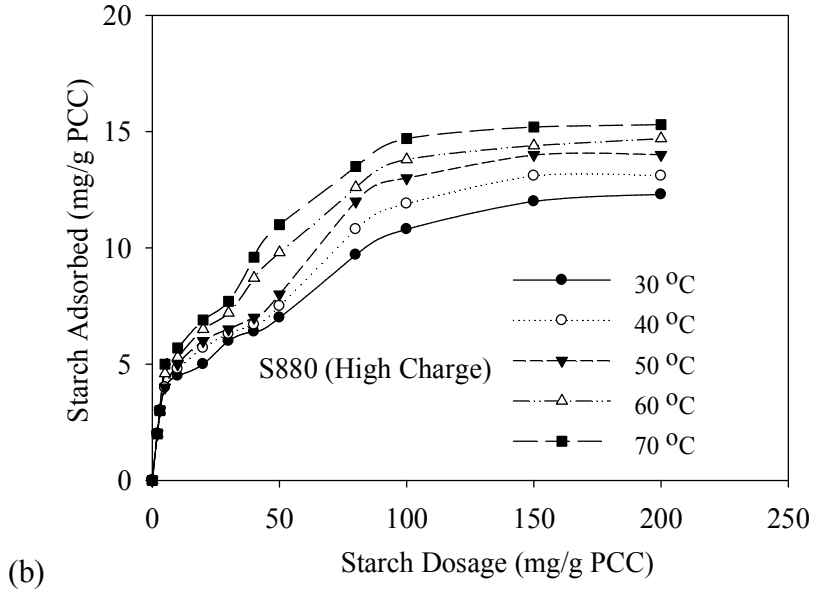

(b)

Fig. 4.8. Adsorption isotherm of (a) S858 and (b) S880 on PCC surface at different temperatures. Experiment conditions: Shear rate = 300 s^{-1}; No electrolyte added

The adsorption amount of cationic starch increased with increasing temperature might be caused by the structure change at higher temperature [157]. It is well known that the starch is a mixture of highly branched amylopectin and linear amylose with a tendency to form clusters. With increase in temperature, the starch clusters separate into smaller agglomerates and even into single macromolecules. These have considerably high diffusion ability than the large clusters and thus favor adsorption.

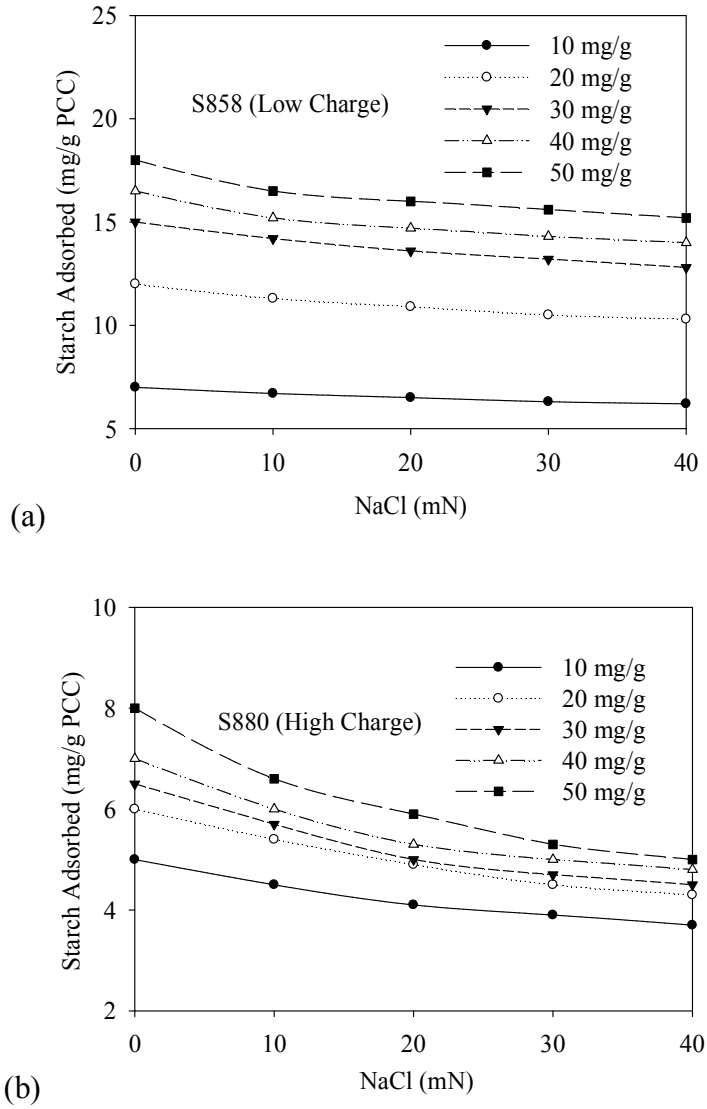

Fig. 4.9. Effect of the NaCl concentration on (a) S858 and (b) S880 adsorption on PCC for various starch dosages. Experimental conditions: Shear rate = 300 s^{-1}; T = 50 ^{o}C

Electrolytes are known to affect polymer flocculation efficiency by interfering with the adsorption process. The effect of NaCl concentration on the steady-state adsorption of starch on PCC was investigated at 0, 10, 20, 30 and 40 mN. As seen in Fig. 4.9, the amount of starch adsorption decreases with the increase of NaCl concentration for both starches. Zakrajsek et al. [141] measured the adsorption of cationic starch on fibres at different concentrations of NaCl and concluded that sodium cations can bind to negative charges of the particles and reduce the adsorption sites available and hence the attractive forces between the particle and cationic starch.

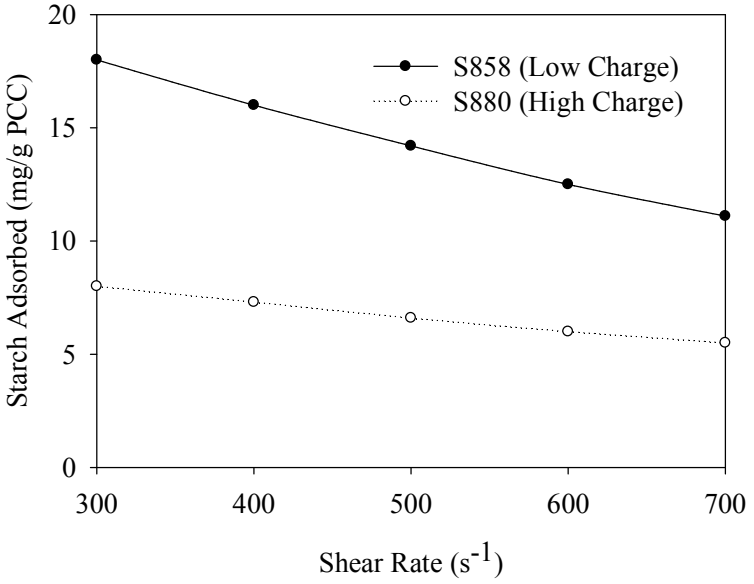

Fig. 4.10. Effect of shear rate on S858 and S880 adsorption on PCC. Experimental conditions: T = 50 ^{o}C; Starch dosage = 50 mg/g PCC

Fig. 4.10 shows that the adsorption amount decreased with the increase of the shear rate for both starches. The adsorption amount decrease is much more pronounced for S858 compared to S880. This is attributed to higher binding strength with the higher charge density S880 and less susceptible to shear than S858.

4.3.5. Zeta potential measurements

Fig. 4.11 shows the zeta potential of PCC in distilled deionized water for two starches. The zeta potential of PCC increases rapidly at low dosages and then reaches a plateau at about 10 mg/g. At the starch dosage of 2 mg/g PCC, the zeta potential of PCC was reversed to +6.9 ± 3.3 mV for S858 and +7.1 ± 2.4 mV for S880. The zeta potential of PCC reached the maximum values of +24.0 ± 0.5 mV for S858 and +26.4 ± 0.2 mV for S880 at about 10 mg/g.

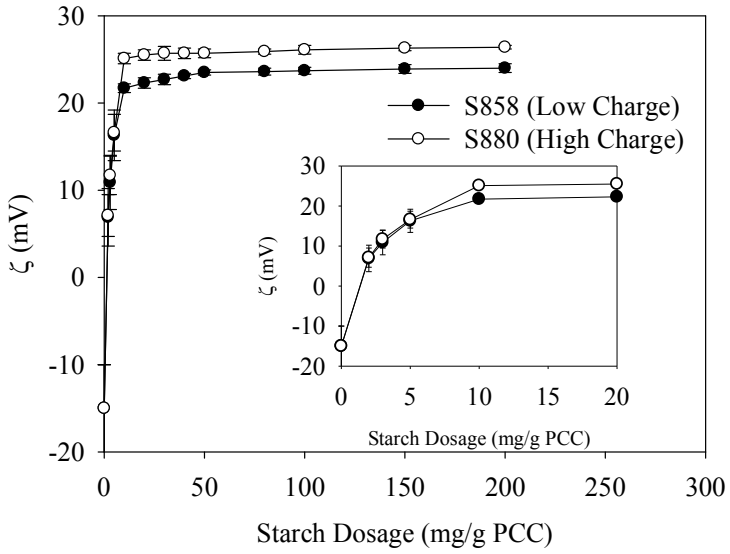

Fig. 4.11. Zeta potential of PCC in distilled deionized water for two starches at different dosages measured after one minute contact between PCC and starch

As seen in Fig. 4.12, a starch dosage of 30 mg/g can reverse the PCC zeta potential value in one minute. The PCC surface charge then decays for both systems in the same fashion to about 10 mV. The PCC surface charge decay may be due to the starch re-conformation and diffusion in the PCC porous spaces.

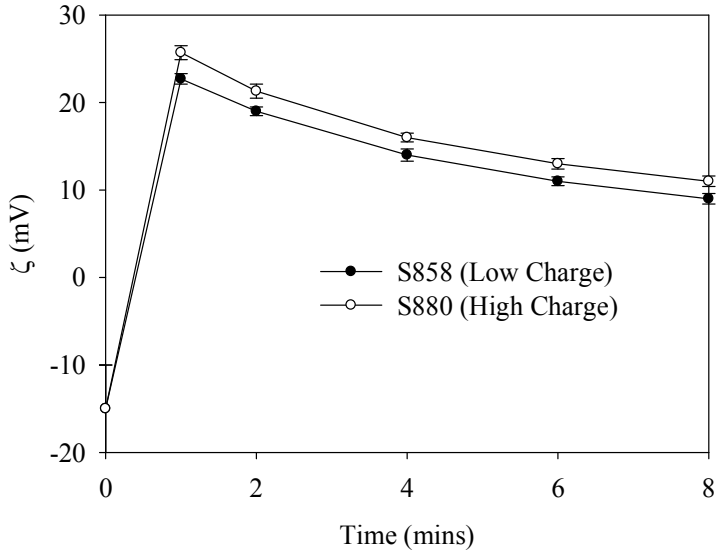

Fig. 4.12. PCC surface charge decay for S858 and S880. Starch dosage = 30 mg/g PCC

4.3.6. Discussion

This study provided direct evidence for the evolution of PCC floc size and structure with time when starch is used as flocculant. As seen the maximum floc size and the maximum positive zeta potential is reached within one minute when a starch dosage of 30 mg/g is used. Interestingly the rate of floc size decay and that of charge decay are similar for both starches used. The floc size decays to a steady state as the large flocs are more susceptible to fragmentation by fluid shear. In fact shear is a significant factor for the floc size as one expects intuitively. The increase in shear was found to decrease the amount of adsorbed starch (the effect was stronger with S858) and also to decrease the floc size. On the other hand, the shear did not affect the floc structure. This indicates even the lowest shear rate (300 s^{-1}) is enough to break up the flocs at the weakest point or restructure the flocs resulting in more compact flocs. The maximum size is higher for the high charge density starch S880 in spite of more S858 starch adsorbed. When the starch is added to the PCC suspension, the high charge density starch S880 can distribute more charge to the PCC

surface resulting in stronger bridges between PCC particles which are then less likely to be broken compared to bridges formed by the low charge density starch S858. If there is only a dynamic equilibrium between floc aggregation and breakage during the flocculation, the floc size would reach a plateau without further decrease in size. The decrease in the floc size indicates floc restructuring which leads to a size decrease. Another possible reason is the PCC surface charge decay that was observed. The PCC surface charge decay possibly due to starch re-conformation and diffusion in the PCC porous spaces may lower the flocculation efficiency.

4.4. Conclusions

The PCC flocculation kinetics and floc structure were studied by Malvern Mastersizer 2000 using the static light scattering technique. Two cationic tapioca starches (S858 and S880) were used. Direct evidence of floc size, structure and their evolution with time was provided. Larger and more compact flocs were produced by the high charge density starch S880. The PCC floc size rapidly increased in size initially, reached a maximum and then decayed gradually to steady state indicating a restructuring accompanied aggregation and breakage. The floc size evolution corrrelates with the zeta potential of the PCC floc. The mass fractal dimension of the flocs which is related to the floc structure continued increasing as the flocculation proceeds indicating more compact flocs formed. The analysis of variance revealed the floc structure is affected mainly by the starch dosage. On the other hand, the floc size is affected by shear rate and the interaction of starch with temperature when using S858. The adsorption experiments showed both starches had high affinity to PCC and the maximum adsorption amount for S858 and S880 is roughly inversely proportional to their degree of substitution suggesting electrostatic interaction is the predominant mechanism.

Chapter 5 Flocculation of Precipitated Calcium Carbonate (PCC) by Cationic Tapioca Starch with Different Charge Densities. II: Population Balance Modeling[4]

Chapter 5 presents a population balance model to describe the floc size evolution and compare it with the experimentally obtained PCC flocculation data. The relationship among collision efficiency, energy dissipation rate, restructure rate and experimental conditions is also established.

5.1. Introduction

In order to understand, predict and control the flocculation of precipitated calcium carbonate (PCC), it is necessary to develop quantitative models which are able to describe aggregation and breakage under various processing conditions. Since the pioneering efforts of Smoluchowski in the early 20th century [106], population balance model has been used widely for modeling the kinetics of granulation [158-160], nucleation [110, 161-163], crystallization [161, 164], sintering [165-167], and flocculation [111, 114, 168-171]. Traditionally, population balance model is one-dimensional which takes size as the only floc property and assumes the floc structure stable throughout the flocculation process [112, 113]. Ding et al. [172] presented a population balance model for activated sludge flocculation and extracted the aggregation rate and selection rate constants through fitting the model to the experimental data without the consideration of the floc structure evolution. Biggs and Lant [108] assumed the activated sludge flocs having a spherical

[4] A version of this chapter has been published online: Sang, Y., Englezos, P. (2012). "Flocculation of Precipitated Calcium Carbonate (PCC) by Cationic Tapioca Starch with Different Charge Densities. II: Population Balance Modeling." Colloids and Surfaces A: Physicochemical and Engineering Aspects. DOI: 10.1016/j.colsurfa.2012.07.028

shape during population balance modeling and pointed out the need of developing a suitable method to monitor the change in structure on-line during flocculation and to incorporate this into the model.

A single moment of floc size cannot provide sufficient information to capture the flocculation kinetics due to the complexity of the aggregation and breakage kernels. A proper incorporation of the fractal dimension is clearly critical for the population balance model reliability. The irregular structure of flocs can be taken into account by incorporating the floc mass fractal dimension into the expression for collision frequency factor [115, 173]. Oles [174] and Marsh et al. [175] showed that the fractal dimension of polystyrene latex particles increased from initial value of 2.1 to 2.5 at the final stages of flocculation. Jullien and Meakin [176] also reported a fractal dimension increase from 1.89 to 2.13 in shear-induced suspensions. Sang and Englezos [137] showed the mass fractal dimension of PCC floc increased from 1.8 to 2.3 induced by cationic tapioca starch. Only a few papers considered the time evolution of mass fractal dimension as another independent moment for the flocculation process modeling though the importance of the floc structure evolution [107, 114, 177]. A fractal population balance model with [178] and without [179] attention to the restructuring effects had been developed for the prediction of the asphaltene aggregate size. The model with consideration of restructuring effects gave more accurate results [178]. Selomulya et al. [114] took into account the floc restructuring effect in the population balance modeling of latex particle flocculation and indicated the shear responsible for creating more compact aggregates. Antunes et al. [107] reported that the PCC flocculation induced by linear cationic polyacrylamide molecules had higher collision efficiency and restructure rate than that from branched molecules. Rasteiro et al. [140] concluded that high charge density cationic polyacrylamide yields more compact and stronger PCC aggregates. It is noted such compact flocs could facilitate drainage [43]. The introduction of the restructuring made the population balance model much richer than in

the case of only flocculation and fragmentation considered [107, 114, 180]. A population balance model including process variables (shear rate, flocculant dosage, primary particle size and solid fraction) has been developed to describe the kinetics of aggregation/breakage of calcite particles with high-molecular-weight flocculant in turbulent flow [109].

While previous work described the evolution of the floc size and structural change with time and extracted the value for the fitting parameters (i.e. collision efficiency, restructure rate, etc). However, they did not establish the relationships between these parameters and the experimental conditions. In order to control the flocculation process and manipulate the floc properties, it is necessary to establish the relationship between its fitting parameters (collision efficiency, energy dissipation rate and restructure rate) and the experimental conditions (shear rate, ionic strength, temperature, and polymer concentration). The objective of this work is to present a population balance model to describe the PCC flocculation process, compare it with the flocculation data in Chapter 4 of Sang and Englezos [137] and establish the relationship between the fitting parameters and the experimental conditions. Finally, this work also relates the floc strength to the energy dissipation rate. It is noted that due to the highly demanding procedures for sample collection and preparation, very little is known about the floc strength.

5.2. Population Balance Model

Parker et al. [181] reported that floc aggregation and breakage are the two main phenomena responsible for the dynamic changes of the particle size distribution during the flocculation process. Hence, the population balance equation describes the rate of change of the particle number concentration as follows:

$$\frac{dn(v)}{dt} = \frac{1}{2}\int_0^v \beta(v-u,u)n(v-u)n(u)du - n(v)\int_0^\infty \beta(v,u)n(u)du + \int_v^\infty b(v/w)S(w)n(w)dw - S(v)n(v) \quad (5\text{-}1)$$

where $\beta(v,u)$ is the frequency of collisions between particles of volume u and v; $n(v)$, $n(u)$ and $n(w)$ are number concentrations of particles of volume u, v and w, respectively; $b(v/w)$ is the breakage probability density function of particles of volume w into particles of volume v; $S(v)$ and $S(w)$ are the specific fragmentation rates for the particles with volume of v and w, respectively.

The evolution of particle size distribution with time is a result of the four terms in Eq. (5-1). The first term on the right hand side of Eq. (5-1) represents the increase in the number concentration of particles with volume v due to aggregation between particles of volume $v–u$ and u (aggregation birth). The second term on the right hand side of Eq. (5-1) denotes the decrease in the number concentration of particles with volume v due to its aggregation with any other particles (aggregation death). The third term on the right describes the increase in the number concentration of particles with volume v when larger particles with volume w break into particles with volume v (breakage birth). The fourth term is the decrease in number concentration when particles with volume v break into smaller particles (breakage death).

Eq. (5-1) is solved by discretizing it with respect to size and convert it into a set of nonlinear ordinary differential equations (ODE). The rate of change of particle number concentration in section i during the simultaneous aggregation and breakage is given by the following population balance Eq. (5-2) [110]:

$$\frac{dN_i}{dt} = N_{i-1}\sum_{j=1}^{i-2} 2^{j-i+1}\alpha_{i-1,j}\beta_{i-1,j}N_j + \frac{1}{2}\alpha_{i-1,i-1}\beta_{i-1,i-1}N_{i-1}^2 - N_i\sum_{j=1}^{i-1} 2^{j-1}\alpha_{i,j}\beta_{i,j}N_j - N_i\sum_{j=i}^{i\max}\alpha_{i,j}\beta_{i,j}N_j - S_iN_i + \sum_{j=i}^{i\max}\Gamma_{i,j}S_jN_j \quad (5\text{-}2)$$

where N_i is the number concentration of particles in section i, $\alpha_{i,j}$ is the collision efficiency, and $\beta_{i,j}$ is the collision frequency for the particles in sections i and j. The floc breakage rate is represented by the fragmentation rate S_j. The volume fraction of the fragments is defined by the breakage probability distribution function $\Gamma_{i,j}$. The breakage distribution function Γ_{ij} describes the distribution of floc fragments in interval i from the break-up of flocs in interval j. The first two terms on the right hand side of Eq. (5-2) represent the birth of floc of size, i, by collision of smaller flocs. The third and fourth terms represent the death of floc of size, i, by its collision with any other flocs. The fifth term is the death of floc of size, i, by itw own breakage. The sixth term is the birth of floc of size, i, by breakage of larger flocs in interval j.

5.2.1. Initial condition for the population balance equation (5-2)

The initial condition (Refer to Appendix I for details) for Eq. (5-2) is:
N_i=[1.67E+08, 2.07E+08, 8.38E+07, 2.55E+07, 1.14E+07, 4.88E+06, 1.38E+06, 2.36E+05].

5.2.2. Collision efficiency

Comparable sized particles are easier to enter regions where the colloidal forces (double layer force or van der Waals forces) and electrostatic forces are significant enough for successful two-body collision compared to the unequal sized particles. The particles are also assumed to be spherical [182]. Eq. (5-3) reflects such relationship between the relative floc size and the collision efficiency and allows higher collision efficiency for flocs with comparable sizes and lower value for unequal sized particles [114, 183].

$$\alpha_{i,j} = \frac{\exp\left(-0.1\left(1-\frac{i}{j}\right)\right)^2}{(i\times j)^{0.1}} \times \alpha_{\max} \qquad (5\text{-}3)$$

where i and j indicate the sections where the colliding aggregates are located. α_{max}=1 denotes maximum coefficiency. The collision efficiency calculated with the above equation was found to decrease exponentially with increasing dimensionless flocs size.

5.2.3. Collision frequency

It is assumed that only binary collisions take place [184]. The overall aggregation rate can be calculated as follows in the case of fully destabilized particles with negligible settling and inertial effects [185]:

$$\beta_{ij} = \beta_{ij,perikinetic} + \beta_{ij,orthokinetic} \quad (5\text{-}4)$$

The frequency of binary collision between particles due to Brownian motion is estimated by Eq. (5-5) [186]:

$$\beta_{ij,perikinetic} = \left(\frac{2k_B T}{3\mu}\right)\frac{\left(R_{ci}+R_{cj}\right)^2}{R_{ci}R_{cj}} \quad (5\text{-}5)$$

where k_B ($\frac{kg\cdot m^2}{K\cdot s^2}$) is the Boltzmann constant, T (K) is the absolute temperature, and μ ($N\ s/m^2$) is the fluid dynamic viscosity. This mechanism is dominant for particles smaller than about one micron. The collision frequency for orthokinetic coagulation in isotropic turbulence is given by the Eq. (5-6) [186]:

$$\beta_{ij,orthokinetic} = 1.294\left(\frac{\varepsilon}{\nu}\right)^{1/2}\left(R_{ci}+R_{cj}\right)^3 \quad (5\text{-}6)$$

Where ε (m^2/s^3) is the average energy dissipation rate, υ is the fluid kinematic viscosity (m^2/s), R_{ci} and R_{cj} (m) are the effective collision radius.

The structure of flocs is taken into account by incorporating the mass fractal dimension to calculate the effective collision radius [186]:

$$R_{Ci} = r_0\left(N/k_c\right)^{1/d_f} \quad (5\text{-}7)$$

where r_0 (m) is the primary particle radius, N is the number of primary particles comprising a floc located in section i and equals to $2^{(i-1)}$, k_c is generally assumed to be unity [173], d_f is the mass fractal dimension of floc. Hence, by substituting R_{ci} in Equations (5-5) and (5-6), the floc structure is taken into account [187].

5.2.4. Energy dissipation rate

A semi-empirical exponential kernel which connects the fragmentation rate S_i and the critical energy dissipation rate were employed in the model through Eq. (5-8) [188]:

$$S_i = \left(\frac{4}{15\pi}\right)^{1/2} \left(\frac{\varepsilon}{\nu}\right)^{1/2} \exp\left(\frac{-\varepsilon_{ci}}{\varepsilon}\right) \qquad (5\text{-}8)$$

where ε_{ci} is the critical energy dissipation rate that results in the break-up. The energy dissipation rate needed for floc breakage is inversely proportional to R_{Ci} [189].

The energy dissipation rate is related to shear rate, G, by Eq. (5-9) [144]:

$$G = \sqrt{\frac{\varepsilon}{\nu}} \qquad (5\text{-}9)$$

where ν (m^2/s) is the kinematic viscosity of water defined as μ/ρ.

5.2.5. Breakage distribution function

Binary breakage refers to the situation where the floc breaks into two pieces of equal size. Ternary breakage refers to breakage into three fragments. In normal breakage, the flocs from the breakage are normally distributed in the lower size ranges. Spicer and Pratsinis [169] showed that the application of any of the breakage functions results in similar self-preserving final floc size distributions. The binary breakage distribution function was selected for use in this study and is expressed as follows [169].

$$\Gamma_{ij} = \frac{V_j}{V_i} = 2 \; for \; j = i+1$$
$$\Gamma_{ij} = 0 \; for \; j \neq i+1 \qquad (5\text{-}10)$$

The number concentration of particles in the intervals (N_i) was used to estimate the volume mean diameter $d_{4,3}(m)$ [188]:

$$d_{4,3} = \frac{\Sigma N_i D_i^4}{\Sigma N_i D_i^3} \qquad (5\text{-}11)$$

The characteristic floc diameter (m) ininterval i is calculated as

$$D_i = \left(2^{(i-1)/d_f}\right) d_0 \qquad (5\text{-}12)$$

where $d_0 = 2.5*10^{-7}\ m$, $d_f = 1.65$ are obtained from the particle size distribution determined experimentally by Malvern Mastersizer 2000 [137].

5.2.6. Variation of floc structure

The compactness of the floc is quantified through the mass fractal dimension. There are several factors that may influence the extent of floc structural changes [113, 190, 191]. The rate of increase of floc compactness is shown in Eq. (5-13) [183]:

$$\frac{dd_f}{dt} = \gamma\left(d_{f,\max} - d_f\right) \qquad (5\text{-}13)$$

where γ (s^{-1}) is the restructure rate as fitting parameter and $d_{f,max}$ is the maximum mass fractal dimension value.

5.2.7. Parameter estimation

The model has the following three adjustable parameters: collision efficiency α, critical energy dissipation rate ε_{ci}, and restructure rate γ. In order to estimate the model parameters, the following least squares objective function is formulated and is shown in Eq. (5-14). The minimization was carried out using the fminsearch solver in Matlab.

$$f(\alpha, \varepsilon_{ci}, \gamma) = \sum_{t=0}^{t=t_{\max}} \left(d_{4,3\exp t} - d_{4,3\mathrm{mod}el} \right)^2 \quad (5\text{-}14)$$

5.3. Results and Discussion

The simulation was performed using the experimental data in Chapter 4. A typical profile of experimental and simulated PCC flocculation kineticsis shown in Fig. 5.1 (Refer to Appendix J for the rest simulated PCC flocculation kinetics). The population balance model provides an excellent approximation of the floc size change with time. At the initial stage of flocculation, the shear force is not strong enough to break the aggregate up and can only rotate the individual aggregates within the solution and restructure is more substantial than fragmentation resulting in the increase of the particle size until the maximum floc size is reached. With further increase of the floc size, the required energy to break down the floc is reduced and flocs are broken into fragments. The collision efficiency (CE), energy dissipation rate (EDR) and restructure rate (RR) were also estimated and their values are shown in Fig. 5.2 to Fig 5.4. The experimental ID numbers refer to Table 4.2.

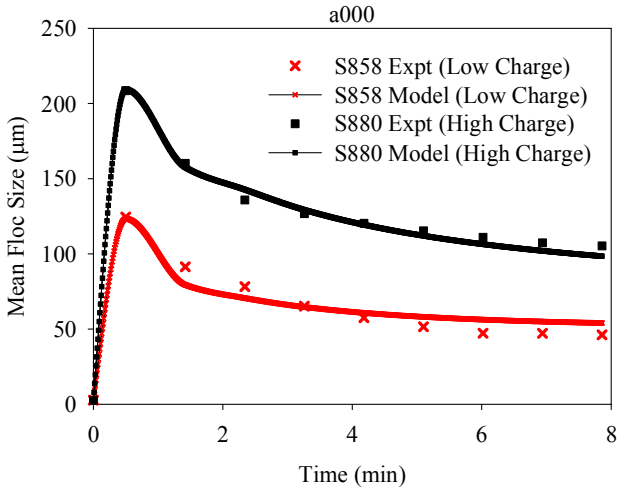

Fig. 5.1. Experimental and simulated PCC flocculation kinetics by starch. Experimental conditions: Temperature = 30 ^{o}C; NaCl = 20 mN; Shear rate = 500 s^{-1}; Starch = 30 mg/g

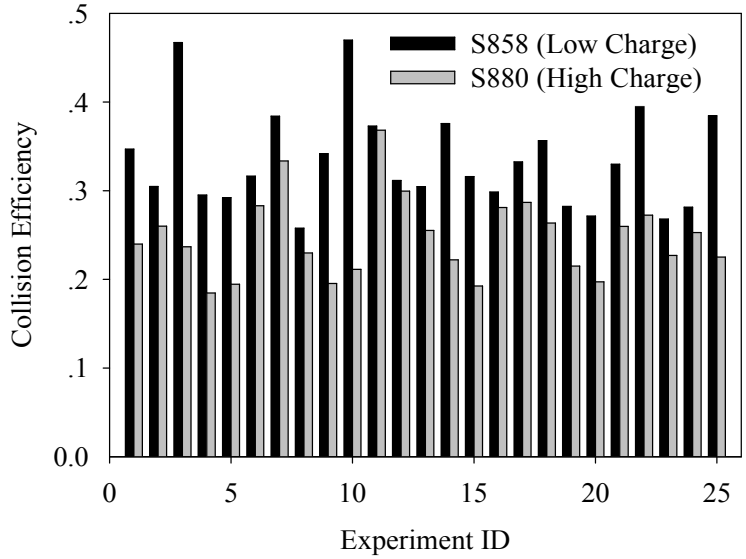

Fig. 5.2. Collision efficiency of S858 and S880 flocculation systems

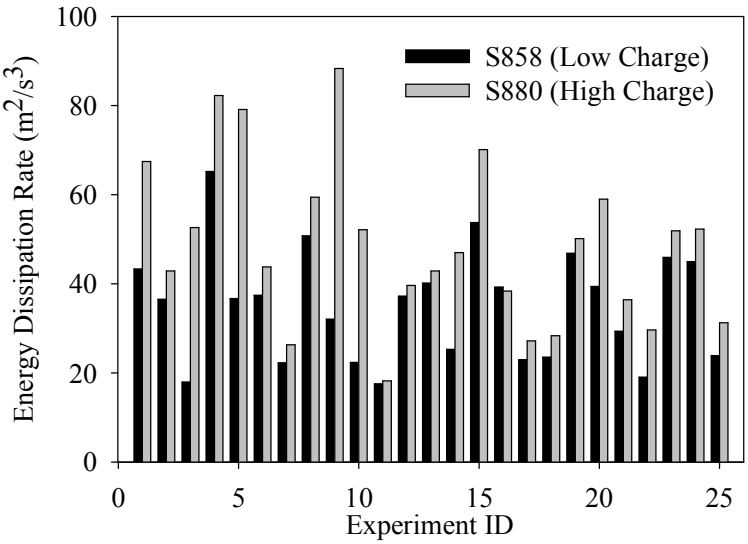

Fig. 5.3. Energy dissipation rate of S858 and S880 flocculation systems

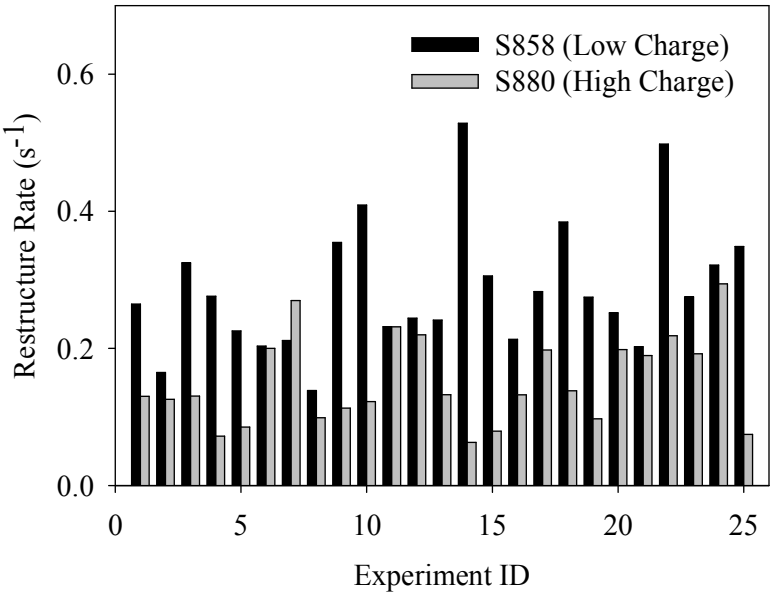

Fig. 5.4. Restructure rate of S858 and S880 flocculation systems

5.3.1. Collision efficiency

As shown in Fig. 5.2, the low charge density starch S858 resulted in higher collision efficiency. The high charge density starch S880 has larger number of contacts with PCC surface compared to S858 and forms more compact polymer layer on the particle surface. The low charge density starch has a much more extended morphology around the particle surface. Thus, the higher collision efficiency for the low charge density starch S858 occurs due to the more significant increase in the effective radius of the particles [182].

5.3.2. Energy dissipation rate

Results in Fig. 5.3 show that flocs induced by S880 system required higher energy dissipation rate to break up. In other words, stronger flocs were formed with S880. The tensile strength of a floc is given by Eq. (5-15) [192, 193]:

$$\sigma_z = \frac{9}{8}\left(\frac{1-\varepsilon_A}{\varepsilon_A}\right)\frac{F_A}{d^2} \qquad (5\text{-}15)$$

where ε_A is the porosity of the floc, d is its size and F_A is the net attractive force binding the particle together. It is evident from Eq. (5-15) that a highly porous floc is much easier to break than a densely packed one. Starch S880 induces more compact (lower porosity) flocs [137]. This may explain why flocs induced by S880 require higher energy dissipation rate to break up. The adhesive strength between flocs is also affected by the molecular mass and charge density of the polymeric flocculant. A large polymer molecule forming a bridge between two particles has many more contacts with the particles and hence a greater force is required to force the particles apart. The charge density of the polymer determines the segment/particle surface adsorption energy and the percent of polymer segments on the surface of the particle. The two cationic starches used in this work have same molecular mass but different charge densities. The high charge density starch distributes more cationic charge on the PCC surface and this enhances the adhesive force. Hence, an increase in the energy dissipation rate is needed to break up the flocs formed by S880.

5.3.3. Restructure rate

As seen in Fig. 5.4, the aggregate induced by low charge density starch S858 has a higher restructure rate. S858 forms weaker flocs than S880 and it should be easier to break up and facilitate the restructure process.

5.3.4. ANOVA results

Based on the ANOVA results shown in Table 5.1 (Refer to Appendix H for ANOVA details), the relationships between model parameters and experimental conditions are

established through empirical models shown in Table 5.2. The factors x_1, x_2, x_3 and x_4 are temperature, NaCl concentration, shear rate and starch dosage as shown in Chapter 4. The prediction profiles in Figs. 5.5 and 5.6, including the 95% confidence intervals for the predicted values, show the positive or negative effect of each significant factor on the collision efficiency, energy dissipation rate, and restructure rate.

Table 5.1. Significant factors for the model parameters of S858 and S880 systems

Factor	Collision Efficiency		Energy Dissipation Rate (m^2/s^3)		Restructure Rate (s^{-1})	
	S858	S880	S858	S880	S858	S880
T	---	---	S	ES	S	---
NaCl	---	VS	---	S	---	---
Shear Rate	VS	ES	ES	ES	---	---
Starch	S	---	ES	---	ES	---
T*Shear Rate	---	---	---	S	---	---
T*Starch	---	---	VS	---	---	---
T*T	---	---	---	S	---	---
Starch* Starch	---	---	---	---	S	---

ES=extremely significant; VS=very significant; S=significant; ----: not significant

Table 5.2. Relationships between the model parameters and the experimental conditions

	S858 Flocculation System	S880 Flocculation System
Collision Efficiency (CE)	$CE_{S858} = 0.31 - 0.03x_3 + 0.02x_4$	$CE_{S880} = 0.26 + 0.01x_2 - 0.03x_3$
Energy Dissipation Rate (EDR)	$EDR_{S858} = 40.17 - 2.74x_1 + 9.38x_3 - 5.13x_4 + 3.93x_1x_4$	$EDR_{S880} = 42.88 - 8.86x_1 - 2.53x_2 + 14.11x_3 - 3.22x_1x_3 + 2.47x_1^2$
Restructure Rate (RR)	$RR_{S858} = 0.24 + 0.03x_1 + 0.06x_4 + 0.03x_4^2$	$RR_{S880} = 0.13$

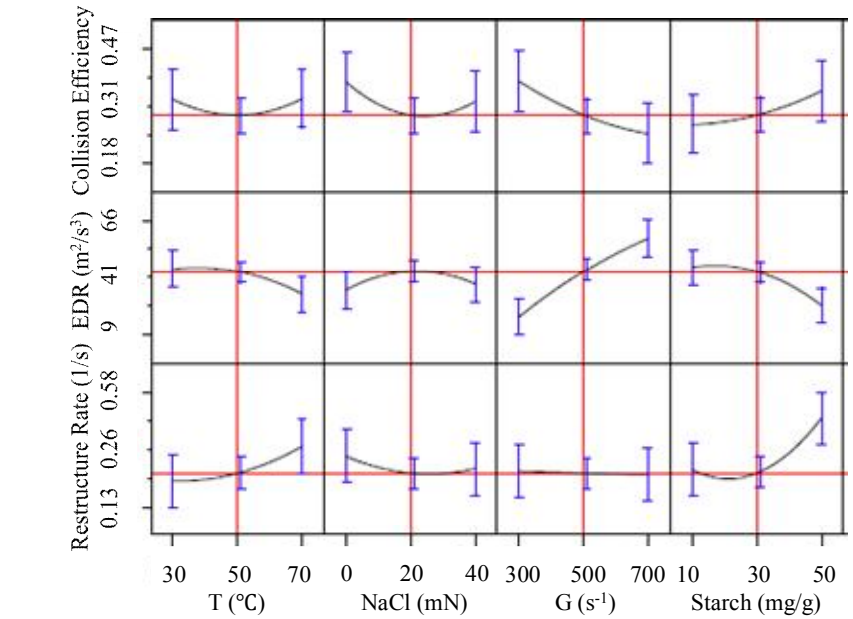

Fig. 5.5. Prediction profiler for S858 flocculation system

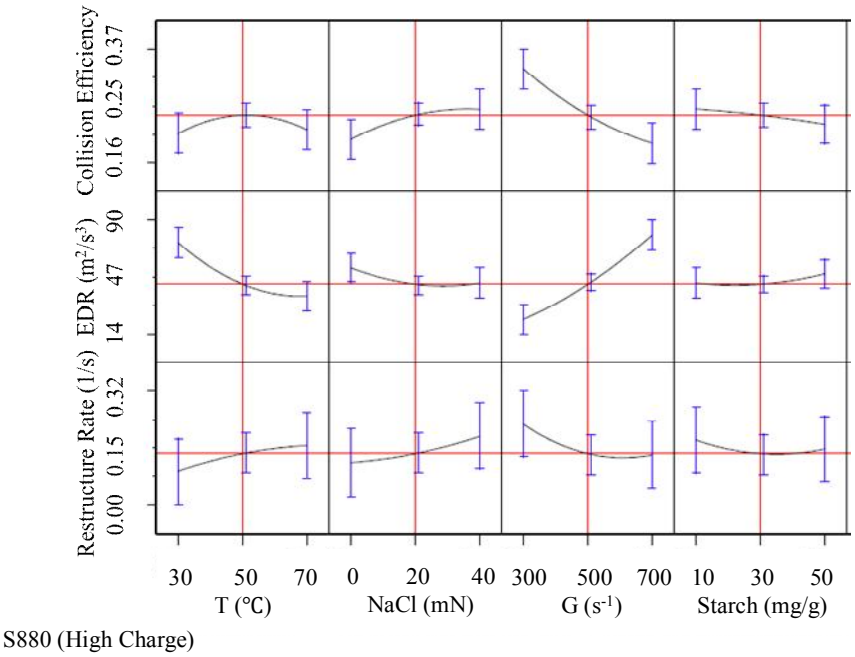

Fig. 5.6. Prediction profiler for S880 flocculation system

5.3.4.1. Effect of temperature

As seen from Table 5.1, temperature has a significant effect on the energy dissipation rate for both flocculation systems. It can be concluded this effect is negative from Table 5.2. The floc strength decreases with increasing temperature and breaks more easily. This is in agreement with the work of Fitzpatrick et al. [194]. As seen from Table 5.1, no temperature effect was found on the restructure rate for the S880 system. However, the increase of temperature significantly increase the restructure rate for the S858 system. This is because the flocs formed by S858 were easier to be broken up (as indicated by the lower energy dissipation rate) and cause more significant restructure.

5.3.4.2. Effect of NaCl

As seen from Table 5.1, the NaCl did not show effect on the three model parameters of S858 system. On the other hand, the collision efficiency and energy dissipation rate were affected by the NaCl when high charge starch S880 was used. As S880 tends to have more compact morphology on the particle surface, the reduction of the electric double layer after the addition of NaCl facilitates the adsorbed S880 polymer layers to extend beyond the electric double layer and this enable the particles to experience a higher collision efficiency [130].

As seen in Fig. 5.6, the energy dissipation rate decreases as the NaCl dosage increases when starch S880 is used. This is probably because high charge density starch S880 occupies more negative points than S858 and thus there are less points available on the PCC surface for the sodium ion to attach. It is then possible the sodium ion could diffuse into the adsorbed starch S880 layer and displace the adsorbed segment from the PCC surface which reduces the number of bonds holding the floc together. This leads to weaker flocs and thus a lower energy dissipation rate is required to break the flocs formed by starch S880 [181, 195]. For the low charge density starch S858, less charge was distributed to the PCC surface and more points on the PCC surface were available for Na^+ ions adsorption from the added NaCl. Less starch displacement was observed [137] and no significant effect was found on energy dissipation rate. Also, according to the Eq. (5-15), the addition of NaCl increases the ionic strength; as a consequence the electrostatic forces decrease. Thus, the attractive force (F_A in the Eq. (5-15)) binding the particles in the floc decreases. Therefore, lower energy dissipation rate was observed.

5.3.4.3. Effect of shear rate

The collision efficiency decreased with the increase of shear rate for both starches as shown in Figs. 5.5 and 5.6. With the increase of shear rate, more polymers were detached from the PCC surface evidenced by the lower adsorption amount at higher shear rate as shown in Chapter 4 [137]. Lower level of agglomeration was thus oberved as the adsorbed starch layer thickness is reduced during the shearing. Another possible reason for the lower collision efficiency at higher shear rate is the faster charge decay rate due to the enhanced starch reconformation/penetration on PCC surface at higher shear rate.

5.3.4.4. Effect of starch dosage

The increase in the dosage of S858 is found to have a positive effect on the collision efficiency and the restructure rate and a negative effect on the energy dissipation rate. However, no effect was observed when S880 was used. The increase of the collision efficiency for S858 at higher starch dosage is probably because the more significant increment of effective diameter of PCC particles coated by S858 due to its more entended morphology compared to S880. Agarwal et al. [196] also showed the collision efficiency has positive correlation with adsorbed layer thickness. An increase in the collision efficiency produces looser flocs compared to the flocs formed at lower collision efficiency [151, 152]. Consequently, lower energy dissipation rate could break the flocs and higher restructure rate is observed with the increase of starch dosage.

5.4. Conclusions

The population balance approach provides a proper framework to describe the dynamics of the flocculation of precipitated calcium carbonate (PCC) by two cationic tapioca

starches. There is an excellent agreement between the experimentally observed evolution of the volume mean floc size with time with the model-based calculated values. The high charge density starch S880 is associated with lower collision efficiency, lower restructure rate and higher energy dissipation rate to break up the flocs compared to the low charge density starch S858. Lower energy dissipation rate is required to break the flocs at higher temperature for both flocculation systems. The presence of the background electrolyte was found to affect the high charge density starch S880 but had no influence on the low charge density starch S858. The collision efficiency decreases with the increase of the shear rate for both starches. Finally, the increase of starch dosage increased the collision efficiency and restructure rate for the low charge density starch S858.

Chapter 6 Conclusions and Recommendations for Future Work

6.1. Conclusions

Under the conventional chemical addition sequence, the retention program using cationic starch S858 gave highest retention and significant drainage improvement, and cationic starch S880 resulted in best drainage. S858 is the most suitable starch in combination with CPAM and silica to achieve the best retention and drainage performance. A significant synergism was found between starch (S858 and S880) and silica, which improves the retention. S858 retention system always gave slightly higher ash content than S880 retention system. S880 retention system resulted in higher breaking length and burst indices possibly because it has a higher affinity to fibres and fines than cationic starch S858.

PCC preflocculation by linear high charge cationic starch S880 with a molecular mass of 3 million Da resulted in highest retention and best drainage performance compared to linear low charge cationic starch S858 and cross linked high charge cationic starch X880. Same charge cationic starch S880 (linear) and X880 (cross-linked) had similar adsorption amount on pulp and are much higher than the low charge cationic starch S858. The linear high charge cationic starch S880 retention system resulted in higher breaking length and burst indices. Finally it is concluded that filler preflocculation by starch resulted in higher breaking length and burst indices compared to the conventional chemical addition sequence for both high charge and low charge cationic starches. Machine trials have also now verified these results. The newly developed starch and nanoparticle silica technologies have proven to be very efficient to increase the retention and drainage performance of the papermaking process.

Larger and more compact flocs were produced by high charge cationic starch S880. The PCC floc size rapidly increased, reached a maximum and then decayed gradually to steady state indicating a restructuring accompanied aggregation and breakage during the flocculation. The mass fractal dimension of the flocs continued increasing as the flocculation proceeds and more compact flocs formed. The adsorption experiments showed that both starches had high affinity to PCC and the maximum adsorption amount for S858 and S880 is inversely proportional to their degree of substitution.

There is an excellent agreement between the experimentally observed evolution of the volume mean floc size with time with the model-based calculated values. The high charge cationic starch S880 is associated with lower collision efficiency, lower restructure rate and higher energy dissipation rate to break up the flocs compared to the low charge cationic starch S858. Lower energy dissipation rate is required to break the flocs at higher temperature for both flocculation systems. The presence of NaCl was found to affect high charge cationic starch S880 but had no influence on the low charge cationic starch S858. The collision efficiency decreases with the increase of the shear rate for both starches. Moreover, the collision efficiency and restructure rate increased with the increase of starch dosage for low charge cationic starch S858.

6.2. Contribution to Knowledge

Knowledge generated from this work enables papermakers to select the appropriate chemicals, the proper dosage of the various chemicals, the addition points and sequence and to manipulate the floc properties for highly filled paper production. The contributions are as follows:

1. An interaction between starch and silica exists and can play an important role in retention, but not in drainage.
2. PCC preflocculation by starch can further improve the retention and drainage. Paper produced with such preflocculated filler has higher breaking length and burst indices.
3. High charge cationic starch S880 induced larger and more compact PCC flocs.
4. Linear high charge cationic starch S880 is associated with lower collision efficiency, lower restructure rate and higher energy dissipation rate required to break up the flocs. The increase of the shear rate lowered the collision efficiency for both starches. The shear applied on the flocs can pattern them to more compact state.

6.3. Recommendations for Future Work

The following are suggested to advance the state of knowledge in the production of highly filled mechanical grade papers:

1. Preflocculate PCC by starch and silica before introducing to pulp to exploit the possibility of higher retention and drainage.
2. Investigate the pasting behavior of starch and correlate this to its papermaking process performance.

References

[1]J.H. Haslam, F.A. Steele, Fillers in the lumens, Paper Trade Journal 102 (1936) 22.
[2]H.V. Green, T.J. Fox, A.M. Scallan, Lumen-loaded paper pulp, Pulp & Paper-Canada 83 (1982) 39-43.
[3]S.R. Middleton, A.M. Scallan, Lumen-loaded paper pulp - mechanism of filler-to-fiber bonding, Colloids and Surfaces 16 (1985) 309-322.
[4]T. Okayama, K. Kumo, A. Hanada, R. Oye, Behaviours of filler particles in lumen-loading, Japan TAPPI J. 43 (1989) 55-66.
[5]S.R. Middleton, J. Desmeules, A.M. Scallan, Lumen loading with calcium carbonate fillers, Journal of Pulp and Paper Science 29 (2003) 241-246.
[6]S.R. Middleton, A.M. Scallan, Partial lumen loading, Nordic Pulp Paper Research Journal 8 (1993) 204-207.
[7]M.L. Miller, D.C. Paliwal, The effects of lumen-loading on strength and optical-properties of paper, Paperi Ja Puu-Paper and Timber 65 (1983) 800-800.
[8]J. Petlicki, T.G.M. Van de ven, Kinetics of lumen loading, Journal of Pulp and Paper Science 20 (1994) J375-J382.
[9]G.G. Allan, J.P. Carroll, A.R. Negri, M. Raghuraman, P. Ritzenthaler, A. Yahiaoui, The microporosity of pulp - the precipitation of inorganic fillers within the micropores of the cell-wall, TAPPI J. 75 (1992) 175-178.
[10]G.G. Allan, Y.C. Ko, P. Ritzenthaler, The microporosity of pulp - the nature of the pore-size distribution, TAPPI J. 74 (1991) 205-212.
[11]G.G. Allan, A.R. Negri, P. Ritzenthaler, The microporosity of pulp - the properties of paper made from pulp fibers internally filled with calcium-carbonate, TAPPI J. 75 (1992) 239-244.
[12]G.G. Allan, Y.C. Ko, The microporosity of pulp. The forces influencing the intra and inter-fiber pore structure and pore size distribution in pulp and paper, Cellulose Chemistry and Technology 29 (1995) 479-485.
[13]J. Klungness, D.F. Caulfield, B. Sachs, M. Sykes, F. Tan, R. Shilts, Method for fiber loading a chemical compound, US Pat. 5,223,090, 1993.
[14]J.H. Klungness, A. Ahmed, S. AbuBakr, M.J. Lentz, E.G. Horn, M. Akhtar, Novel lightweight, high-opacity papers made from mechanical pulps, International Mechanical Pulping Conference 2001, Helsinki, Finland, 2001, pp. 95-101.
[15]L. Cousin, F. Mora, Highly loaded fiber-based composite material, US Pat. 5,731,080, 1998.
[16]L. Cousin, F. Mora, Methods of manufacture for highly loaded fiberbased composite material, US Pat. 5,824,364, 1998.
[17]G. Gavelin, Method for manufacturing filler-containing paper, US Pat. 4,889,594, 1989.

[18] P. Silenius, Improving the combinations of critical properties and process parameters of printing and writing papers and paperboards by new paper-filling methods, Doctoral dissertation, Helsinki University of Technology, Helsinki, Finland, 2002.
[19] R. Subramanian, H. Fordsmand, H. Paulapuro, Precipitated calcium carbonate (PCC) - Cellulose composite fillers: effect of PCC particle structure on the production and properties of uncoated fine paper, Bioresources 2 (2007) 91-105.
[20] R. Subramanian, H. Fordsmand, J. Paltakari, H. Paulapuro, A new composite fine paper with high filler loading and functional cellulosic microfines, Journal of Pulp and Paper Science 34 (2008) 146-152.
[21] R.A. Gill, Cationic polymer modified filler material, process for its preparation and method for its use in papermaking, US Pat. 5,147,507, 1992.
[22] B. Alince, Cationic latex as a multifunctional wet-end additive in highly filled paper, TAPPI J. 3 (2004) 16-18.
[23] B. Alince, Cationic latex as a multifunctional papermaking wet-end additive, TAPPI J. 82 (1999) 175-187.
[24] S.Y. Yoon, Y.L. Deng, Clay-starch composites and their application in papermaking, J Appl Polym Sci 100 (2006) 1032-1038.
[25] Y. Zhao, Z. Hu, A. Ragauskas, Y. Deng, Improvement of paper properties using starch-modified precipitated calcium carbonate filler, TAPPI J. 4 (2005) 3-7.
[26] S.Y. Yoon, Y. Deng, Starch-fatty complex modified filler for papermaking, TAPPI J. 5 (2006) 3-9.
[27] S.-Y. Yoon, Bonding material coated clay for improving paper properties, Doctoral dissertation, Georgia Institute of Technology, Atlanta, 2007.
[28] R.D. Harvey, R.E. Klem, Preparation of filler compositions for paper, US Pat. 4,799,964, 1989.
[29] D.E. Smith, Producing dispersions of preflocculated fillers for use in papermaking, US Pat. 3,873,336, 1975.
[30] L.E. Shiel, Preflocculated filler compositions for use in the manufacture of paper, US Pat. 4,174,998, 1979.
[31] K. Brooks, L.E. Shiel, D.E. Smith, Compositions for use with papermaking fillers, US Pat. 4,272,297, 1981.
[32] R.F. Palmer, M.S.D. Juang, J.S. Johnson, B.R. Atha, D.T. Lee, L.L. Malcom, Paper products comprising filler materials preflocculated using starch granules and/or polymerized mineral networks, US Pat. 6,494,991, 2002.
[33] S. Mabee, R. Harvey, Filler flocculation technology - increasing sheet filler content without loss in strength or runnability parameters, 2000 TAPPI Papermakers Conference and Trade Fair, TAPPI Press, Vancouver, BC, Canada, April 2000, pp. 797-810.
[34] S.W. Mabee, Controlled filler preflocculation - improved formation, strength and machine performance, 2001 Papermakers Conference, TAPPI Press, Cincinnati, OH, March 2001.

[35] J. Novak, K. Stark, R. Eichinger, The influence of filler pretreatment on paper, Paper 207 (1987) 22-24.
[36] S.H. Park, D.S. Shin, Effects of the preflocculated domestic fillers on the strength and optical properties in highly-filled papermaking, Korea TAPPI J. 19 (1987) 44-61.
[37] W.G. Cheng, R.T. Gray, Controllable filler prefloculation using a dual polymer system, Pub. No. US 2009/0267258, 20090267258, 2009.
[38] K.W. Britt, J.E. Unbehend, Water removal during paper formation, TAPPI J. 68 (1985) 104-107.
[39] S. Modgi, M.E. McQuaid, P. Englezos, SEM/EDX analysis of Z-direction distribution of mineral content in paper along the cross-direction, Pulp & Paper-Canada 107 (2006) 48-51.
[40] J. Gregory, Rates of flocculation of latex particles by cationic polymers, Journal of Colloid and Interface Science 42 (1973) 448-456.
[41] M.A. Hubbe, Detachment of colloidal hydrous oxide spheres from flat solids exposed to flow. 4. Effect of polyelectrolytes, Colloids and Surfaces 25 (1987) 325-339.
[42] T. Asselman, B. Alince, G. Garnier, T.G.M. van de Ven, Mechanism of polyacrylamide-bentonite - microparticulate retention aids, Nordic Pulp & Paper Research Journal 15 (2000) 515-519.
[43] M.A. Hubbe, Mechanistic aspects of microparticle systems, TAPPI J. 4 (2005) 23-28.
[44] K.W. Britt, J.E. Unbehend, Electrophoresis in paper stock suspensions as measured by mass-transport analysis, TAPPI J. 57 (1974) 81-84.
[45] L. Wagberg, T. Lindstrom, Kinetics of polymer-induced flocculation of cellulosic fibers in turbulent-flow, Colloids and Surfaces 27 (1987) 29-42.
[46] M. Zempel, S. Trahan, EKA new nanoparticle silica technology introduction, PAPTAC 95th Annual Meeting and EXFOR 2009, Montreal, Canada, 2009, pp. 441-442.
[47] M. Zempel, New nanoparticle silica technology pushes retention and drainage performance, PAPTAC 95th Annual Meeting and EXFOR 2009, Montreal, Canada, 2009, pp. 35-39.
[48] M.A. Hubbe, Reversibility of polymer-induced fiber flocculation by shear. 1. Experimental methods, Nordic Pulp & Paper Research Journal 16 (2001) 375-375.
[49] M.A. Hubbe, Reversibility of polymer-induced fiber flocculation by shear. 2. Multi-component chemical treatments, Nordic Pulp & Paper Research Journal 16 (2001) 369-375.
[50] S.G. Mason, Fiber motions and flocculation, TAPPI J. 37 (1954) 494-501.
[51] M. Bjorklund, L. Wagberg, Flocculation of cellulosic fibres following addition of cationic starch, Colloids and Surfaces A-Physicochemical and Engineering Aspects 105 (1995) 199-209.
[52] R.J. Kerekes, C.J. Schell, Characterization of fiber flocculation regimes by a crowding factor, Journal of Pulp and Paper Science 18 (1992) J32-J38.
[53] P. Huber, C. Pierre, C. Bermond, B. Carre, Comparing the fiber flocculation behavior of several wet-end retention systems, TAPPI J. 3 (2004) 19-24.

[54] A. Kiviranta, C.T.J. Dodson, Evaluating fourdrinier formation performance, Journal of Pulp and Paper Science 21 (1995) J379-J383.
[55] B.-U. Cho, G. Garnier, T.G.M. van de Ven, M. Perrier, A bridging model for the effects of a dual component flocculation system on the strength of fiber contacts in flocs of pulp fibers: Implications for control of paper uniformity, Colloids and Surfaces A-Physicochemical and Engineering Aspects 287 (2006) 117-125.
[56] A. Swerin, U. Sjodin, L. Odberg, Flocculation of cellulosic fibre suspensions by model microparticulate retention aid systems: Effect of polymer charge density and type of microparticle, Nordic Pulp & Paper Research Journal 8 (1993) 389-398.
[57] E. Dickinson, L. Eriksson, Particle flocculation by adsorbing polymers, Advances in Colloid and Interface Science 34 (1991) 1-29.
[58] A. Swerin, L. Odberg, Flocculation and floc strength in suspensions flocculated by retention aids, Nordic Pulp & Paper Research Journal 8 (1993) 141-147.
[59] C.F. Schmid, L.H. Switzer, D.J. Klingenberg, Simulations of fiber flocculation: Effects of fiber properties and interfiber friction, Journal of Rheology 44 (2000) 781-809.
[60] C.J. Albinsson, A. Swerin, L. Odberg, Formation and retention during twin-wire blade forming of a fine paper stock, TAPPI J. 78 (1995) 121-128.
[61] A. Gerli, B.A. Keiser, M. Strand, The use of a flocculation sensor as a predictive tool for paper machine retention program performance, TAPPI J. 83 (2000) 1-16.
[62] J.C. Alfano, P.W. Carter, A. Gerli, Characterization of the flocculation dynamics in a papermaking system by non-imaging reflectance scanning laser microscopy (SLM), Nordic Pulp Paper Research Journal 13 (1998) 159-165.
[63] B. Krogerus, Impact of retention polymers on flocculation, retention, drainage and sheet formation, 1994 Papermakers Conference, TAPPI Press, San Francisco, CA US, 1994, pp. 445-452.
[64] J.G. Langley, E. Litchfield, Dewatering aids for paper applications, 1986 Papermakers Conference, TAPPI Press, New Orleans, LA US, 1986, pp. 89-92.
[65] H. Tanaka, A. Swerin, L. Odberg, Cleavage of polymer-chains during transfer of cationic polyacrylamide from cellulose fibers to polystyrene latex, Journal of Colloid and Interface Science 153 (1992) 13-22.
[66] L.H. Allen, I.M. Yaraskavitch, Effects of retention and drainage aids on paper-machine drainage - A review, TAPPI J. 74 (1991) 79-84.
[67] Y. Sang, M. McQuaid, P. Englezos, Optimization of chemical use for highly filled mechanical grade papers with precipitated calcium carbonate, Bioresources 6 (2011) 656-671.
[68] G. Ionides, Adding value for improved market competitiveness of mechanical printing papers, Pulp & Paper-Canada 105 (2004) 40-44.
[69] L. Li, A. Collis, R. Pelton, A new analysis of filler effects on paper strength, J.Pulp Paper Sci. 28 (2002) 267-273.
[70] G.H. Fairchild, Increasing the filler content of PCC-filled alkaline papers, TAPPI J. 75 (1992) 85-90.

[71]G.H. Fairchild, E.B. Clark, PCC morphology and particle size effects in alkaline paper, 50th Appita Annual General Conference Proceedings, New Generation Print & Copy, Brunswick East, Victoria, Australia, 1996, pp. 427-433.
[72]K.M. Beazley, H. Pereit, Effect of china clay and calcium carbonate on paper properties, Wochenbl. Papierfabr 103 (1975) 143-147.
[73]T. Lindstrom, T. Floren, The effect of filler particle size on the dry-strengthening effect of cationic starch wet-end addition, Nordic Pulp & Paper Research Journal 4 (1987) 142-145.
[74]T.G.M. van de Ven, Filler and fines retention in papermaking, Advances in Paper Science and Technology, The 13th FRC Symposium, Pulp & Paper Fundamental Research Society, Bury Lancashire, UK, 2005, pp. 1193-1224.
[75]J.M. Adams, Particle-size and shape effects in materials science - examples from polymer and paper systems, Clay Minerals 28 (1993) 509-530.
[76]J. Papp, The use of calcined clay in lightweight papers, Nordic Pulp & Paper Research Journal 1 (1989) 4-7.
[77]R. Bown, Particle size, shape and structure of paper fillers and their effect on paper properties, Paper Technology 39 (1998) 44-48.
[78]H. Schott, Adhesion of montmorillonite clay to cellulose and effect of particulate fillers on mechanical properties of paper, TAPPI J. 54 (1971) 748-&.
[79]Y. Xu, R. Pelton, A new look at how fines influence the strength of filled papers, Journal of Pulp and Paper Science 31 (2005) 147-152.
[80]S. Modgi, M.E. McQuaid, P. Englezos, Effect of cationic tapioca and potato starches on TMP fibres loaded with PCC, Journal of Pulp and Paper Science 33 (2007) 156-162.
[81]R. Pelton, On the design of polymers for increased paper dry strength - A review, Appita J. 57 (2004) 181-190.
[82]J. Zhang, R. Pelton, L. Wagberg, M. Rundlof, The effect of molecular weight on the performance of paper strength-enhancing polymers, J.Pulp Paper Sci. 27 (2001) 145-151.
[83]K.S. Kontturi, T. Tammelin, L.S. Johansson, P. Stenius, Adsorption of cationic starch on cellulose studied by QCM-D, Langmuir 24 (2008) 4743-4749.
[84]M. Shirazi, T.G.M. van de Ven, G. Garnier, Adsorption of modified starches on pulp fibers, Langmuir 19 (2003) 10835-10842.
[85]H.G.M. Vandesteeg, A. Dekeizer, M.A.C. Stuart, B.H. Bijsterbosch, Adsorption of Cationic Potato Starch on Microcrystalline Cellulose, Colloids and Surfaces A-Physicochemical and Engineering Aspects 70 (1993) 91-103.
[86]E. Brannvall, M. Eriksson, M.E. Lindstrom, L. Wagberg, Fibre surface modifications of market pulp by consecutive treatments with cationic and anionic starch, Nordic Pulp & Paper Research Journal 22 (2007) 244-248.
[87]D. Glittenberg, J.L. Hemmes, N.O. Bergh, Cationic starches in systems with high levels of anionic trash, Paper Technology 35 (1994) 18-27.
[88]D. Glittenberg, R.J. Tippett, P. Leonhardt, Wet-end starches-still up to date for high speed papermaking?, Paper Technology 45 (2004) 27-33.

[89]S. Modgi, Interaction of fibres and additives in mechanical pulp suspensions, Doctoral dissertation, University of British Columbia, Vancouver, BC, Canada, 2007.
[90]S. Modgi, J. Lauter, M.E. McQuaid, P. Englezos, Assessment of the need for a coagulant (poly DADMAC or PAC) with tapioca or potato starch in mechanical papers filled with PCC, Pulp and Paper Canada 111 (2010) 22-22.
[91]J. Laine, T. Lindstrom, G.G. Nordmark, G. Risinger, Studies on topochemical modification of cellulosic fibres Part 1. Chemical conditions for the attachment of carboxymethyl cellulose onto fibres, Nordic Pulp & Paper Research Journal 15 (2000) 520-526.
[92]J. Laine, T. Lindstrom, G.G. Nordmark, G. Risinger, Studies on topochemical modification of cellulosic fibres - Part 2. The effect of carboxymethyl cellulose attachment on fibre swelling and paper strength, Nordic Pulp & Paper Research Journal 17 (2002) 50-56.
[93]R.A. Stratton, Dependency of sheet properties on the location of adsorbed polymer, Nordic Pulp & Paper Research Journal 4 (1989) 104-112.
[94]L. Gardlund, L. Wagberg, R. Gernandt, Polyelectrolyte complexes for surface modification of wood fibres II. Influence of complexes on wet and dry strength of paper, Colloids and Surfaces A-Physicochemical and Engineering Aspects 218 (2003) 137-149.
[95]R. Gernandt, L. Wagberg, L. Gardlund, H. Dautzenberg, Polyelectrolyte complexes for surface modification of wood fibres - I. Preparation and characterisation of complexes for dry and wet strength improvement of paper, Colloids and Surfaces A-Physicochemical and Engineering Aspects 213 (2003) 15-25.
[96]R. Gaudreault, N. Di Cesare, D. Weitz, T.G.M. van de Ven, Flocculation kinetics of precipitated calcium carbonate, Colloids and Surfaces A-Physicochemical and Engineering Aspects 340 (2009) 56-65.
[97]W. Cheng, K. Broadus, M. Ancona, New technology for increased filler use and fiber savings in graphic grades, 2011 TAPPI PaperCon Conference, TAPPI Press, Covington, KY USA, 2011, pp. 616-620.
[98]S. Tang, Y. Ma, C. Shiu, Modelling the mechanical strength of fractal aggregates, Colloids and Surfaces A-Physicochemical and Engineering Aspects 180 (2001) 7-16.
[99]M. Hermawan, G. Bushell, G. Bickert, R. Amal, Relationship between floc short range structure and sediment compaction, Particle & Particle Systems Characterization 20 (2003) 327-334.
[100]M. Hermawan, G. Bushell, G. Bickert, R. Amal, Characterisation of short-range structure of silica aggregates - implication to sediment compaction, International Journal of Mineral Processing 73 (2004) 65-81.
[101]R. Gaudreault, N. Di Cesare, T.G.M. van de Ven, D.A. Weitz, S.J. Ianson, The structure and strength of flocs of precipitated calcium carbonate induced by various polymers used in papermaking, 14th Fundamental Research Symposium on Advances in Pulp and Paper Research, Oxford, England, 2009, pp. 1193-1219.

[102]A.K.C. Yeung, R. Pelton, Micromechanics: A new approach to studying the strength and breakup of flocs, J.Colloid Interface Sci. 184 (1996) 579-585.
[103]P. Jarvis, B. Jefferson, J. Gregory, S.A. Parsons, A review of floc strength and breakage, Water research 39 (2005) 3121-3137.
[104]H. Liimatainen, A. Haapala, J. Tomperi, J. Niinimaki, Fiber floc morphology and dewaterability of a pulp suspension: Role of flocculation kinetics and characteristics of flocculation agents, Bioresources 4 (2009) 640-658.
[105]Y. Sang, M. McQuaid, P. Englezos, Pre-flocculation of precipitated calcium carbonate filler by cationic starch for highly filled mechanical grade paper, Bioresources 7 (2012) 354-373.
[106]M.V. von Smoluchowski, Mathematical theory of the kinetics of the coagulation of colloidal solutions, Zeitschriftfuer Physikalische Chemie 92 (1917) 129-168.
[107]E. Antunes, F.A.P. Garcia, P. Ferreira, A. Blanco, C. Negro, M.G. Rasteiro, Modelling PCC flocculation by bridging mechanism using population balances: Effect of polymer characteristics on flocculation, Chemical Engineering Science 65 (2010) 3798-3807.
[108]C.A. Biggs, P.A. Lant, Modelling activated sludge flocculation using population balances, Powder Technology 124 (2002) 201-211.
[109]A.R. Heath, P.A. Bahri, P.D. Fawell, J.B. Farrow, Polymer flocculation of calcite: Population balance model, AICHE Journal 52 (2006) 1641-1653.
[110]M.J. Hounslow, R.L. Ryall, V.R. Marshall, A discretized population balance for nucleation, growth, and aggregation, AICHE Journal 34 (1988) 1821-1832.
[111]A.S. Bramley, M.J. Hounslow, R.L. Ryall, Aggregation during precipitation from solution: A method for extracting rates from experimental data, Journal of Colloid and Interface Science 183 (1996) 155-165.
[112]T. Serra, X. Casamitjana, Modeling the aggregation and break-up of fractal aggregates in a shear flow, Applied Scientific Research 59 (1998) 255-268.
[113]J.C. Flesch, P.T. Spicer, S.E. Pratsinis, Laminar and turbulent shear-induced flocculation of fractal aggregates, AICHE Journal 45 (1999) 1114-1124.
[114]C. Selomulya, G. Bushell, R. Amal, T.D. Waite, Understanding the role of restructuring in flocculation: The application of a population balance model, Chemical Engineering Science 58 (2003) 327-338.
[115]K.A. Kusters, J.G. Wijers, D. Thoenes, Aggregation kinetics of small particles in agitated vessels, Chemical Engineering Science 52 (1997) 107-121.
[116]A.R. Heath, P.T.L. Koh, Combined population balance and CFD modelling of particle aggregation by polymeric flocculant, Third International Conference on CFD in the Minerals and Process Industries, CSIRO, Melbourne, Australia, 2003, pp. 339-344.
[117]C.F. Baker, Emerging technologies for fillers and pigments, Pira International, Surrey, UK, 2005.
[118]J. Yoshizawa, A. Isogai, F. Onabe, Analysis and retention behaviour of cationic and amphoteric starches on handsheets, Journal of Pulp and Paper Science 24 (1998) 213-218.

[119]S. Malton, K. Kuys, I. Parker, N. Vanderhoek, Adsorption of cationic starch on eucalypt pulp fibres and fines, Appita Journal 51 (1998) 292-298.
[120]A. Blennow, A.M. Bay-Smidt, P. Leonhardt, O. Bandsholm, M.H. Madsen, Starch paste stickiness is a relevant native starch selection criterion for wet-end paper manufacturing, Starch-Starke 55 (2003) 381-389.
[121]L. Wagberg, K. Kolar, Adsorption of cationic starch on fibres from mechanical pulps, Berichte Der Bunsen-Gesellschaft-Physical Chemistry Chemical Physics 100 (1996) 984-993.
[122]B. Alince, F. Bednar, T.G.M. van de Ven, Deposition of calcium carbonate particles on fiber surfaces induced by cationic polyelectrolyte and bentonite, Colloids and Surfaces A-Physicochemical and Engineering Aspects 190 (2001) 71-80.
[123]C. Ovenden, H.N. Xiao, Flocculation behaviour and mechanisms of cationic inorganic microparticle/polymer systems, Colloids and Surfaces A-Physicochemical and Engineering Aspects 197 (2002) 225-234.
[124]O.J. Rojas, M.A. Hubbe, The dispersion science of papermaking, Journal of Dispersion Science and Technology 25 (2004) 713-732.
[125]Y. Wiputri, Microparticle retention aid systems in mechanical pulp suspensions, M.A.Sc. Thesis, University of British Columbia, Vancouver, BC, Canada, 2008.
[126]Y. Wiputri, P. Englezos, Microparticle retention aid systems in mechanical pulp suspensions, Recent Patents on Engineering 1 (2007) 177-186.
[127]N.K. Singh, A. Parmar, D. Madamwar, Optimization of medium components for increased production of C-phycocyanin from Phormidium ceylanicum and its purification by single step process, Bioresource Technology 100 (2009) 1663-1669.
[128]Y.H. Ni, A review of recent technological advances in the brightening of high-yield pulps, Canadian Journal of Chemical Engineering 83 (2005) 610-617.
[129]M. Preissinger, Interactions of starch with the pulp suspension components, M.A.Sc. Thesis, Technical University of Darmstadt, Darmstadt, Germany, 2009.
[130]Y. Sang, H. Xiao, Clay flocculation improved by cationic poly(vinyl alcohol)/anionic polymer dual-component system, Journal of Colloid and Interface Science 326 (2008) 420-425.
[131]J. Montgomery, The role of suction boxes on forming section retention and filler migration, M.A.Sc. Thesis, The University of British Columbia, Vancouver, BC, Canada, 2010.
[132]A. Khosravani, A.J. Latibari, S.A. Mirshokraei, M. Rahmaninia, M.M. Nazhad, Studying the effect of cationic starch-anionic nanosilica system on retention and drainage, Bioresources 5 (2010) 939-950.
[133]M. Shirazi, T.G.M. van de Ven, G. Garnier, Adsorption of modified starches on porous glass, Langmuir 19 (2003) 10829-10834.
[134]P. Kumar, Y.S. Negi, S.P. Singh, Filler loading in the lumen or/and cell wall of fibers - A literature review, BioResources 6 (2011) 3526-3546.

[135]V. Nguyen, W. Yoshida, Y. Cohen, Graft polymerization of vinyl acetate onto silica, J Appl Polym Sci 87 (2003) 300-310.
[136]Y. Sang, H. Xiao, Preparation and application of cationic cellulose fibers modified by in situ grafting of cationic PVA, Colloids and Surfaces A-Physicochemical and Engineering Aspects 335 (2009) 121-127.
[137]Y. Sang, P. Englezos, Flocculation of precipitated calcium carbonate (PCC) by cationic tapioca starch with different charge densities. I: Experimental, Colloids and Surfaces A: Physicochemical and Engineering Aspects (2012) DOI: 10.1016/j.colsurfa.2012.07.019.
[138]Y. Sang, P. Englezos, Flocculation of precipitated calcium carbonate (PCC) by cationic tapioca starch with different charge densities. II: Population balance modeling, Colloids and Surfaces A: Physicochemical and Engineering Aspects (2012) DOI: 10.1016/j.colsurfa.2012.07.028.
[139]S. Modgi, M.E. McQuaid, P. Englezos, Interaction of precipitated calcium carbonate (PCC) with starch in distilled and deionized water (DDW) and process water (PW), Nordic Pulp & Paper Research Journal 21 (2006) 716-723.
[140]M.G. Rasteiro, F.A.P. Garcia, P.J. Ferreira, E. Antunes, D. Hunkeler, C. Wandrey, Flocculation by cationic polyelectrolytes: Relating efficiency with polyelectrolyte characteristics, Journal of Applied Polymer Science 116 (2010) 3603-3612.
[141]N. Zakrajsek, E. Fuente, A. Blanco, J. Golob, Influence of cationic starch adsorption on fiber flocculation, Chem. Eng. Technol. 32 (2009) 1259-1265.
[142]P. Pang, P. Englezos, Kinetics of the aggregation of polyethylene oxide at temperatures above the polyethylene oxide-water cloud point temperature, Colloids and Surfaces A-Physicochemical and Engineering Aspects 204 (2002) 23-30.
[143]P.A. Tam Doo, R.J. Kerekes, R.H. Pelton, Estimates of maximum hydrodynamic shear stresses on fiber surfaces in papermaking, J. Pulp Paper Sci. 10 (1984) J80-J88.
[144]J.Y. Oldshue, Fluid mixing technology, McGraw Hill Publication Co., New York, 1982.
[145]J.A.S. Perez, E.M.R. Porcel, J.L.C. Lopez, J.M.F. Sevilla, Y. Chisti, Shear rate in stirred tank and bubble column bioreactors, Chemical Engineering Journal 124 (2006) 1-5.
[146]K. Muhle, B. Dobias, Floc stability in laminar and turbulent flow, Coagulation and Flocculation: Theory and Applications, Marcel Dekker, 1993, pp. 355-390.
[147]W.L. McCabe, J.C. Smith, P. Harriott, Unit operations of chemical engineering (5th edition), McGraw-Hill, 1993.
[148]J. Teixeira, Small-angle scattering by fractal systems, Journal of Applied Crystallography 21 (1988) 781-785.
[149]G.C. Bushell, Y.D. Yan, D. Woodfield, J. Raper, R. Amal, On techniques for the measurement of the mass fractal dimension of aggregates, Advances in Colloid and Interface Science 95 (2002) 1-50.
[150]N.H.G. Rahmani, T. Dabros, J.H. Masliyah, Online optical monitoring of asphaltene aggregation, Industrial & Engineering Chemistry Research 44 (2005) 75-84.

[151]P. Meakin, Fractal aggregates, Advances in Colloid and Interface Science 28 (1988) 249-331.
[152]M.M. Clark, J.R.V. Flora, Floc restructuring in varied turbulent mixing, Journal of Colloid and Interface Science 147 (1991) 407-421.
[153]F.E. Torres, W.B. Russel, W.R. Schowalter, Simulations of coagulation in viscous flows, Journal of Colloid and Interface Science 145 (1991) 51-73.
[154]A. Blanco, C. Negro, A. Hooimeijer, J. Tijero, Polymer optimization in paper mills by means of a particle size analyser: An alternative to zeta potential measurements, Appita Journal 49 (1996) 113-116.
[155]V.K. La Mer, T.W. Healy, Adsorption-flocculation reactions of macromolecules at solid-liquid interface, Review of Pure and Applied Chemistry 13 (1963) 112-133.
[156]R. Hogg, Collision efficiency factors for polymer flocculation, Journal of Colloid and Interface Science 102 (1984) 232-236.
[157]M.P. Nedelcheva, G.V. Stoilkov, Cationic starch adsorption by cellulose, Journal of Colloid and Interface Science 66 (1978) 475-482.
[158]A.A. Adetayo, J.D. Litster, S.E. Pratsinis, B.J. Ennis, Population balance modeling of drum granulation of materials with wide size distribution, Powder Technology 82 (1995) 37-49.
[159]M.J. Hounslow, J.M.K. Pearson, T. Instone, Tracer studies of high-shear granulation: II. Population balance modeling, AICHE Journal 47 (2001) 1984-1999.
[160]H.S. Tan, M.J.V. Goldschmidt, R. Boerefijn, M.J. Hounslow, A.D. Salman, J.A.M. Kuipers, Population balance modelling of fluidized bed melt granulation - An overview, Chemical Engineering Research & Design 83 (2005) 871-880.
[161]J.R.V. Gooch, M.J. Hounslow, Monte Carlo simulation of size-enlargement mechanisms in crystallization, AICHE Journal 42 (1996) 1864-1874.
[162]B.J. McCoy, A population balance framework for nucleation, growth, and aggregation, Chemical Engineering Science 57 (2002) 2279-2285.
[163]S. Qamar, G. Warnecke, M.P. Elsner, On the solution of population balances for nucleation, growth, aggregation and breakage processes, Chemical Engineering Science 64 (2009) 2088-2095.
[164]M.J. Hounslow, A.E. Lewis, S.J. Sanders, R. Bondy, Generic crystallizer model: 1. A model framework for a well-mixed compartment, AICHE Journal 51 (2005) 2942-2955.
[165]Y. Xiong, S.E. Pratsinis, Formation of agglomerate particles by coagulation and sintering. 1. A 2-dimensional solution of the population balance equation, Journal of Aerosol Science 24 (1993) 283-300.
[166]Y. Xiong, M.K. Akhtar, S.E. Pratsinis, Formation of agglomerate particles by coagulation and sintering. 2. The evolution of the morphology of aerosol-made titania, silica and silica-doped titania powders, Journal of Aerosol Science 24 (1993) 301-313.
[167]H.J. Schmid, B. Al-Zaitone, C. Artelt, W. Peukert, Evolution of the fractal dimension for simultaneous coagulation and sintering, Chemical Engineering Science 61 (2006) 293-305.

[168]T. Hamalainen, J. Hamalainen, Fibre floc evolution model, Part I: Flocculation in a headbox, Nordic Pulp & Paper Research Journal 25 (2010) 39-47.
[169]P.T. Spicer, S.E. Pratsinis, Coagulation and fragmentation: Universal steady-state particle-size distribution, AICHE Journal 42 (1996) 1612-1620.
[170]T.A. Kramer, M.M. Clark, Incorporation of aggregate breakup in the simulation of orthokinetic coagulation, Journal of Colloid and Interface Science 216 (1999) 116-126.
[171]P. Somasundaran, V. Runkana, Modeling flocculation of colloidal mineral suspensions using population balances, International Journal of Mineral Processing 72 (2003) 33-55.
[172]A. Ding, M.J. Hounslow, C.A. Biggs, Population balance modelling of activated sludge flocculation: Investigating the size dependence of aggregation, breakage and collision efficiency, Chemical Engineering Science 61 (2006) 63-74.
[173]M.R. Wiesner, Kinetics of aggregate formation in rapid mix, Water Research 26 (1992) 379-387.
[174]V. Oles, Shear-induced aggregation and breakup of polystyrene latex-particles Journal of Colloid and Interface Science 154 (1992) 351-358.
[175]P. Marsh, G. Bushell, R. Amal, Scattering behavior of restructured aggregates: A simulation study, Journal of Colloid and Interface Science 241 (2001) 286-288.
[176]R. Jullien, P. Meakin, Simple models for the restructuring of 3-dimensional ballistic aggregates, Journal of Colloid and Interface Science 127 (1989) 265-272.
[177]M. Soos, J. Sefcik, M. Morbidelli, Investigation of aggregation, breakage and restructuring kinetics of colloidal dispersions in turbulent flows by population balance modeling and static light scattering, Chemical Engineering Science 61 (2006) 2349-2363.
[178]H. Rahimi, A.R.S. Nazar, Asphaltene aggregates fractal restructuring model, a population balance approach, Energy & Fuels 24 (2010) 1088-1093.
[179]A.R. Solaimany-Nazar, H. Rahimi, Dynamic determination of asphaltene aggregate size distribution in shear induced organic solvents, Energy & Fuels 22 (2008) 3435-3442.
[180]C. Selomulya, R. Amal, G. Bushell, T.D. Waite, Evidence of shear rate dependence on restructuring and breakup of latex aggregates, Journal of Colloid and Interface Science 236 (2001) 67-77.
[181]D.S. Parker, A.M. Asce, W.J. Kaufman, D. Jenkins, Floc breakup in turbulent flocculation processes, Journal of the Sanitary Engineering Division-ASCE 98 (1972) 79-99.
[182]T.G.M. van de Ven, Effects of polymer bridging on selective shear flocculation, Journal of Colloid and Interface Science 81 (1981) 290-291.
[183]E. Bonanomi, J. Sefcik, M. Morari, M. Morbidelli, Analysis and control of a turbulent coagulator, Industrial & Engineering Chemistry Research 43 (2004) 6112-6124.
[184]L.B. Brakalov, A connection between the orthokinetic coagulation capture efficiency of aggregates and their maximum size, Chemical Engineering Science 42 (1987) 2373-2383.

[185]D.L. Swift, S.K. Friedlander, The coagulation of hydrosols by Brownian motion + laminar shear flow, Journal of Colloid Science 19 (1964) 621-647.
[186]P.G. Saffman, J.S. Turner, On the collision of drops in turbulent clouds, Journal of Fluid Mechanics 1 (1956) 16-30.
[187]Q. Jiang, B.E. Logan, Fractal dimensions of aggregates determined from steady-state size distributions, Environmental Science & Technology 25 (1991) 2031-2038.
[188]K.A. Kusters, The influence of turbulence on aggregation of small particles in agitated vessels, Doctoral dissertation, Eindhoven University of Technology, Netherlands, 1991.
[189]N. Tambo, Y. Watanabe, Physical characteristics of flocs .1. Floc density-function and aluminum floc, Water research 13 (1979) 409-419.
[190]M.Y. Lin, R. Klein, H.M. Lindsay, D.A. Weitz, R.C. Ball, P. Meakin, The structure of fractal colloidal aggregates of finite extent, Journal of Colloid and Interface Science 137 (1990) 263-280.
[191]C. Selomulya, G. Bushell, R. Amal, T.D. Waite, Aggregation mechanisms of latex of different particle sizes in a controlled shear environment, Langmuir 18 (2002) 1974-1984.
[192]H. Rumpf, W.A. Knepper, The strength of granules and agglomerates, Agglomeration, Interscience Publishers, New York, 1962, pp. 379-418.
[193]S. Agarwal, Efficiency of shear-induced agglomeration of particulate suspensions subjected to bridging flocculation, Doctoral dissertation, West Virginia University, Morgantown, West Virginia, 2002, p. 138.
[194]C.S.B. Fitzpatrick, E. Fradin, J. Gregory, Temperature effects on flocculation, using different coagulants, Water Science and Technology 50 (2004) 171-175.
[195]D.H. Bache, C. Johnson, J.F. McGilligan, E. Rasool, A conceptual view of floc structure in the sweep floc domain, Water Science and Technology 36 (1997) 49-56.
[196]S. Agarwal, R.K. Gupta, D. Doraiswamy, A model for the collision efficiency of shear-induced agglomeration involving polymer bridging, Colloids and Surfaces A-Physicochemical and Engineering Aspects 345 (2009) 224-230.

Appendices

Appendix A: Chapter 2 ANOVA results for the retention systems (conventional chemical addition sequence)

Table A1 ANOVA for total retention using S858

Source	DF	Sum of Squares	F Ratio	Prob > F	Comments
PCC	1	13.95375	46.5608	<.0001	extremely statistically significant
Starch	1	6.72042	22.4246	0.0004	extremely statistically significant
CPAM	1	136.80375	456.486	<.0001	extremely statistically significant
Silica	1	49.88167	166.445	<.0001	extremely statistically significant
PCC*Starch	1	0.39062	1.3034	0.2742	---
PCC*CPAM	1	0	0	1	---
Starch*CPAM	1	1.05062	3.5057	0.0838	---
PCC*Silica	1	0.18063	0.6027	0.4514	---
Starch*Silica	1	3.0625	10.2189	0.007	very statistically significant
CPAM*Silica	1	0.03063	0.1022	0.7543	---
PCC*PCC	1	0.52646	1.7567	0.2079	---
Starch*Starch	1	0.31574	1.0536	0.3234	---
CPAM*CPAM	1	0.83003	2.7696	0.12	---
Silica*Silica	1	0.07146	0.2384	0.6335	---

RSquare=0.982359; RSquare Adj=0.960647; Root Mean Square Error=0.547439; Mean of Response=89.47333; DF: Degree of freedom; ---: Not statistically significant

Table A2 ANOVA for filler retention using S858

Source	DF	Sum of Squares	F Ratio	Prob > F	Comments
PCC	1	20.25844	44.1573	<.0001	extremely statistically significant
Starch	1	13.4251	29.2627	0.0001	extremely statistically significant
CPAM	1	260.37094	567.5304	<.0001	extremely statistically significant
Silica	1	109.01344	237.6165	<.0001	extremely statistically significant
PCC*Starch	1	2.28766	4.9864	0.0438	statistically significant
PCC*CPAM	1	1.65766	3.6132	0.0797	---
Starch*CPAM	1	2.76391	6.0245	0.029	statistically significant
PCC*Silica	1	1.47016	3.2045	0.0967	---
Starch*Silica	1	4.89516	10.67	0.0061	very statistically significant
CPAM*Silica	1	0.21391	0.4663	0.5067	---
PCC*PCC	1	0.11626	0.2534	0.6231	---
Starch*Starch	1	0.63876	1.3923	0.2592	---
CPAM*CPAM	1	3.07626	6.7053	0.0225	statistically significant
Silica*Silica	1	0.00019	0.0004	0.9842	---

RSquare=0.986096; RSquare Adj=0.968982; Root Mean Square Error=0.677332; Mean of Response=88.78333

DF: Degree of freedom; ---: Not statistically significant

Table A3 ANOVA for drainage using S858

Source	DF	Sum of Squares	F Ratio	Prob > F	Comments
PCC	1	2480.667	37.478	<.0001	extremely statistically significant
Starch	1	368.167	5.5623	0.0347	statistically significant
CPAM	1	28290.667	427.42	<.0001	extremely statistically significant
Silica	1	20827.042	314.66	<.0001	extremely statistically significant
PCC*Starch	1	105.062	1.5873	0.2299	---
PCC*CPAM	1	85.562	1.2927	0.2761	---
Starch*CPAM	1	150.062	2.2672	0.156	---
PCC*Silica	1	324	4.895	0.0454	statistically significant
Starch*Silica	1	0.25	0.0038	0.9519	---
CPAM*Silica	1	361	5.454	0.0362	statistically significant
PCC*PCC	1	542.646	8.1984	0.0133	statistically significant
Starch*Starch	1	1.074	0.0162	0.9006	---
CPAM*CPAM	1	13.36	0.2018	0.6606	---
Silica*Silica	1	199.646	3.0163	0.1061	---

RSquare=0.984277; RSquare Adj=0.964927; Root Mean Square Error=8.135688; Mean of response=560.4333; DF: Degree of freedom; ---: Not statistically significant

Table A4 ANOVA for total retention using S880

Source	DF	Sum of Squares	F Ratio	Prob > F	Comments
PCC	1	12.760417	12.1455	0.004	very statistically significant
Starch	1	50.170417	47.7528	<.0001	extremely statistically significant
CPAM	1	3.450417	3.2841	0.0931	---
Silica	1	29.70375	28.2724	0.0001	extremely statistically significant
PCC*Starch	1	0.390625	0.3718	0.5525	---
PCC*CPAM	1	0.765625	0.7287	0.4087	---
Starch*CPAM	1	0.680625	0.6478	0.4354	---
PCC*Silica	1	2.030625	1.9328	0.1878	---
Starch*Silica	1	7.425625	7.0678	0.0197	statistically significant
CPAM*Silica	1	0.525625	0.5003	0.4919	---
PCC*PCC	1	2.915744	2.7752	0.1196	---
Starch*Starch	1	0.21503	0.2047	0.6584	---
CPAM*CPAM	1	1.401458	1.3339	0.2689	---
Silica*Silica	1	0.526458	0.5011	0.4915	---

RSquare=0.899597; RSquare Adj=0.776024; Root Mean Square Error=1.025002; Mean of Response=85.42333; DF: Degree of freedom; ---: Not statistically significant

Table A5 ANOVA for filler retention using S880

Source	DF	Sum of Squares	F Ratio	Prob > F	Comments
PCC	1	83.25375	31.9339	<.0001	extremely statistically significant
Starch	1	122.85375	47.1234	<.0001	extremely statistically significant
CPAM	1	8.28375	3.1774	0.098	---
Silica	1	65.01042	24.9363	0.0002	extremely statistically significant
PCC*Starch	1	0.45562	0.1748	0.6827	---
PCC*CPAM	1	1.38063	0.5296	0.4797	---
Starch*CPAM	1	2.64062	1.0129	0.3326	---
PCC*Silica	1	1.15563	0.4433	0.5172	---
Starch*Silica	1	15.01562	5.7596	0.0321	statistically significant
CPAM*Silica	1	2.48062	0.9515	0.3471	---
PCC*PCC	1	4.18527	1.6054	0.2274	---
Starch*Starch	1	1.93527	0.7423	0.4045	---
CPAM*CPAM	1	4.18527	1.6054	0.2274	---
Silica*Silica	1	1.1317	0.4341	0.5215	---

RSquare=0.912816; RSquare Adj=0.805513; Root Mean Square Error=1.614641; Mean of Response=82.3

DF: Degree of freedom; ---: Not statistically significant

Table A6 ANOVA for drainage using S880

Source	DF	Sum of Squares	F Ratio	Prob > F	Comments
PCC	1	1734	5.6449	0.0336	statistically significant
Starch	1	10837.5	35.2805	<.0001	extremely statistically significant
CPAM	1	44376	144.462	<.0001	extremely statistically significant
Silica	1	39690.667	129.21	<.0001	extremely statistically significant
PCC*Starch	1	272.25	0.8863	0.3637	---
PCC*CPAM	1	81	0.2637	0.6162	---
Starch*CPAM	1	462.25	1.5048	0.2417	---
PCC*Silica	1	20.25	0.0659	0.8014	---
Starch*Silica	1	256	0.8334	0.3779	---
CPAM*Silica	1	240.25	0.7821	0.3926	---
PCC*PCC	1	1064.298	3.4647	0.0855	---
Starch*Starch	1	86.012	0.28	0.6056	---
CPAM*CPAM	1	332.012	1.0808	0.3175	---
Silica*Silica	1	0.583	0.0019	0.9659	---

RSquare=0.963491; RSquare Adj=0.918556; Root Mean Square Error=17.52657; Mean of Response=649.7667; DF: Degree of freedom; ---: Not statistically significant

Appendix B: Chapter 3 ANOVA results for the retention systems (PCC preflocculation strategy)

Table B1 ANOVA for total retention using S858

Source	DF	Sum of Squares	F Ratio	Prob > F	Comments
PCC	1	28.601667	26.6673	0.0002	extremely statistically significant
Starch	1	0.041667	0.0388	0.8468	----
CPAM	1	33.606667	31.3338	<.0001	extremely statistically significant
Silica	1	80.666667	75.211	<.0001	extremely statistically significant
PCC*Starch	1	0.9025	0.8415	0.3757	----
PCC*CPAM	1	0.1225	0.1142	0.7408	----
Starch*CPAM	1	2.7225	2.5384	0.1351	----
PCC*Silica	1	1.96	1.8274	0.1995	----
Starch*Silica	1	0.16	0.1492	0.7056	----
CPAM*Silica	1	0.04	0.0373	0.8499	----
PCC*PCC	1	1.950476	1.8186	0.2005	----
Starch*Starch	1	2.201905	2.053	0.1755	----
CPAM*CPAM	1	3.440476	3.2078	0.0966	----
Silica*Silica	1	0.190476	0.1776	0.6803	----

RSquare = 0.920828; RSquare Adj = 0.823385; Root Mean Square Error = 1.035634; Mean of Response = 88.83667; DF: Degree of Freedom; ----: Not statistically significant

Table B2 ANOVA for filler retention using S858

Source	DF	Sum of Squares	F Ratio	Prob > F	Comments
PCC	1	10.53375	6.5693	0.0236	statistically significant
Starch	1	1.76042	1.0979	0.3138	----
CPAM	1	66.33375	41.3688	<.0001	extremely statistically significant
Silica	1	174.42042	108.7766	<.0001	extremely statistically significant
PCC*Starch	1	0.52562	0.3278	0.5767	----
PCC*CPAM	1	1.75562	1.0949	0.3145	----
Starch*CPAM	1	6.37562	3.9761	0.0676	----
PCC*Silica	1	0.05063	0.0316	0.8617	----
Starch*Silica	1	0.45563	0.2841	0.6030	----
CPAM*Silica	1	0.05063	0.0316	0.8617	----
PCC*PCC	1	0.49527	0.3089	0.5878	----
Starch*Starch	1	0.02170	0.0135	0.9092	----
CPAM*CPAM	1	3.30027	2.0582	0.1750	----
Silica*Silica	1	3.66670	2.2867	0.1544	----

RSquare = 0.93075; RSquare Adj = 0.84552; Root Mean Square Error = 1.266284; Mean of Response = 87.95333

DF: Degree of Freedom; ----: Not statistically significant

Table B3 ANOVA for drainage using S858

Source	DF	Sum of Squares	F Ratio	Prob > F	Comments
PCC	1	4004.167	19.5218	0.0007	extremely statistically significant
Starch	1	3504.167	17.0841	0.0012	very statistically significant
CPAM	1	10584.000	51.6009	<.0001	extremely statistically significant
Silica	1	28290.667	137.9273	<.0001	extremely statistically significant
PCC*Starch	1	4.000	0.0195	0.8911	----
PCC*CPAM	1	49.000	0.2389	0.6331	----
Starch*CPAM	1	49.000	0.2389	0.6331	----
PCC*Silica	1	1332.250	6.4952	0.0243	statistically significant
Starch*Silica	1	156.250	0.7618	0.3986	----
CPAM*Silica	1	90.250	0.4400	0.5187	----
PCC*PCC	1	1551.440	7.5638	0.0165	statistically significant
Starch*Starch	1	63.440	0.3093	0.5876	----
CPAM*CPAM	1	70.583	0.3441	0.5675	----
Silica*Silica	1	293.440	1.4306	0.2530	----

RSquare = 0.951633; RSquare Adj = 0.892104; Root Mean Square Error = 14.32176; Mean of Response = 568.9333

DF: Degree of Freedom; ----: Not statistically significant

Table B4 ANOVA for total retention using S880

Source	DF	Sum of Squares	F Ratio	Prob > F	Comments
PCC	1	8.760417	13.0127	0.0032	very statistically significant
Starch	1	18.200417	27.0350	0.0002	extremely statistically significant
CPAM	1	23.403750	34.7640	<.0001	extremely statistically significant
Silica	1	25.833750	38.3735	<.0001	extremely statistically significant
PCC*Starch	1	0.050625	0.0752	0.7882	----
PCC*CPAM	1	0.140625	0.2089	0.6552	----
Starch*CPAM	1	0.455625	0.6768	0.4255	----
PCC*Silica	1	0.600625	0.8922	0.3621	----
Starch*Silica	1	0.225625	0.3351	0.5725	----
CPAM*Silica	1	0.275625	0.4094	0.5334	----
PCC*PCC	1	7.351458	10.9199	0.0057	very statistically significant
Starch*Starch	1	0.008601	0.0128	0.9117	----
CPAM*CPAM	1	0.055030	0.0817	0.7795	----
Silica*Silica	1	0.660744	0.9815	0.3399	----

RSquare = 0.912505; RSquare Adj = 0.804819; Root Mean Square Error = 0.820499; Mean of Response = 92.83333

DF: Degree of Freedom; ----: Not statistically significant

Table B5 ANOVA for filler retention using S880

Source	DF	Sum of Squares	F Ratio	Prob > F	Comments
PCC	1	23.010417	131.555	<.0001	extremely statistically significant
Starch	1	32.433750	185.308	<.0001	extremely statistically significant
CPAM	1	43.470417	248.5298	<.0001	extremely statistically significant
Silica	1	46.203750	264.1569	<.0001	extremely statistically significant
PCC*Starch	1	0.330625	1.8903	0.1924	----
PCC*CPAM	1	0.390625	2.2333	0.1589	----
Starch*CPAM	1	1.050625	6.0067	0.0292	statistically significant
PCC*Silica	1	0.005625	0.0322	0.8604	----
Starch*Silica	1	0.390625	2.2333	0.1589	----
CPAM*Silica	1	0.765625	4.3772	0.0566	----
PCC*PCC	1	0.660744	3.7776	0.0739	----
Starch*Starch	1	0.303601	1.7358	0.2104	----
CPAM*CPAM	1	0.050030	0.2860	0.6018	----
Silica*Silica	1	3.965030	22.6689	0.0004	extremely statistically significant

RSquare = 0.98575; RSquare Adj = 0.968212; Root Mean Square Error = 0.418223; Mean of Response = 92.60333

DF: Degree of Freedom; ----: Not statistically significant

Table B6 ANOVA for drainage using S880

Source	DF	Sum of Squares	F Ratio	Prob > F	Comments
PCC	1	4732.042	28.7929	0.0001	extremely statistically significant
Starch	1	17876.042	108.7698	<.0001	extremely statistically significant
CPAM	1	15150.375	92.1850	<.0001	extremely statistically significant
Silica	1	37842.042	230.2564	<.0001	extremely statistically significant
PCC*Starch	1	27.562	0.1677	0.6888	----
PCC*CPAM	1	495.062	3.0123	0.1063	----
Starch*CPAM	1	390.062	2.3734	0.1474	----
PCC*Silica	1	27.562	0.1677	0.6888	----
Starch*Silica	1	7.563	0.0460	0.8335	----
CPAM*Silica	1	410.063	2.4951	0.1382	----
PCC*PCC	1	314.360	1.9128	0.1899	----
Starch*Starch	1	108.574	0.6606	0.4310	----
CPAM*CPAM	1	15.003	0.0913	0.7673	----
Silica*Silica	1	584.074	3.5539	0.0820	----

RSquare = 0.973622; RSquare Adj = 0.941156; Root Mean Square Error = 12.81981; Mean of Response = 654.5

DF: Degree of Freedom; ----: Not statistically significant

Table B7 ANOVA for total retention using X880

Source	DF	Sum of Squares	F Ratio	Prob > F	Comments
PCC	1	10.666667	54.0751	<.0001	extremely statistically significant
Starch	1	17.001667	86.1907	<.0001	extremely statistically significant
CPAM	1	33.606667	170.3705	<.0001	extremely statistically significant
Silica	1	51.041667	258.7580	<.0001	extremely statistically significant
PCC*Starch	1	0.122500	0.6210	0.4448	----
PCC*CPAM	1	0.810000	4.1063	0.0637	----
Starch*CPAM	1	0.562500	2.8516	0.1151	----
PCC*Silica	1	1.440000	7.3001	0.0181	statistically significant
Starch*Silica	1	0.302500	1.5335	0.2375	----
CPAM*Silica	1	0.090000	0.4563	0.5112	----
PCC*PCC	1	0.026786	0.1358	0.7184	----
Starch*Starch	1	0.001071	0.0054	0.9424	----
CPAM*CPAM	1	0.026786	0.1358	0.7184	----
Silica*Silica	1	0.009643	0.0489	0.8284	----

RSquare = 0.978595; RSquare Adj = 0.952251; Root Mean Square Error = 0.444136; Mean of Response = 90.33

DF: Degree of Freedom; ----: Not statistically significant

Table B8 ANOVA for filler retention using X880

Source	DF	Sum of Squares	F Ratio	Prob > F	Comments
PCC	1	24.401667	82.4024	<.0001	extremely statistically significant
Starch	1	26.881667	90.7771	<.0001	extremely statistically significant
CPAM	1	69.360000	234.2229	<.0001	extremely statistically significant
Silica	1	94.406667	318.8034	<.0001	extremely statistically significant
PCC*Starch	1	0.062500	0.2111	0.6535	----
PCC*CPAM	1	0.002500	0.0084	0.9282	----
Starch*CPAM	1	0.902500	3.0477	0.1044	----
PCC*Silica	1	0.022500	0.0760	0.7872	----
Starch*Silica	1	0.562500	1.8995	0.1914	----
CPAM*Silica	1	0.562500	1.8995	0.1914	----
PCC*PCC	1	1.214405	4.1009	0.0639	----
Starch*Starch	1	0.100119	0.3381	0.5709	----
CPAM*CPAM	1	0.414405	1.3994	0.258	----
Silica*Silica	1	0.820119	2.7695	0.12	----

RSquare = 0.983116; RSquare Adj = 0.962336; Root Mean Square Error = 0.544177; Mean of Response = 88.99667

DF: Degree of Freedom; ----: Not statistically significant

Table B9 ANOVA for drainage using X880

Source	*DF*	*Sum of Squares*	*F Ratio*	*Prob > F*	Comments
PCC	1	7597.042	71.7058	<.0001	extremely statistically significant
Starch	1	9009.375	85.0363	<.0001	extremely statistically significant
CPAM	1	11051.042	104.307	<.0001	extremely statistically significant
Silica	1	17120.042	161.59	<.0001	extremely statistically significant
PCC*Starch	1	52.563	0.4961	0.4936	----
PCC*CPAM	1	430.562	4.0639	0.065	----
Starch*CPAM	1	52.563	0.4961	0.4936	----
PCC*Silica	1	10.563	0.0997	0.7572	----
Starch*Silica	1	540.562	5.1022	0.0417	statistically significant
CPAM*Silica	1	175.563	1.6571	0.2204	----
PCC*PCC	1	13.36	0.1261	0.7282	----
Starch*Starch	1	568.36	5.3645	0.0375	statistically significant
CPAM*CPAM	1	235.003	2.2181	0.1603	----
Silica*Silica	1	396.503	3.7424	0.0751	----

RSquare = 0.972004; RSquare Adj = 0.937548; Root Mean Square Error = 10.29308; Mean of Response = 564.5333; DF: Degree of Freedom; ----: Not statistically significant

Appendix C: Chapter 4 ANOVA results for PCC flocculation

Table C1 ANOVA for floc size induced by S858

Source	DF	Sum of Squares	F Ratio	Prob > F	Comments
T	1	721.8041	4.6495	0.0504	---
NaCl	1	39.501	0.2544	0.6224	---
Shear Rate	1	2959.8823	19.0662	0.0008	extremely statistically significant
Starch	1	148.902	0.9592	0.3453	---
T*NaCl	1	155.3887	1.0009	0.3353	---
T*Shear Rate	1	1.5675	0.0101	0.9215	---
NaCl*Shear Rate	1	106.0797	0.6833	0.4234	---
T*Starch	1	2592.8973	16.7023	0.0013	very statistically significant
NaCl*Starch	1	144.9134	0.9335	0.3516	---
Shear Rate*Starch	1	30.5864	0.197	0.6644	---
T*T	1	379.5675	2.445	0.1419	---
NaCl*NaCl	1	185.6847	1.1961	0.294	---
Shear Rate*Shear Rate	1	119.4527	0.7695	0.3963	---
Starch*Starch	1	9.9237	0.0639	0.8044	---

RSquare=0.792964; RSquare Adj=0.53815; Root Mean Square Error=12.45962; Mean of Response=63.8478; DF: Degree of freedom; ---: Not statistically significant

Table C2 ANOVA for mass fractal dimension induced by S858

Source	DF	Sum of Squares	F Ratio	Prob > F	Comments
T	1	0.00770417	0.6966	0.419	---
NaCl	1	0.0108375	0.9799	0.3403	---
Shear Rate	1	0.0030375	0.2746	0.6091	---
Starch	1	0.1890375	17.0922	0.0012	very significant
T*NaCl	1	0.02805625	2.5368	0.1352	---
T*Shear Rate	1	0.03150625	2.8487	0.1153	---
NaCl*Shear Rate	1	0.00950625	0.8595	0.3708	---
T*Starch	1	0.00005625	0.0051	0.9442	---
NaCl*Starch	1	0.00180625	0.1633	0.6927	---
Shear Rate*Starch	1	0.00005625	0.0051	0.9442	---
T*T	1	0.03921696	3.5459	0.0823	---
NaCl*NaCl	1	0.04185268	3.7842	0.0737	---
Shear Rate*Shear Rate	1	0.05027411	4.5456	0.0527	---
Starch*Starch	1	0.04738125	4.2841	0.059	---

RSquare=0.753327; RSquare Adj=0.449729; Root Mean Square Error=0.105166; Mean of Response=2.241; DF: Degree of freedom; ---: Not statistically significant

Table C3 ANOVA for floc size induced by S880

Source	DF	Sum of Squares	F Ratio	Prob > F	Comments
T	1	119.7245	0.5508	0.4712	---
NaCl	1	3136.941	14.4325	0.0022	Very Significant
Shear Rate	1	2521.418	11.6006	0.0047	Very Significant
Starch	1	2137.745	9.8353	0.0079	Very Significant
T*NaCl	1	1521.156	6.9985	0.0202	Significant
T*Shear Rate	1	0.1376	0.0006	0.9803	---
NaCl*Shear Rate	1	13.5829	0.0625	0.8065	---
T*Starch	1	2.5648	0.0118	0.9152	---
NaCl*Starch	1	690.2705	3.1758	0.0981	---
Shear Rate*Starch	1	161.7221	0.7441	0.404	---
T*T	1	1452.032	6.6805	0.0227	Significant
NaCl*NaCl	1	288.9608	1.3295	0.2697	---
Shear Rate*Shear Rate	1	352.0799	1.6199	0.2254	---
Starch*Starch	1	317.3347	1.46	0.2485	---

RSquare=0.833577; RSquare Adj=0.628749; Root Mean Square Error=14.74291; Mean of Response=102.3637; DF: Degree of freedom; ---: Not statistically significant

Table C4 ANOVA for mass fractal dimension induced by S880

Source	DF	Sum of Squares	F Ratio	Prob > F	Comments
T	1	0.01215	1.0661	0.3207	---
NaCl	1	0.016017	1.4054	0.257	---
Shear Rate	1	0.01215	1.0661	0.3207	---
Starch	1	0.0486	4.6701	0.0499	Significant
T*NaCl	1	0.0361	3.1676	0.0985	---
T*Shear Rate	1	0	0	1	---
NaCl*Shear Rate	1	0.0001	0.0088	0.9268	---
T*Starch	1	0.030625	2.6872	0.1251	---
NaCl*Starch	1	0.000025	0.0022	0.9634	---
Shear Rate*Starch	1	0.011025	0.9674	0.3433	---
T*T	1	0.032019	2.8095	0.1176	---
NaCl*NaCl	1	0.016019	1.4056	0.257	---
Shear Rate*Shear Rate	1	0.032019	2.8095	0.1176	---
Starch*Starch	1	0.001219	0.107	0.7488	---

RSquare=0.631992; RSquare Adj =0.17906; Root Mean Square Error=0.106755; Mean of Response=2.290667; DF: Degree of freedom; ---: Not statistically significant

Appendix D: Chapter 4 Experimental PCC flocculation kinetics by starch

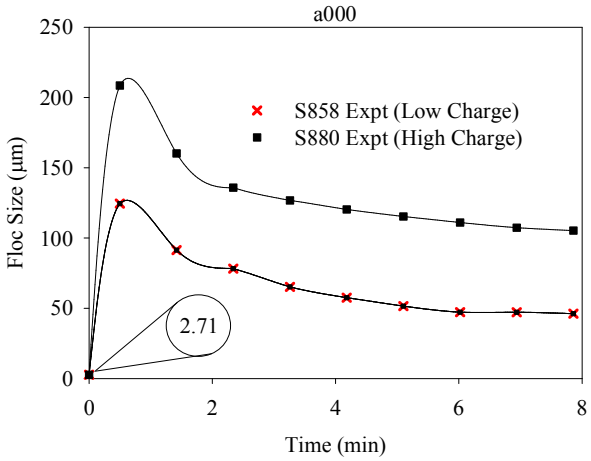

Fig. D1. Flocculation kinetics induced by S858 and S880 at condition "a000"

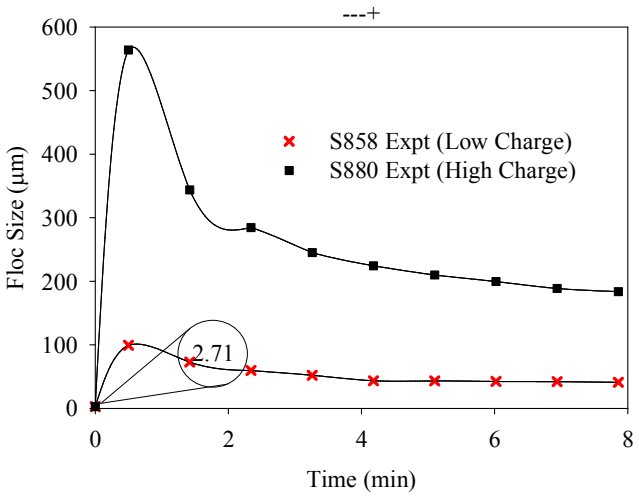

Fig. D2. Flocculation kinetics induced by S858 and S880 at condition "---+"

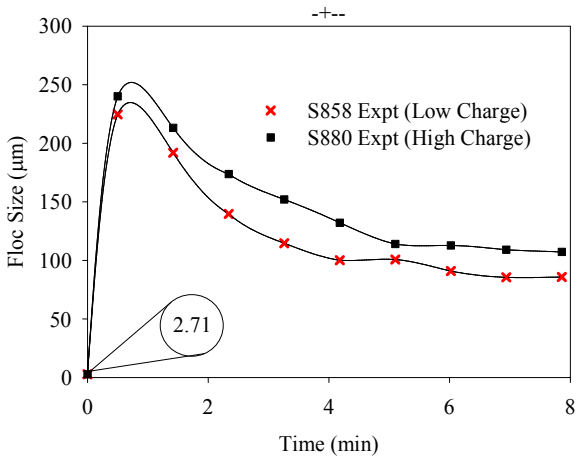

Fig. D3. Flocculation kinetics induced by S858 and S880 at condition "-+--"

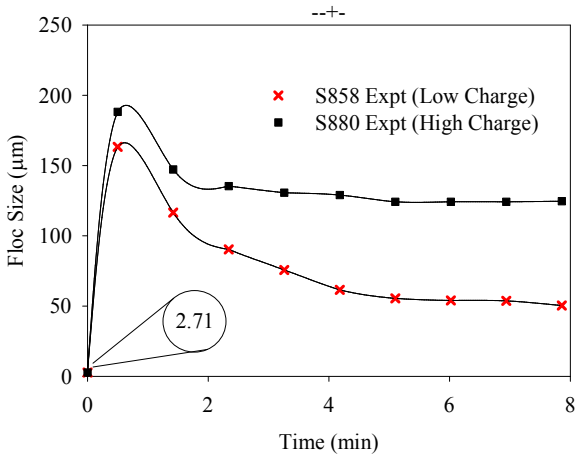

Fig. D4. Flocculation kinetics induced by S858 and S880 at condition "--+-"

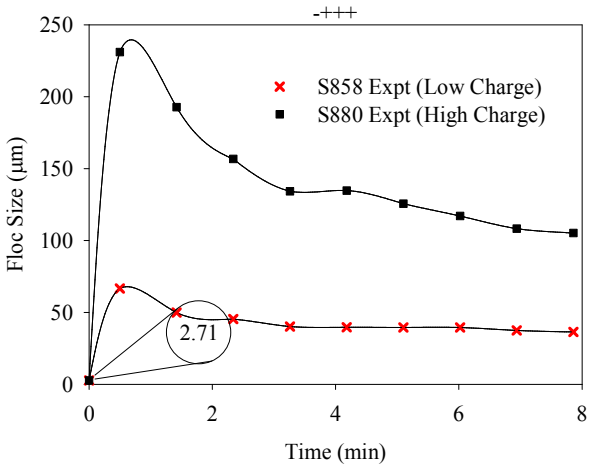

Fig. D5. Flocculation kinetics induced by S858 and S880 at condition "-+++"

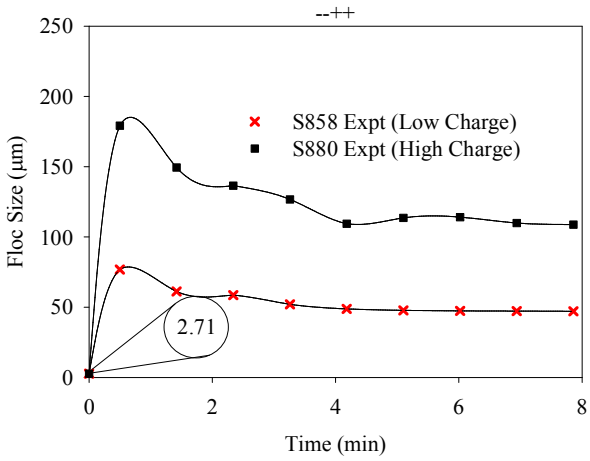

Fig. D6. Flocculation kinetics induced by S858 and S880 at condition "--++"

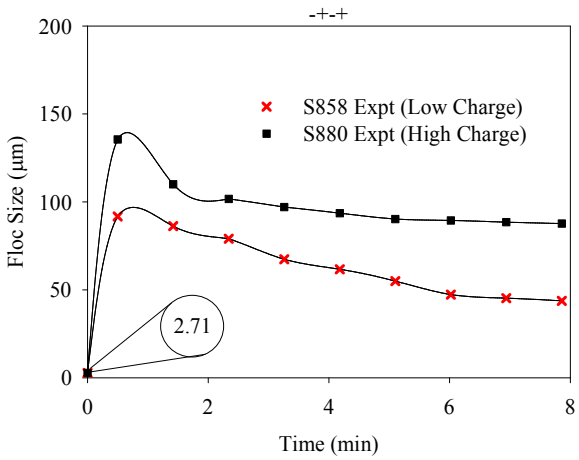

Fig. D7. Flocculation kinetics induced by S858 and S880 at condition "-+-+"

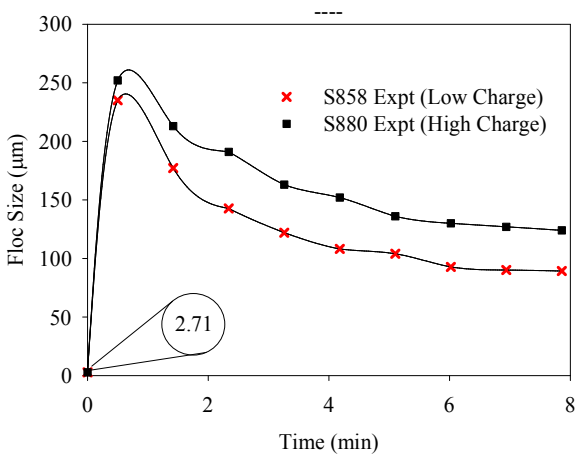

Fig. D8. Flocculation kinetics induced by S858 and S880 at condition "----"

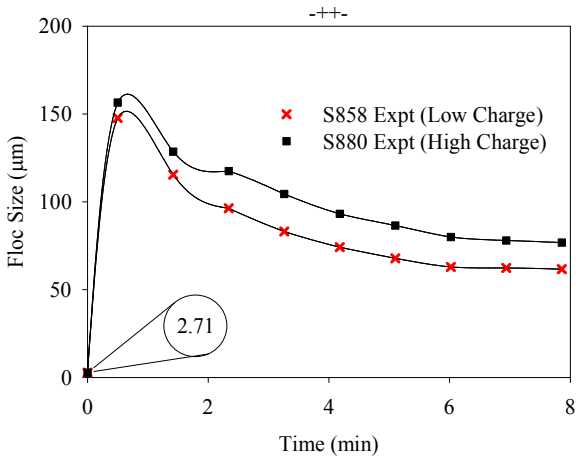

Fig. D9. Flocculation kinetics induced by S858 and S880 at condition "-++-"

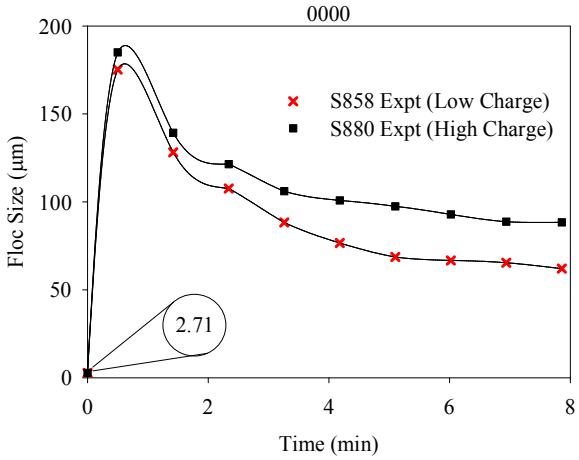

Fig. D10. Flocculation kinetics induced by S858 and S880 at condition "0000"

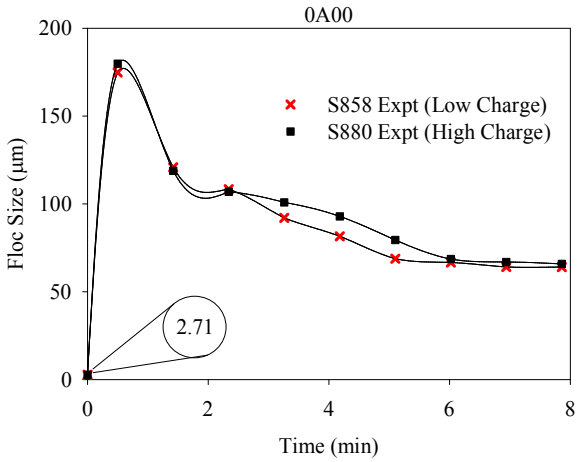

Fig. D11. Flocculation kinetics induced by S858 and S880 at condition "0A00"

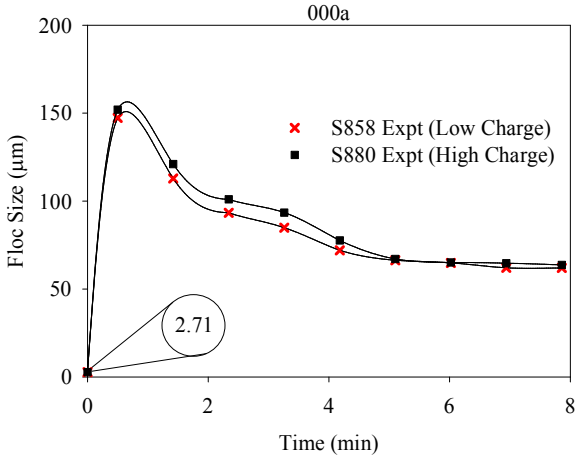

Fig. D12. Flocculation kinetics induced by S858 and S880 at condition "000a"

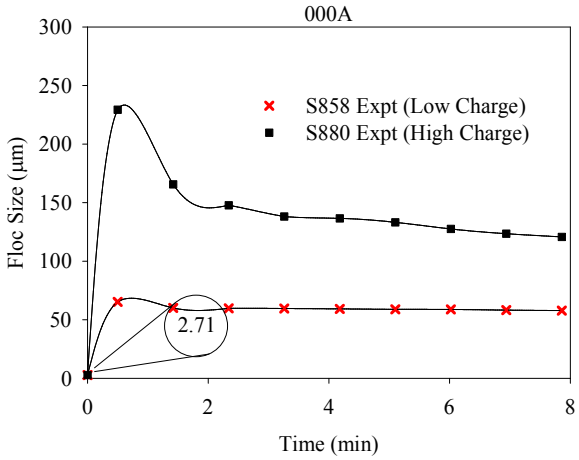

Fig. D13. Flocculation kinetics induced by S858 and S880 at condition "000A"

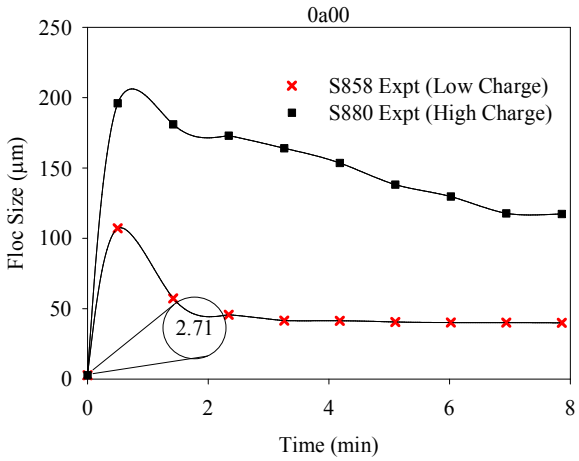

Fig. D14. Flocculation kinetics induced by S858 and S880 at condition "0a00"

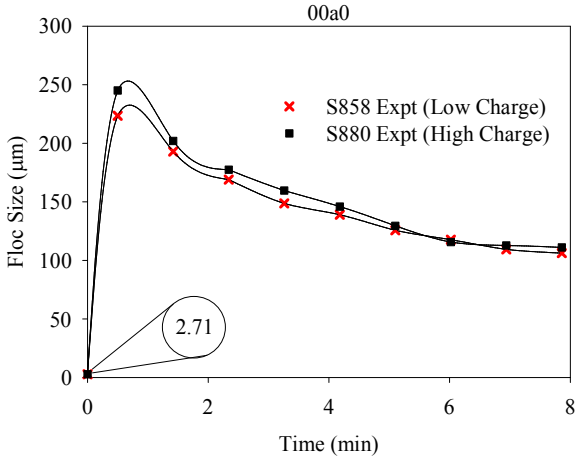

Fig. D15. Flocculation kinetics induced by S858 and S880 at condition "00a0"

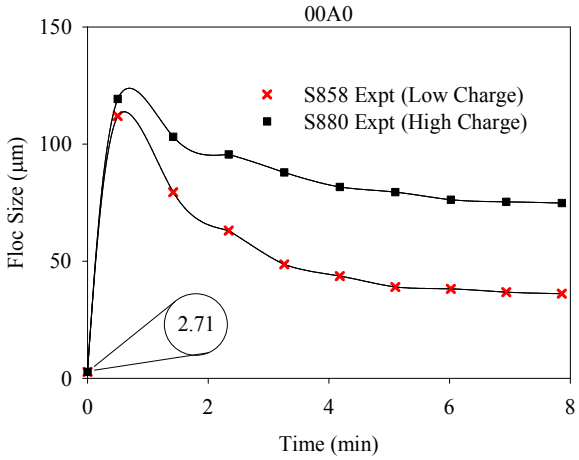

Fig. D16. Flocculation kinetics induced by S858 and S880 at condition "00A0"

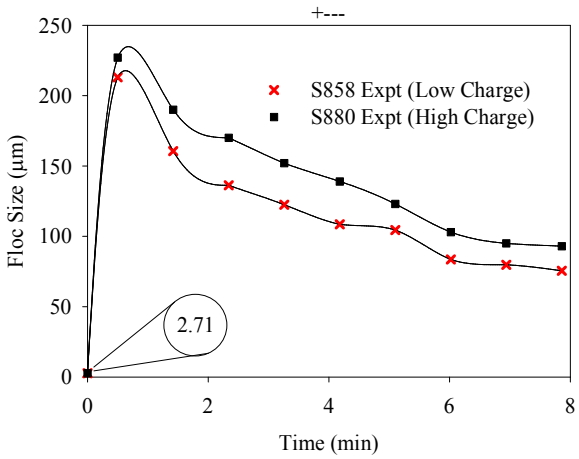

Fig. D17. Flocculation kinetics induced by S858 and S880 at condition "+---"

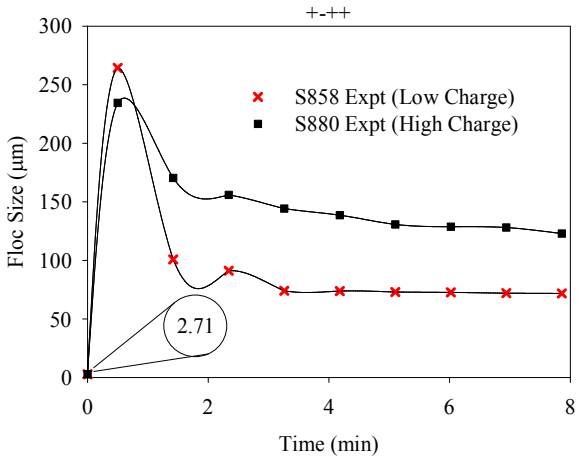

Fig. D18. Flocculation kinetics induced by S858 and S880 at condition "+-++"

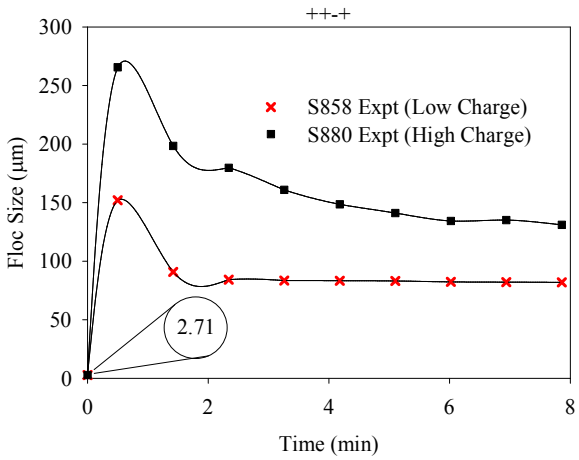

Fig. D19. Flocculation kinetics induced by S858 and S880 at condition "++-+"

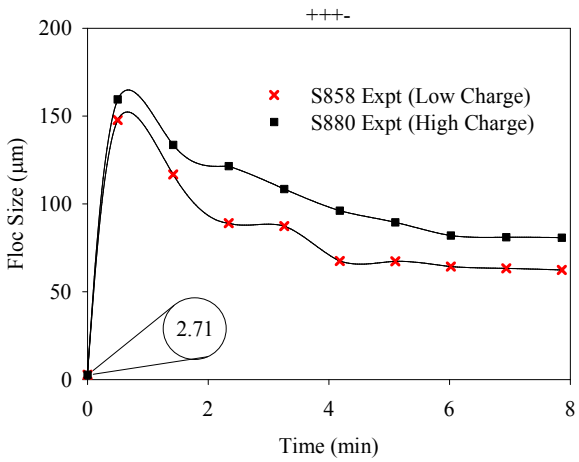

Fig. D20. Flocculation kinetics induced by S858 and S880 at condition "+++-"

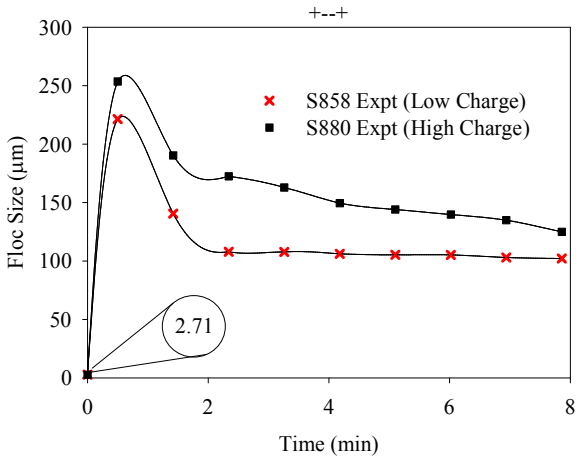

Fig. D21. Flocculation kinetics induced by S858 and S880 at condition "+--+"

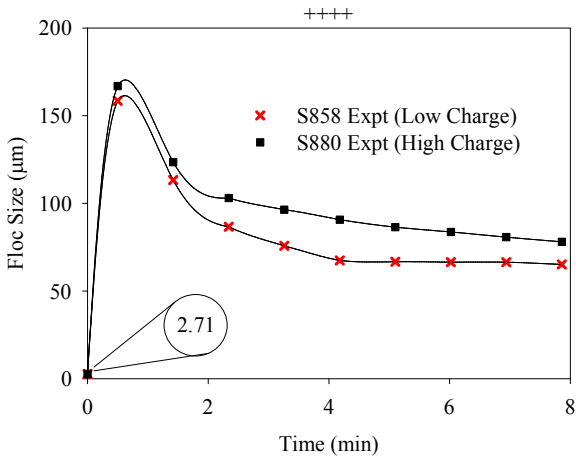

Fig. D22. Flocculation kinetics induced by S858 and S880 at condition "++++"

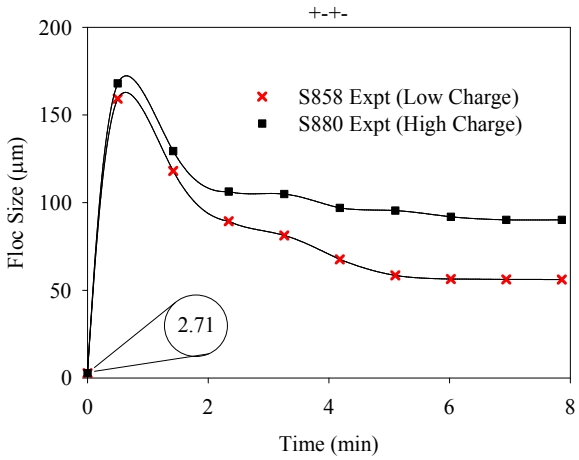

Fig. D23. Flocculation kinetics induced by S858 and S880 at condition "+-+-"

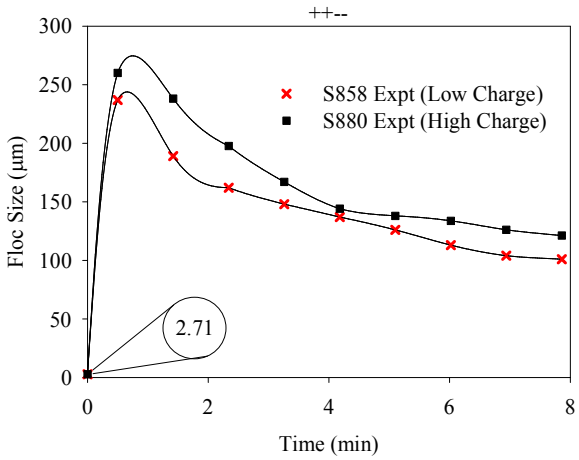

Fig. D24. Flocculation kinetics induced by S858 and S880 at condition "++--"

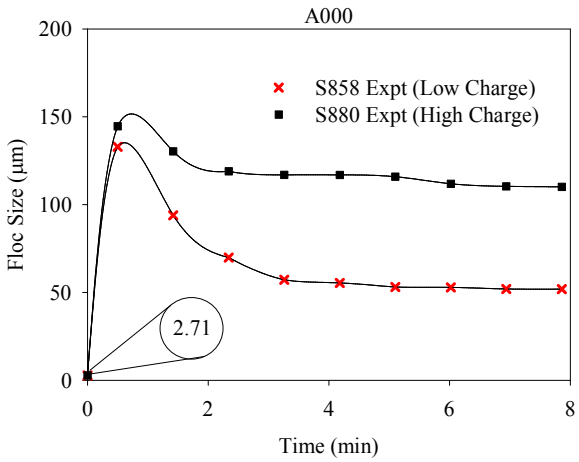

Fig. D25. Flocculation kinetics induced by S858 and S880 at condition "A000"

Appendix E: Chapter 4 Particle size distribution induced by S858 at condition “a000”

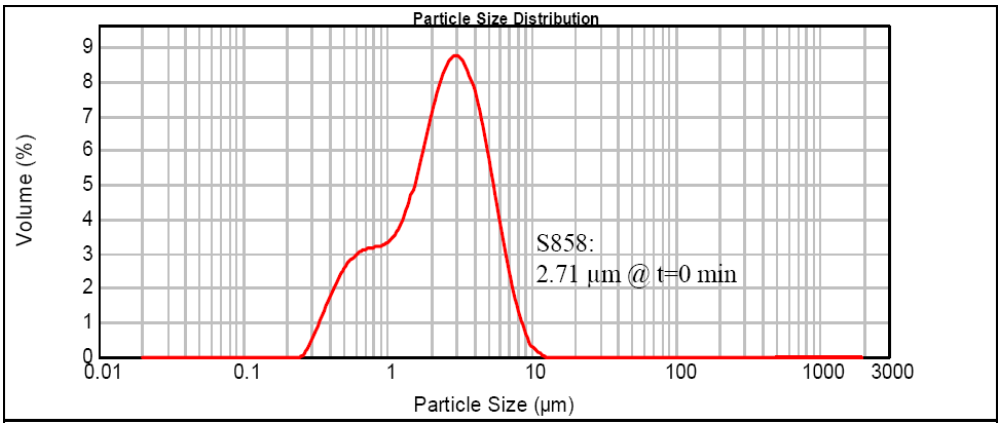

Fig. E1. Particle size distribution induced by S858 at t=0 min at condition “a000”

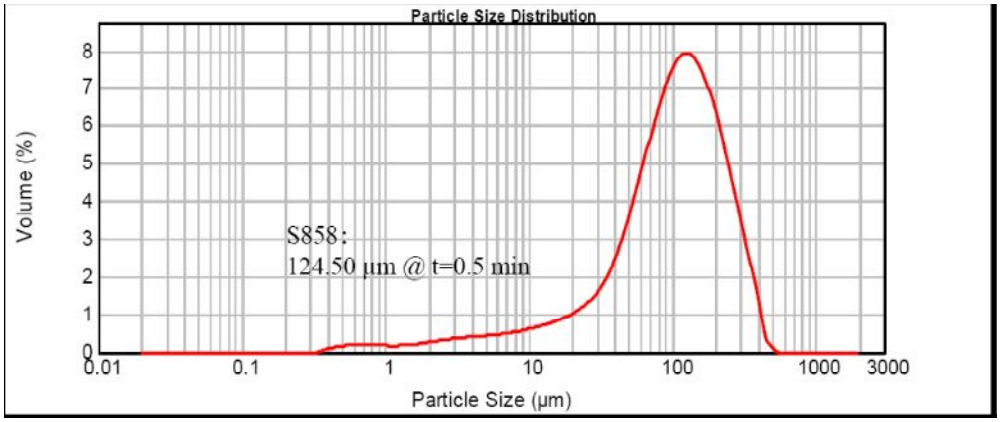

Fig. E2. Particle size distribution induced by S858 at t=0.5 min at condition “a000”

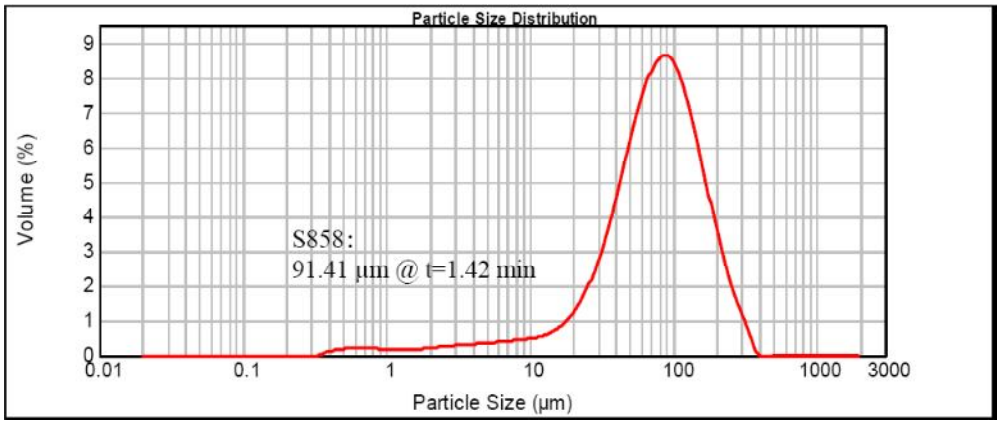

Fig. E3. Particle size distribution induced by S858 at t=1.42 min at condition “a000”

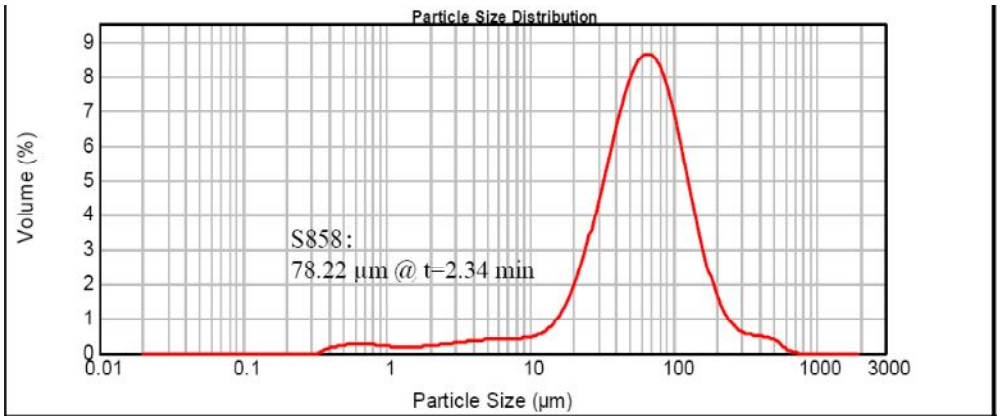

Fig. E4. Particle size distribution induced by S858 at t=2.34 min at condition “a000”

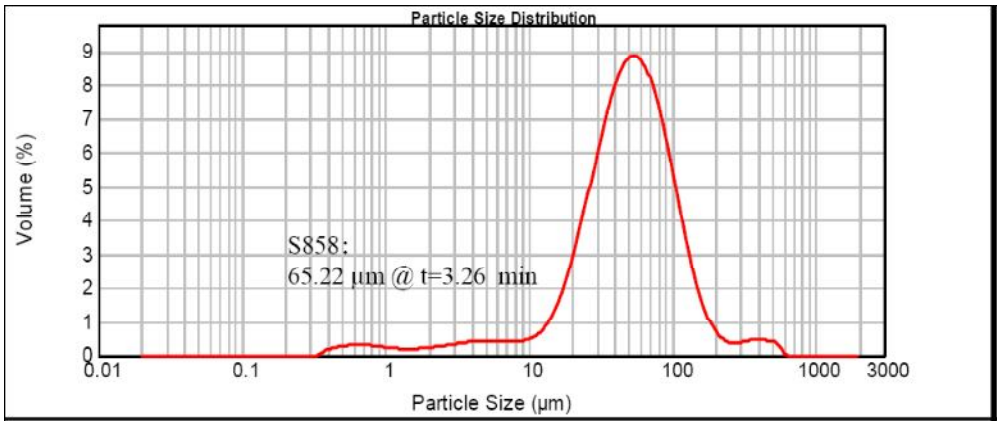

Fig. E5. Particle size distribution induced by S858 at t=3.26 min at condition “a000”

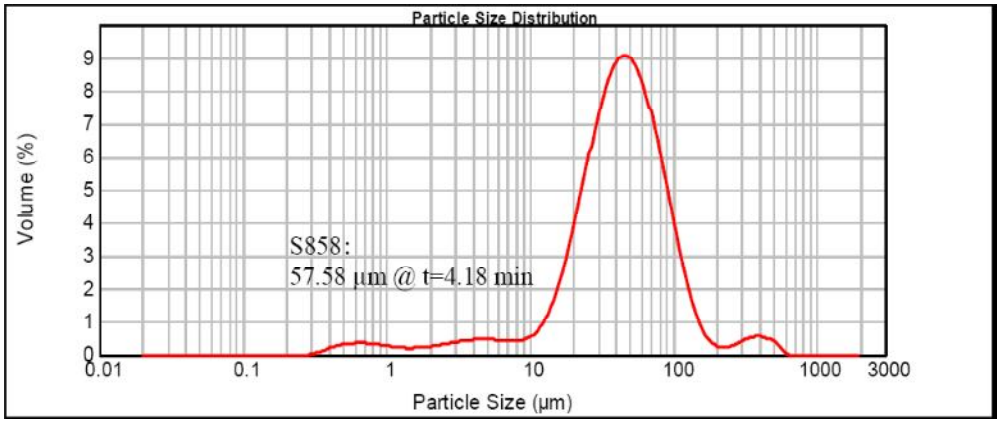

Fig. E6. Particle size distribution induced by S858 at t=4.18 min at condition “a000”

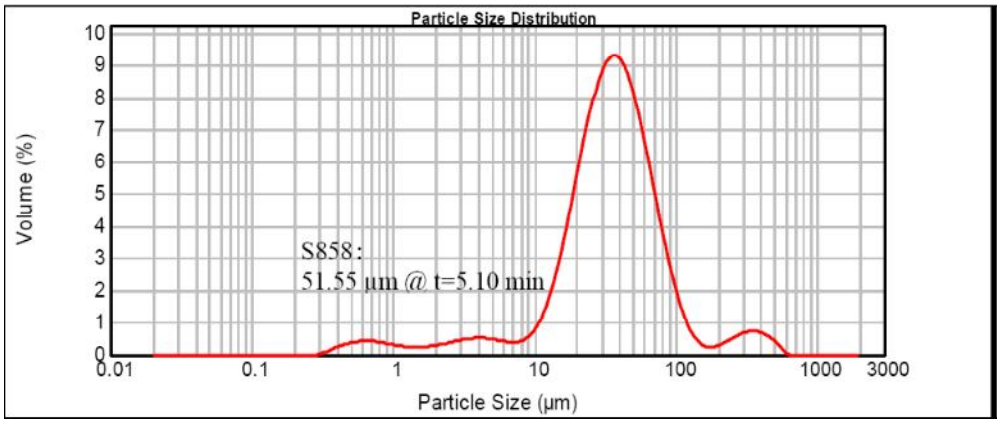

Fig. E7. Particle size distribution induced by S858 at t=5.10 min at condition “a000”

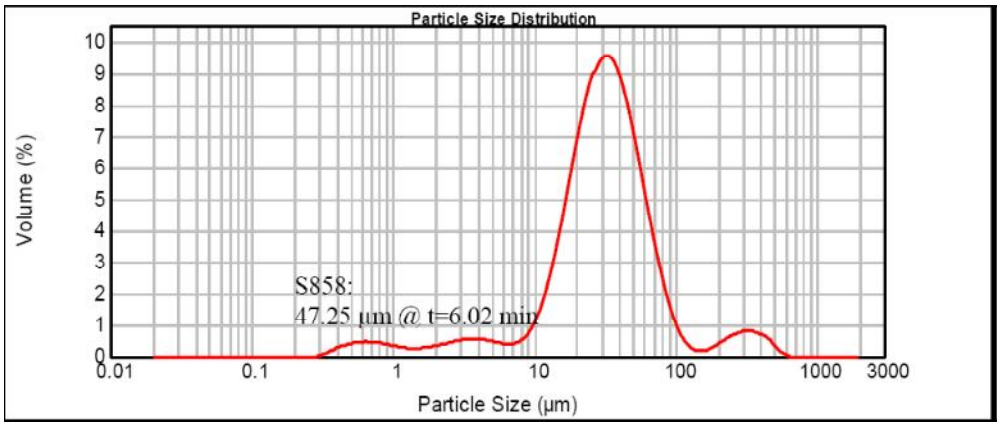

Fig. E8. Particle size distribution induced by S858 at t=6.02 min at condition “a000”

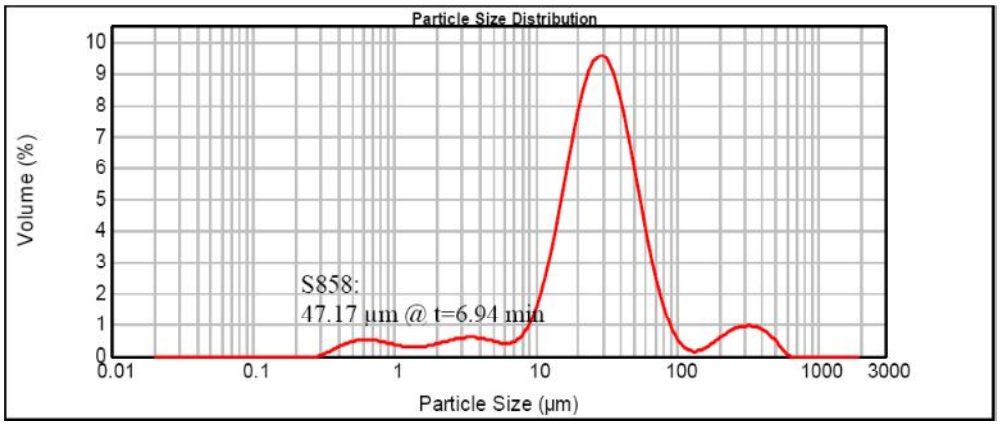

Fig. E9. Particle size distribution induced by S858 at t=6.94 min at condition “a000”

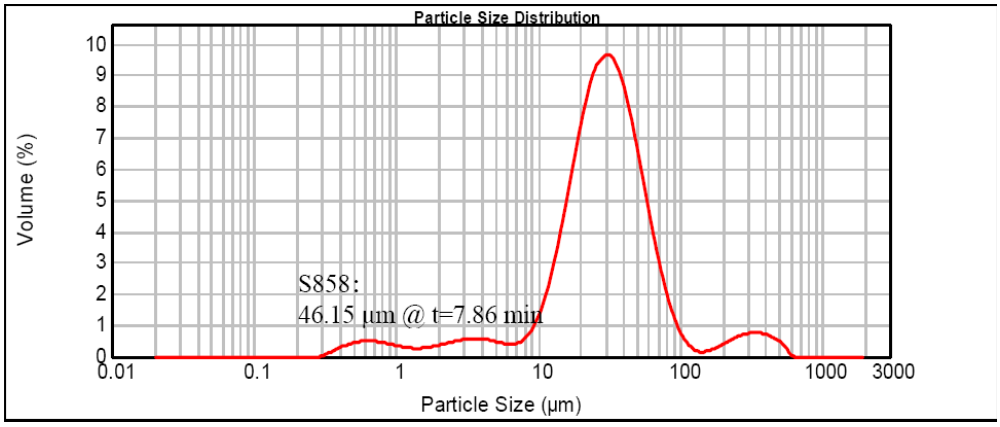

Fig. E10. Particle size distribution induced by S858 at t=7.86 min at condition “a000”

Appendix F: Chapter 4 Particle size distribution induced by S880 at condition “a000”

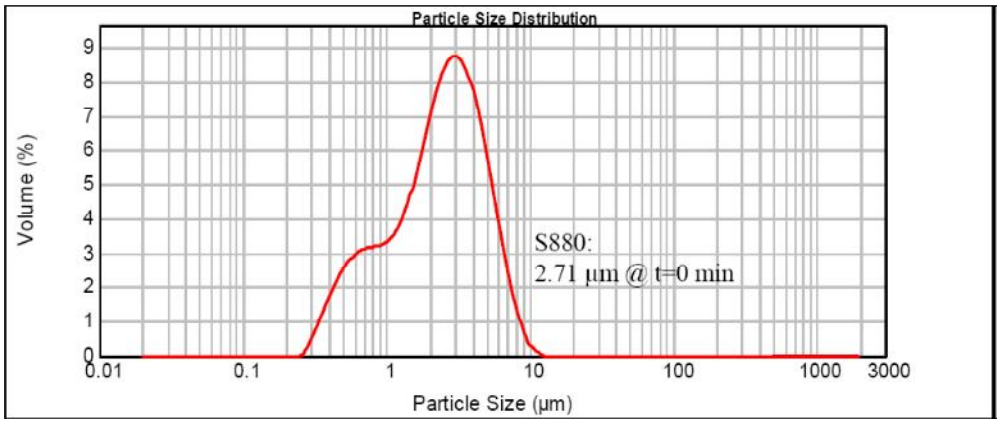

Fig. F1. Particle size distribution induced by S880 at t=0 min at condition “a000”

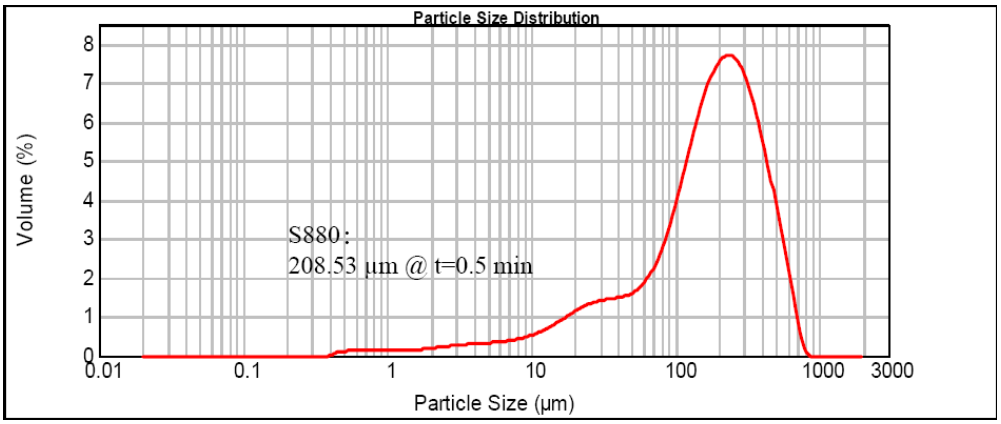

Fig. F2. Particle size distribution induced by S880 at t=0.5 min at condition “a000”

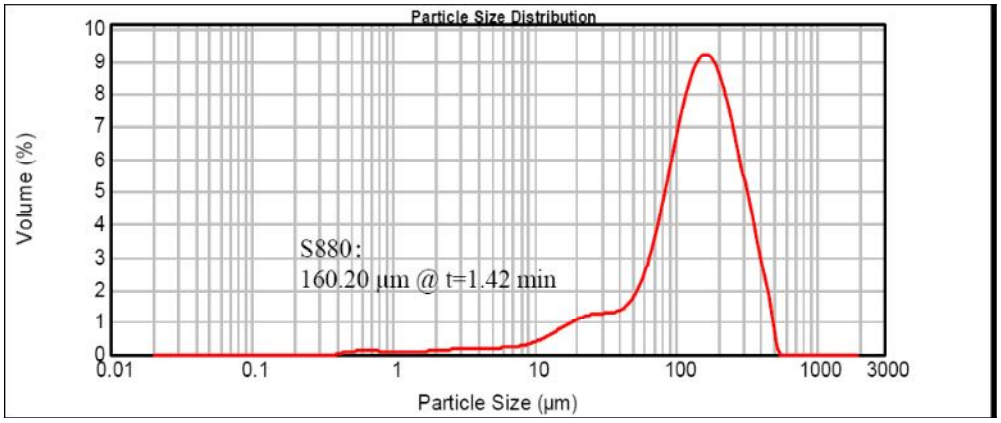

Fig. F3. Particle size distribution induced by S880 at t=1.42 min at condition “a000”

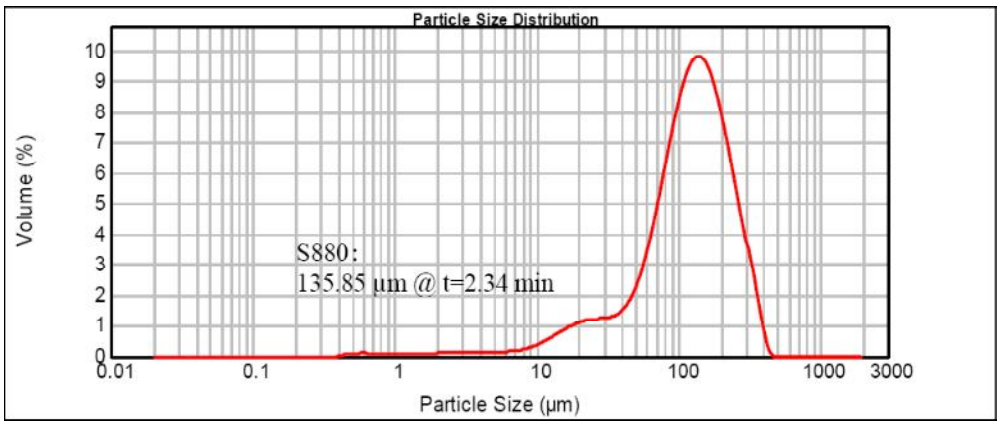

Fig. F4. Particle size distribution induced by S880 at t=2.34 min at condition "a000"

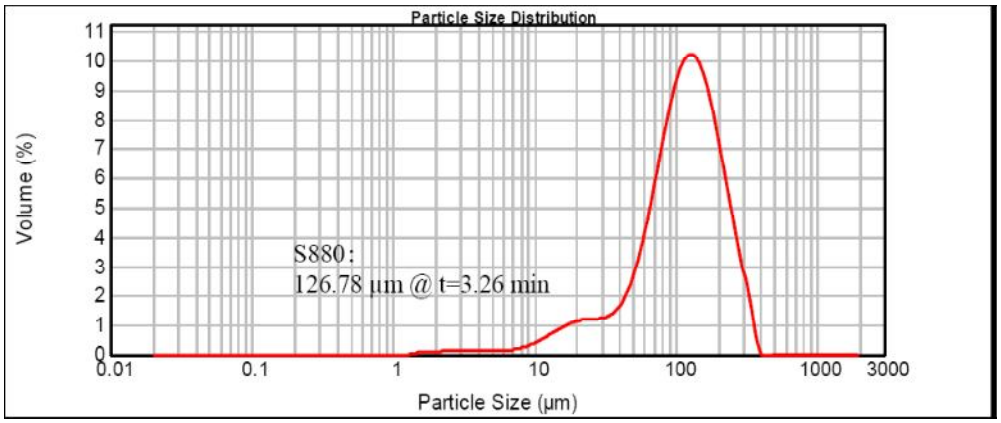

Fig. F5. Particle size distribution induced by S880 at t=3.26 min at condition "a000"

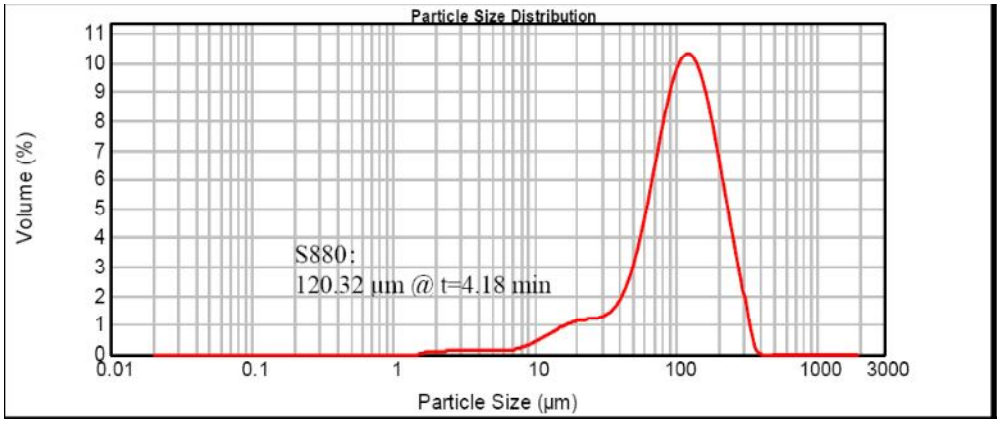

Fig. F6. Particle size distribution induced by S880 at t=4.18 min at condition "a000"

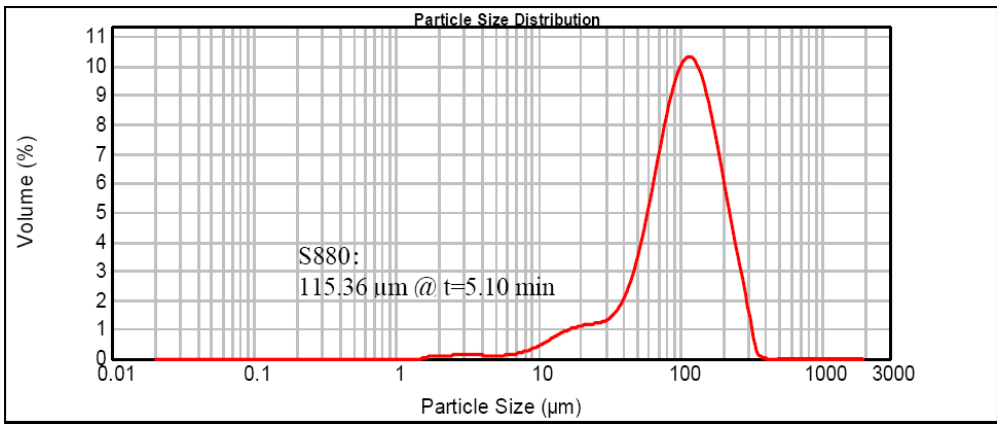

Fig. F7. Particle size distribution induced by S880 at t=5.10 min at condition “a000”

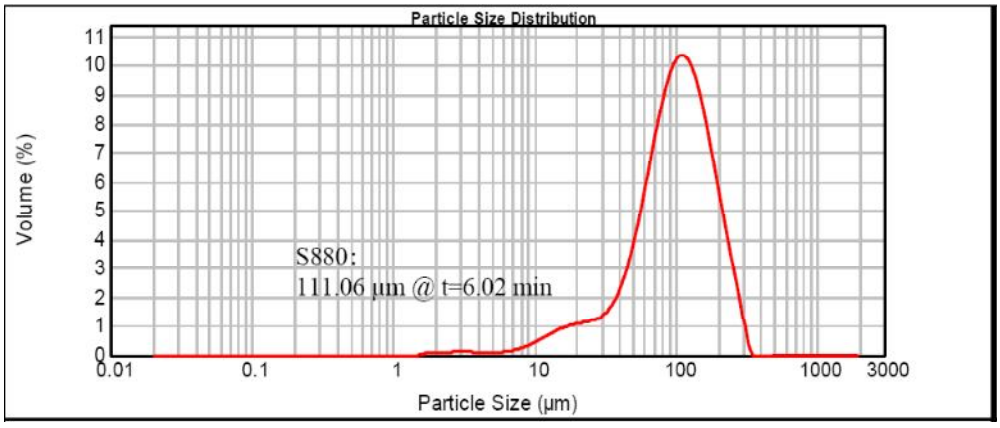

Fig. F8. Particle size distribution induced by S880 at t=6.02 min at condition “a000”

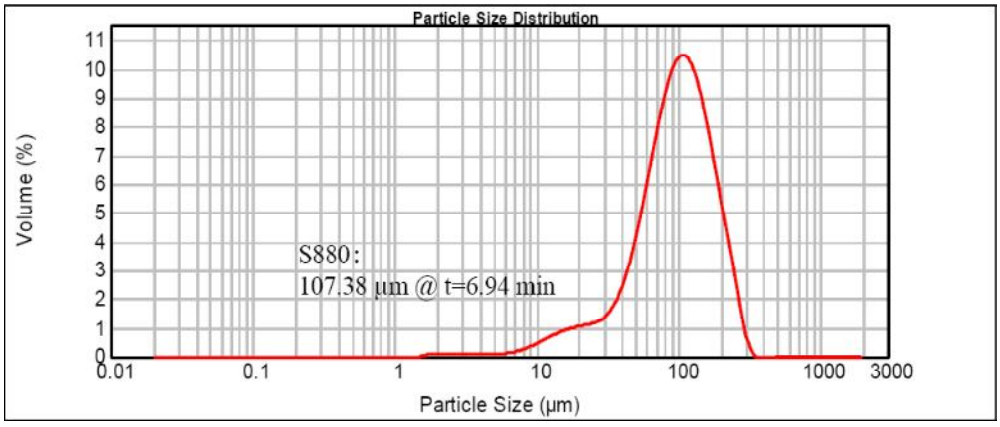

Fig. F9. Particle size distribution induced by S880 at t=6.94 min at condition “a000”

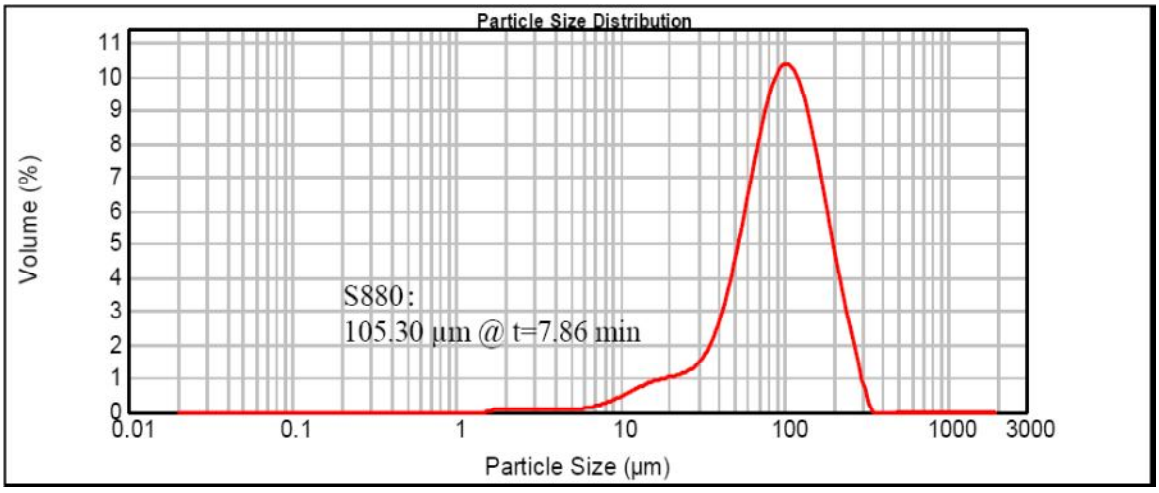

Fig. F10. Particle size distribution induced by S880 at t=7.86 min at condition “a000”

Appendix G: Chapter 4 Mass fractal dimension evolution induced by starches

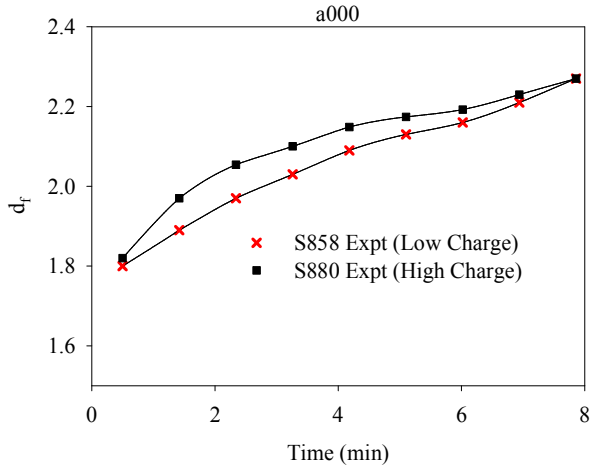

Fig. G1. Mass fractal dimension evolution induced S858 and S880 at condition "a000"

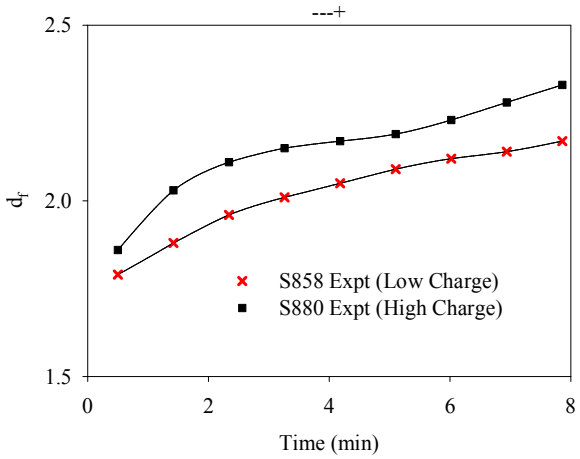

Fig. G2. Mass fractal dimension evolution induced S858 and S880 at condition "---+"

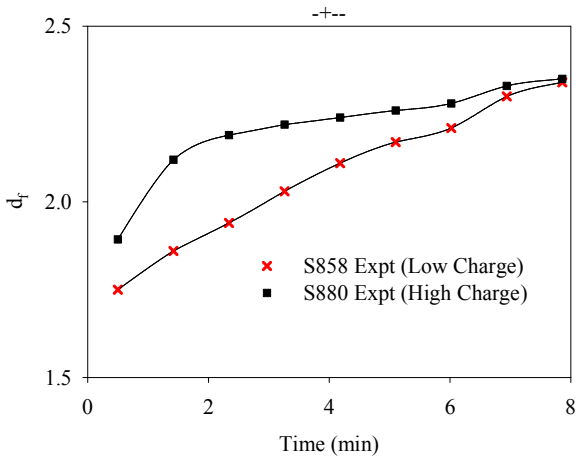

Fig. G3. Mass fractal dimension evolution induced S858 and S880 at condition "-+--"

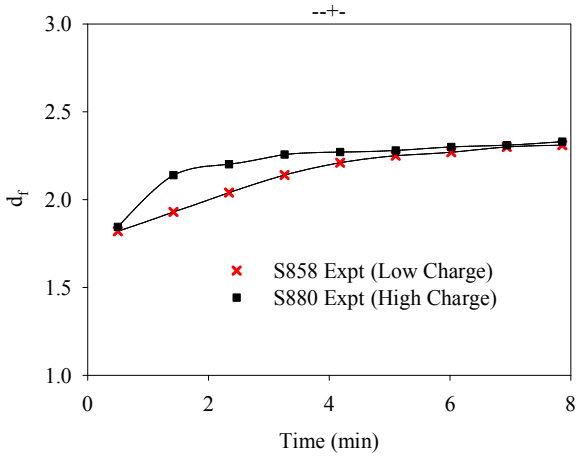

Fig. G4. Mass fractal dimension evolution induced S858 and S880 at condition "--+-"

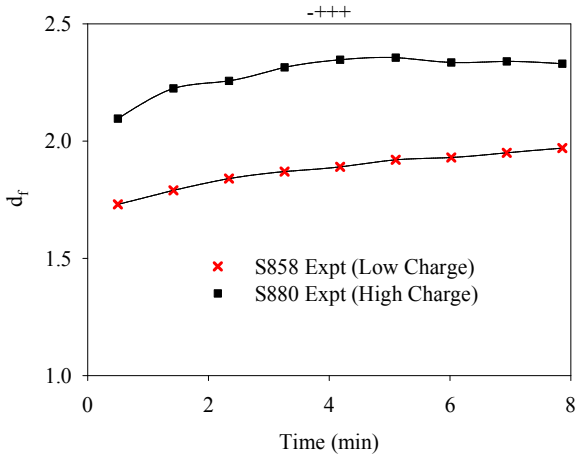

Fig. G5. Mass fractal dimension evolution induced S858 and S880 at condition "-+++"

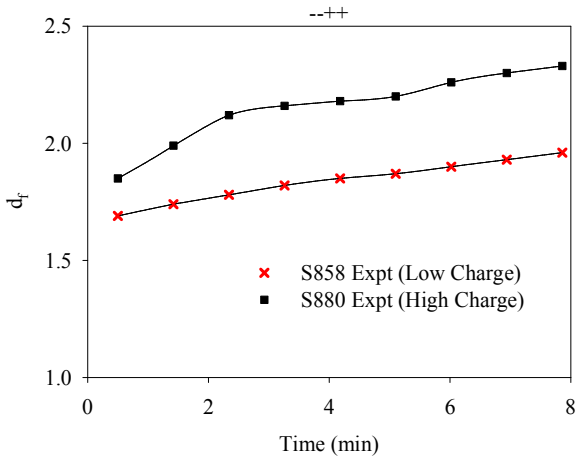

Fig. G6. Mass fractal dimension evolution induced S858 and S880 at condition "--++"

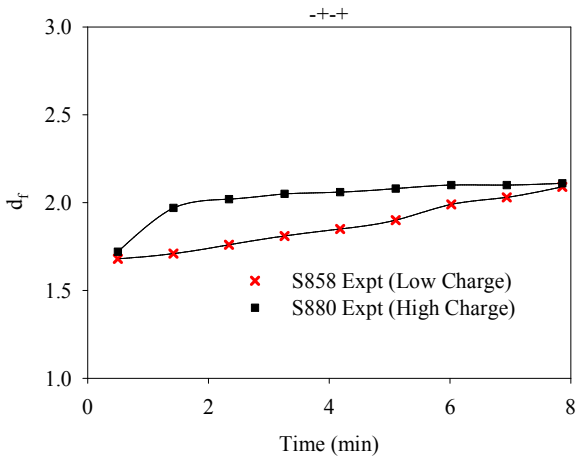

Fig. G7. Mass fractal dimension evolution induced S858 and S880 at condition "-+-+"

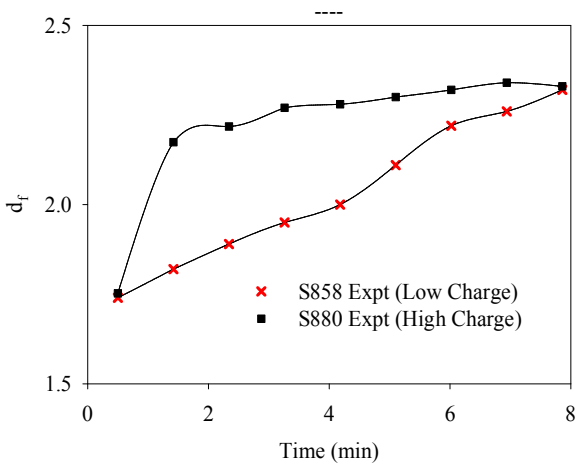

Fig. G8. Mass fractal dimension evolution induced S858 and S880 at condition "----"

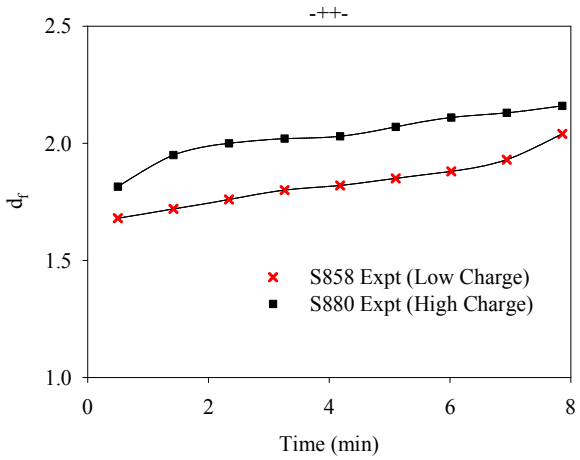

Fig. G9. Mass fractal dimension evolution induced S858 and S880 at condition "-++-"

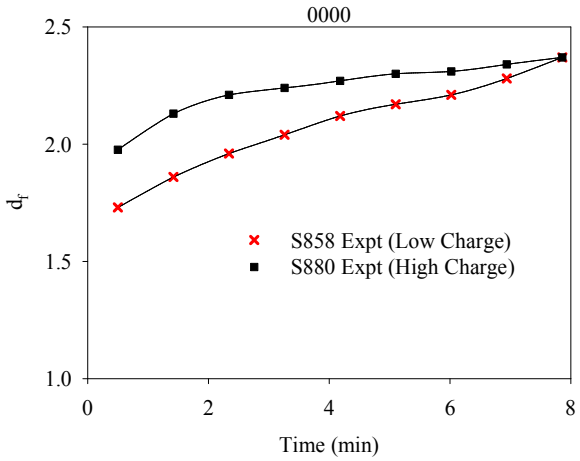

Fig. G10. Mass fractal dimension evolution induced S858 and S880 at condition "0000"

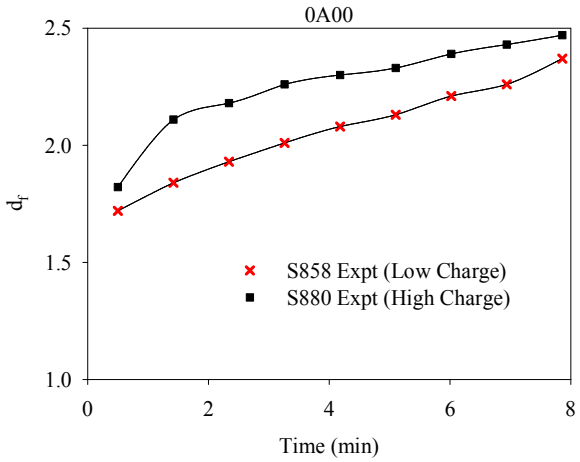

Fig. G11. Mass fractal dimension evolution induced S858 and S880 at condition "0A00"

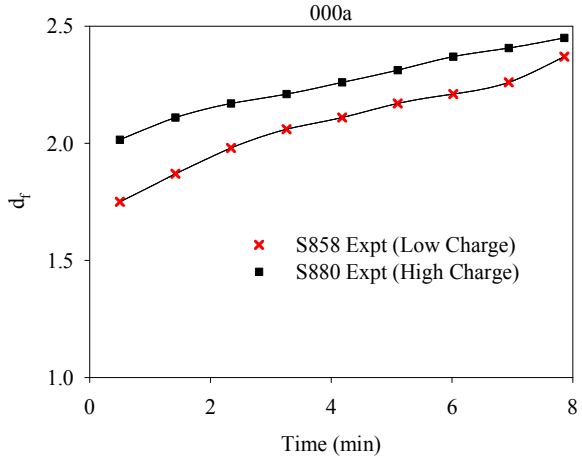

Fig. G12. Mass fractal dimension evolution induced S858 and S880 at condition "000a"

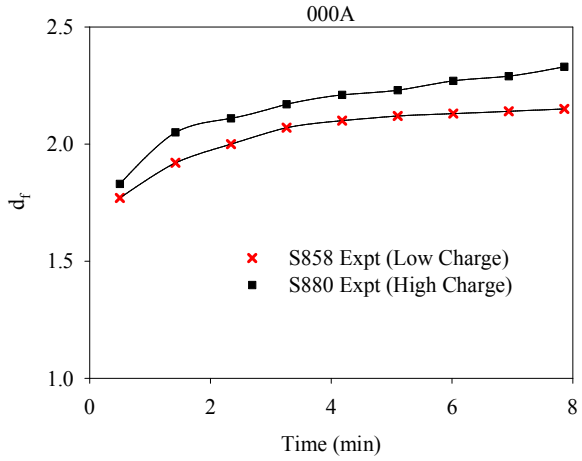

Fig. G13. Mass fractal dimension evolution induced S858 and S880 at condition "000A"

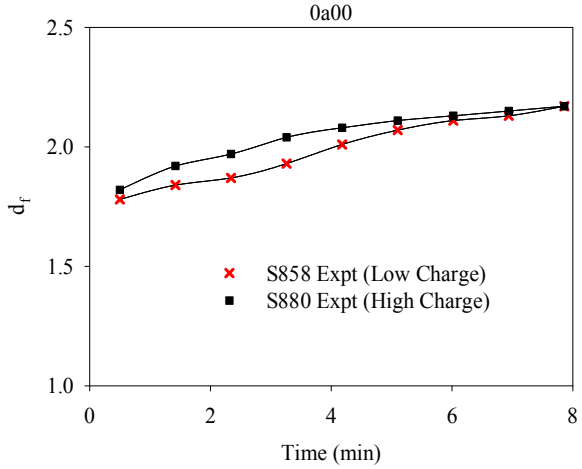

Fig. G14. Mass fractal dimension evolution induced S858 and S880 at condition "0a00"

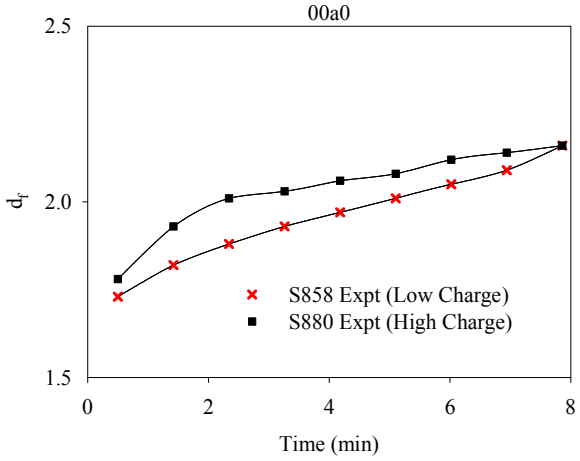

Fig. G15. Mass fractal dimension evolution induced S858 and S880 at condition "00a0"

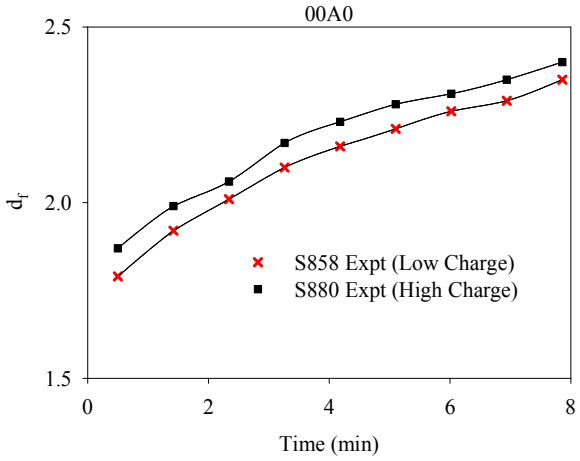

Fig. G16. Mass fractal dimension evolution induced S858 and S880 at condition "00A0"

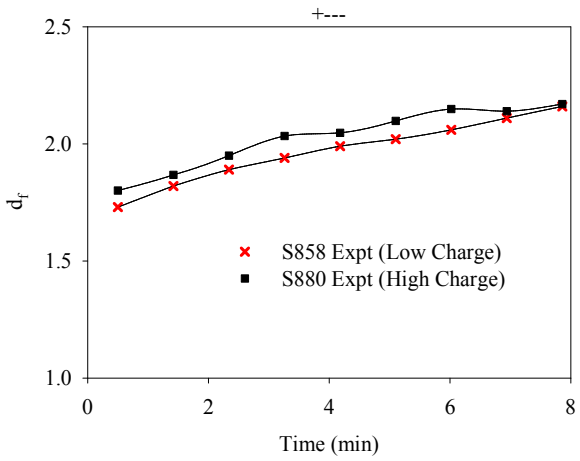

Fig. G17. Mass fractal dimension evolution induced S858 and S880 at condition "+---"

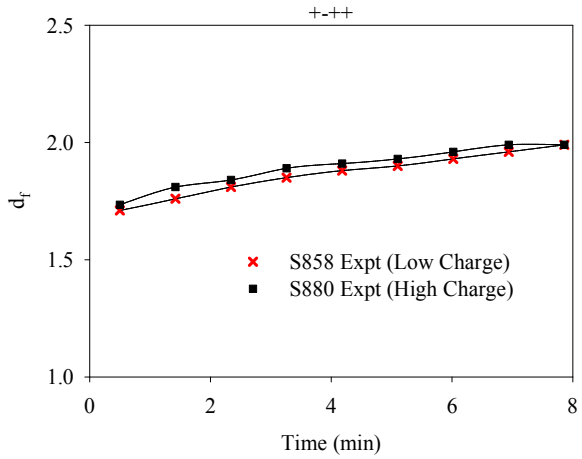

Fig. G18. Mass fractal dimension evolution induced S858 and S880 at condition "+-++"

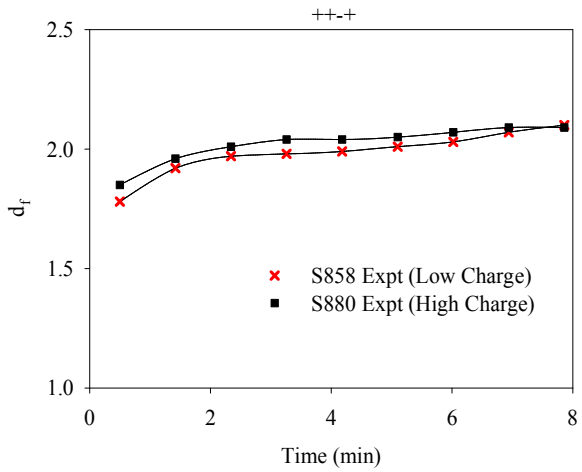

Fig. G19. Mass fractal dimension evolution induced S858 and S880 at condition "++-+"

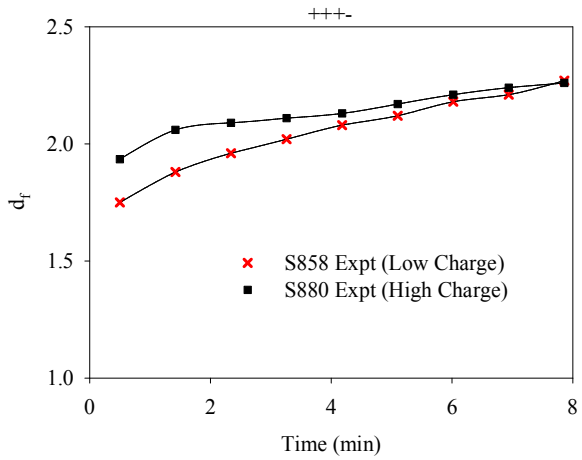

Fig. G20. Mass fractal dimension evolution induced S858 and S880 at condition "+++-"

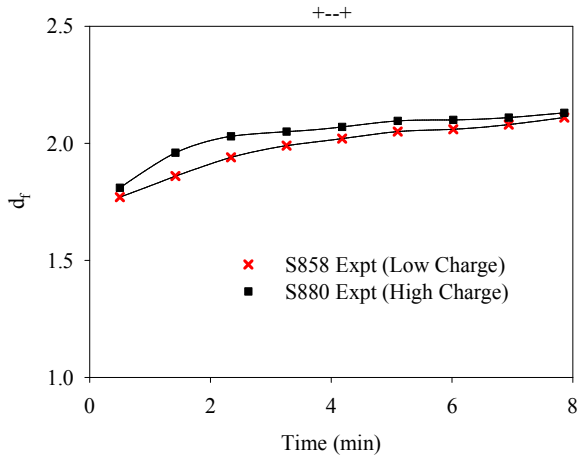

Fig. G21. Mass fractal dimension evolution induced S858 and S880 at condition "+--+"

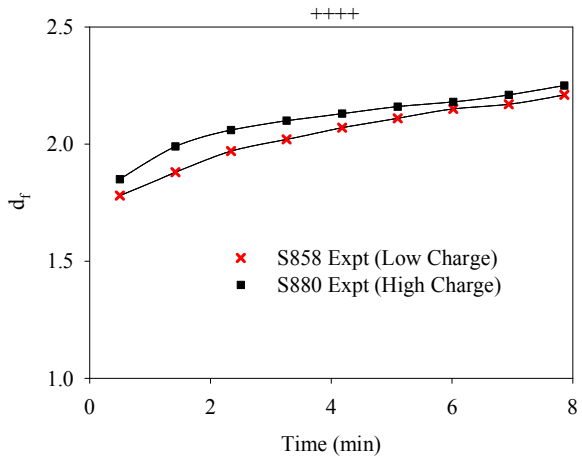

Fig. G22. Mass fractal dimension evolution induced S858 and S880 at condition "++++"

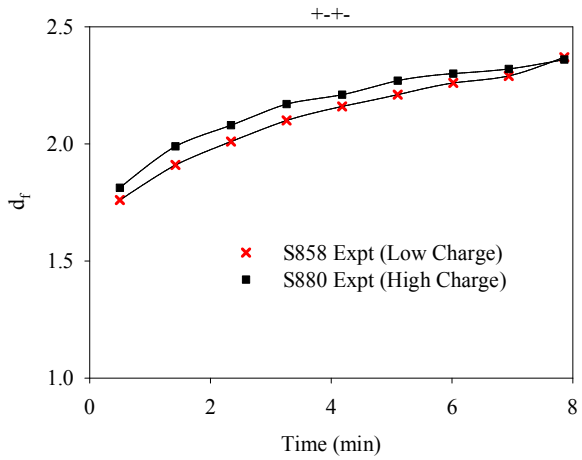

Fig. G23. Mass fractal dimension evolution induced S858 and S880 at condition "+-+-"

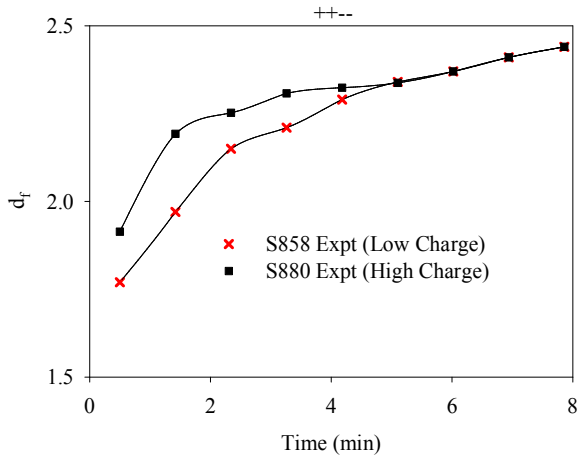

Fig. G24. Mass fractal dimension evolution induced S858 and S880 at condition "++--"

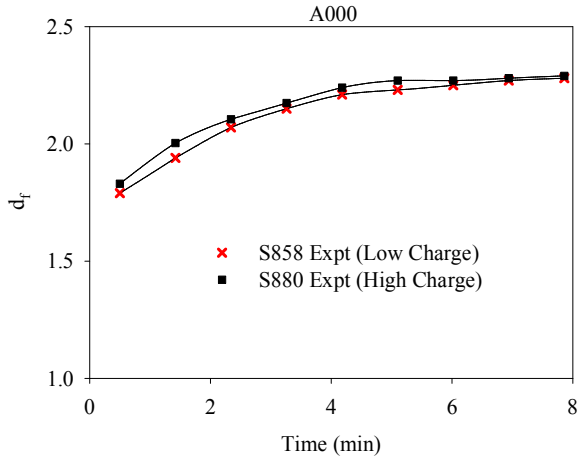

Fig. G25. Mass fractal dimension evolution induced S858 and S880 at condition "A000"

Appendix H: Chapter 5 ANOVA results for the population balance modeling

Table H1 ANOVA for collision efficiency of S858 system

Source	DF	Sum of Squares	F Ratio	Prob > F	Comments
T	1	6.63E-05	0.0424	0.84	---
NaCl	1	0.004899	3.1318	0.1002	---
Shear Rate	1	0.022638	14.4713	0.0022	Very Significant
Starch	1	0.012969	8.2903	0.0129	Significant
T*NaCl	1	0.000872	0.5572	0.4687	---
T*Shear Rate	1	0.000172	0.1101	0.7453	---
NaCl*Shear Rate	1	1.66E-05	0.0106	0.9195	---
T*Starch	1	0.002306	1.4744	0.2463	---
NaCl*Starch	1	0.000453	0.2893	0.5997	---
Shear Rate*Starch	1	0.0043	2.7488	0.1212	---
T*T	1	0.002513	1.6064	0.2272	---
NaCl*NaCl	1	0.005519	3.5277	0.083	---
Shear Rate*Shear Rate	1	0.000492	0.3144	0.5845	---
Starch*Starch	1	0.000449	0.2872	0.6011	---

RSquare=0.757242; RSquare Adj=0.458462; Root Mean Square Error=0.039552; Mean of Response=0.33023; DF: Degree of freedom; ---: Not statistically significant

Table H2 ANOVA for energy dissipation rate of S858 system

Source	DF	Sum of Squares	F Ratio	Prob > F	Comments
T	1	180.3578	6.6732	0.0227	Significant
NaCl	1	29.3289	1.0852	0.3165	---
Shear Rate	1	2111.13	78.1112	<.0001	Extremely Significant
Starch	1	631.1009	23.3506	0.0003	Extremely Significant
T*NaCl	1	25.957	0.9604	0.345	---
T*Shear Rate	1	8.4001	0.3108	0.5867	---
NaCl*Shear Rate	1	29.1163	1.0773	0.3182	---
T*Starch	1	246.4335	9.118	0.0099	Very Significant
NaCl*Starch	1	4.9856	0.1845	0.6746	---
Shear Rate*Starch	1	9.1721	0.3394	0.5702	---
T*T	1	37.0909	1.3724	0.2624	---
NaCl*NaCl	1	94.8254	3.5085	0.0837	---
Shear Rate*Shear Rate	1	11.5417	0.427	0.5248	---
Starch*Starch	1	83.8139	3.1011	0.1017	---

RSquare=0.908483; RSquare Adj=0.795847; Root Mean Square Error=5.198772; Mean of Response=35.83173; DF: Degree of freedom; ---: Not statistically significant

Table H3 ANOVA for restructure rate of S858 system

Source	DF	Sum of Squares	F Ratio	Prob > F	Comments
T	1	0.024029	7.2239	0.0186	Significant
NaCl	1	0.005747	1.7279	0.2114	---
Shear Rate	1	1.31E-06	0.0004	0.9845	---
Starch	1	0.072886	21.9122	0.0004	Extremely Significant
T*NaCl	1	0.002176	0.6542	0.4332	---
T*Shear Rate	1	0.007006	2.1062	0.1704	---
NaCl*Shear Rate	1	0.000666	0.2001	0.662	---
T*Starch	1	0.000475	0.1429	0.7115	---
NaCl*Starch	1	0.008949	2.6904	0.1249	---
Shear Rate*Starch	1	0.008845	2.6592	0.1269	---
T*T	1	0.002234	0.6716	0.4273	---
NaCl*NaCl	1	0.002826	0.8495	0.3735	---
Shear Rate*Shear Rate	1	6.19E-06	0.0019	0.9663	---
Starch*Starch	1	0.022928	6.8931	0.021	Significant

RSquare=0.805529; RSquare Adj=0.566181; Root Mean Square Error=0.057674; Mean of Response=0.27949; DF: Degree of freedom; ---: Not statistically significant

Table H4 ANOVA for collision efficiency of S880 system

Source	DF	Sum of Squares	F Ratio	Prob > F	Comments
T	1	0.00003174	0.0645	0.8035	---
NaCl	1	0.00523331	10.6379	0.0062	Very Significant
Shear Rate	1	0.03018923	61.3663	<.0001	Extremely Significant
Starch	1	0.00099588	2.0244	0.1783	---
T*NaCl	1	0.00084681	1.7213	0.2122	---
T*Shear Rate	1	0.0008732	1.775	0.2057	---
NaCl*Shear Rate	1	0.000009	0.0183	0.8945	---
T*Starch	1	0.00000196	0.004	0.9506	---
NaCl*Starch	1	0.00074256	1.5094	0.241	---
Shear Rate*Starch	1	0.00006889	0.14	0.7143	---
T*T	1	0.0015982	3.2487	0.0947	---
NaCl*NaCl	1	0.00048288	0.9816	0.3399	---
Shear Rate*Shear Rate	1	0.00051703	1.051	0.324	---
Starch*Starch	1	0.0000078	0.0159	0.9017	---

RSquare=0.871049; RSquare Adj=0.712339; Root Mean Square Error=0.02218; Mean of Response=0.248783; DF: Degree of freedom; ---: Not statistically significant

Table H5 ANOVA for energy dissipation rate of S880 system

Source	DF	Sum of Squares	F Ratio	Prob > F	Comments
T	1	1877.1125	59.3259	<.0001	Extremely Significant
NaCl	1	155.2832	4.9077	0.0452	Significant
Shear Rate	1	4790.5364	151.404	<.0001	Extremely Significant
Starch	1	55.1166	1.742	0.2097	---
T*NaCl	1	123.9064	3.916	0.0694	---
T*Shear Rate	1	168.0828	5.3122	0.0383	Significant
NaCl*Shear Rate	1	0.8644	0.0273	0.8713	---
T*Starch	1	12.9634	0.4097	0.5332	---
NaCl*Starch	1	8.3257	0.2631	0.6166	---
Shear Rate*Starch	1	146.1119	4.6179	0.0511	---
T*T	1	166.9089	5.2751	0.0389	Significant
NaCl*NaCl	1	56.9025	1.7984	0.2029	---
Shear Rate*Shear Rate	1	37.4884	1.1848	0.2961	---
Starch*Starch	1	25.144	0.7947	0.3889	---

RSquare=0.950179; RSquare Adj=0.888861; Root Mean Square Error=5.625004; Mean of Response=47.70696; DF: Degree of freedom; ---: Not statistically significant

Table H6 ANOVA for restructure rate of S880 system

Source	DF	Sum of Squares	F Ratio	Prob > F	Comments
T	1	0.00763623	2.6656	0.1265	---
NaCl	1	0.00812912	2.8376	0.1159	---
Shear Rate	1	0.01101245	3.8441	0.0717	---
Starch	1	0.0009238	0.3225	0.5798	---
T*NaCl	1	0.00067211	0.2346	0.6362	---
T*Shear Rate	1	0.00510153	1.7808	0.205	---
NaCl*Shear Rate	1	0.00028985	0.1012	0.7555	---
T*Starch	1	0.00201826	0.7045	0.4164	---
NaCl*Starch	1	0.00013283	0.0464	0.8329	---
Shear Rate*Starch	1	0.00545013	1.9025	0.1911	---
T*T	1	0.00029776	0.1039	0.7523	---
NaCl*NaCl	1	0.00023551	0.0822	0.7788	---
Shear Rate*Shear Rate	1	0.00271152	0.9465	0.3484	---
Starch*Starch	1	0.00113852	0.3974	0.5393	---

RSquare=0.557207; RSquare Adj=0.01223; Root Mean Square Error=0.058756; Mean of Response=0.148947; DF: Degree of freedom; ---: Not statistically significant

Appendix I: Chapter 5 Initial condition calculation

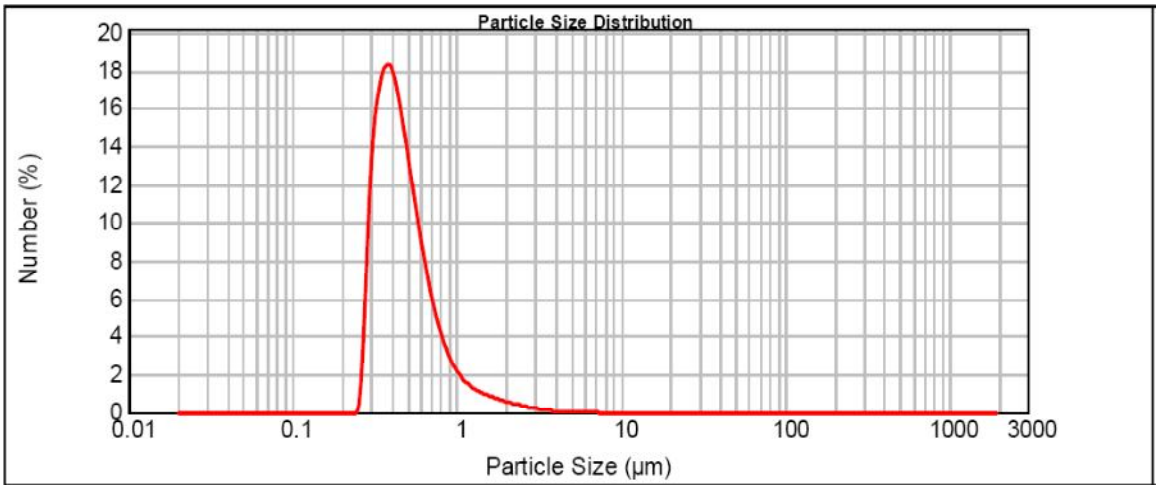

Size (µm)	Number In %
0.250	33.40
0.380	41.24
0.580	

Size (µm)	Number In %
0.580	16.71
0.890	5.09
1.350	

Size (µm)	Number In %
1.350	2.27
2.060	0.97
3.130	

Size (µm)	Number In %
3.130	0.28
4.770	0.05
7.260	

Fig. I1: Particle number distribution

The characteristic length D_i is calculated using the following equation:

$$D_i = \left(2^{(i-1)/d_f}\right) d_0$$

where d_0 = 2.50E-07 m, d_f = 1.65 are obtained from the Malvern Mastersizer 2000 measurement.

For example, D_1 is 2.50E-07 m.

The representative diameter for each band is taken to be the geometric mean of the size band limits:

$$D_{ir} = \sqrt{D_i D_{i+1}}$$

For example, the size band 2.50E-07 – 3.84E-07 *m* has a geometric mean of 3.10E-07 *m*.

Based on the representative diameter of each band, the volume of a single particle is calculated as:

$$V = \frac{4}{3}\pi r^3$$

For example, a single particle in the size band 2.50E-07 – 3.84E-07 *m* has a volume of 1.56E-20 m^3.

The mass of a single particle is calculated as:

$$m = \rho V$$

where ρ=2.71E+06 g/m^3 for PCC.

For example, a single particle in the size band 2.50E-07 – 3.84E-07 *m* has a mass of 4.23E-14 g.

The number percentage for the particles in the size band 2.50E-07 – 3.84E-07 *m* is 33.40% as shown in Table I1. Assuming the total particle number in the reactor is N, the total number of particles in the size band 2.50E-07 – 3.84E-07 *m* is (33.40%N).

Thus, the total mass of particles in the size band 2.50E-07 – 3.84E-07 *m* is:
4.23E-14 * (33.40%N) =(1.41E-14*N) g.

Adding the total mass of particles in all the size band, the total mass in the reactor is (9.97E-13*N) g. 0.30 g PCC was added to the reactor for the PCC flocculation experiment.

Doing the mass balance, 9.97E-13*N=0.30→N=3.01E+11

Thus, the total number of particles in the size band 2.50E-07 – 3.84E-07 m is (33.40%N)= 1.00E+11.

The number concentration of particles in each size band can be obtained by dividing the total number of particles in each size band by the total volume of the PCC suspension, here is 600 ml.

For example, the number concentation of particles in the size band 2.50E-07 – 3.84E-07 m is 1.67E+08/cm^3.

The number concentation of particles in each size band is used as the initial condition for the discretized population balance equation (5-2) shown in Chapter 5.

The final results are shown in Table I1.

Table I1: Results for initial condition calculation

i	Characteristic Length $D_i\,(m)$	Representative diameter $D_{ir}\,(m)$	A single particle volume (m^3)	Number (%)	Mass (g)	Total number in each size band	Number Concentration $(\#/cm^3)$
1	2.50E-07	3.10E-07	1.56E-20	33.40	1.4E-14	1.00E+11	1.67E+08
2	3.84E-07	4.74E-07	5.56E-20	41.24	6.2E-14	1.24E+11	2.07E+08
3	5.84E-07	7.21E-07	1.96E-19	16.71	8.9E-14	5.03E+10	8.38E+07
4	8.89E-07	1.10E-06	6.91E-19	5.09	9.5E-14	1.53E+10	2.55E+07
5	1.35E-06	1.67E-06	2.43E-18	2.27	1.5E-13	6.83E+09	1.14E+07
6	2.06E-06	2.54E-06	8.57E-18	0.97	2.3E-13	2.93E+09	4.88E+06
7	3.13E-06	3.86E-06	3.02E-17	0.28	2.3E-13	8.27E+08	1.38E+06
8	4.77E-06	5.88E-06	1.07E-16	0.05	1.4E-13	1.42E+08	2.36E+05
9	7.26E-06						

Note: Number distribution in Fig. I1 is transformed from the volume distribution in Fig. E1

Appendix J: Chapter 5 Experimental and simulated PCC flocculation kinetics by starch

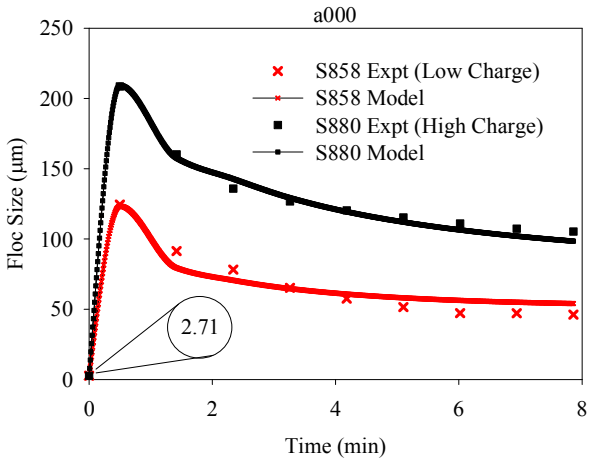

Fig. J1. Experimental and simulated PCC flocculation kinetics at condition "a000"

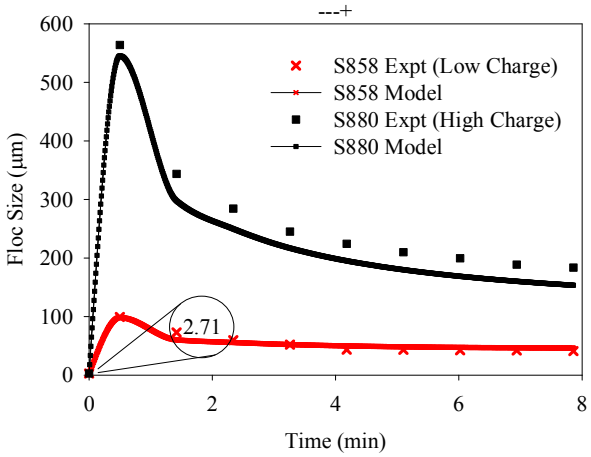

Fig. J2. Experimental and simulated PCC flocculation kinetics at condition "---+"

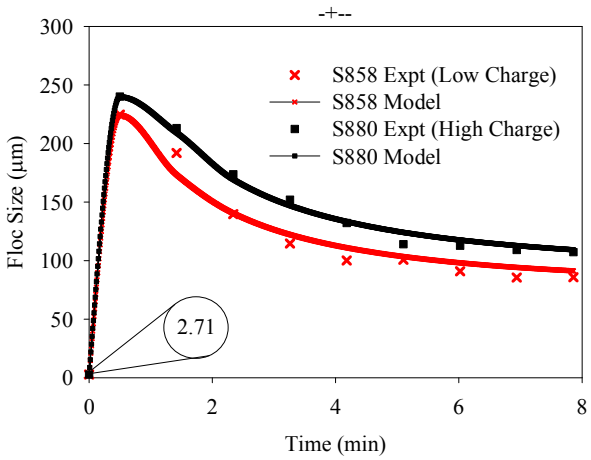

Fig. J3. Experimental and simulated PCC flocculation kinetics at condition "-+--"

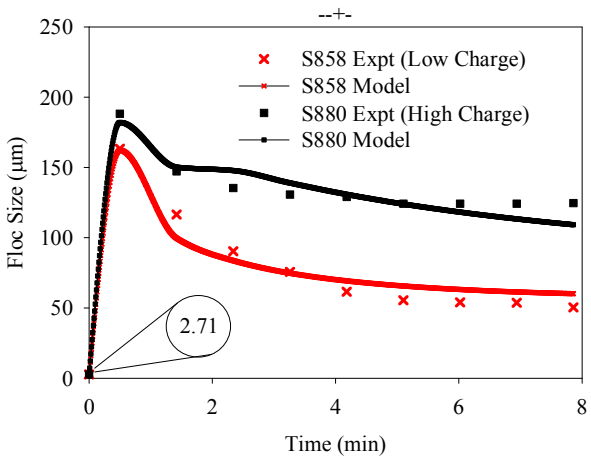

Fig. J4. Experimental and simulated PCC flocculation kinetics at condition "--+-"

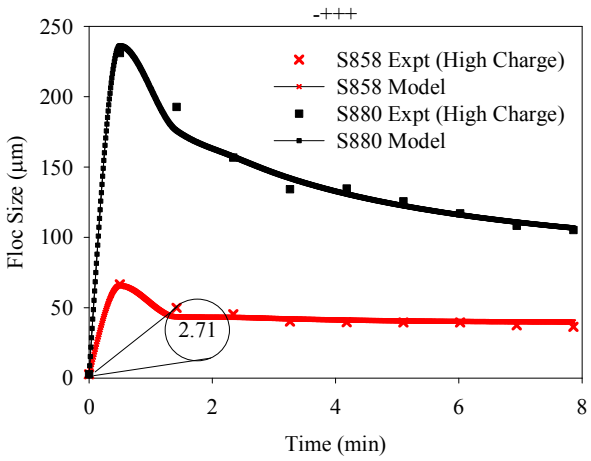

Fig. J5. Experimental and simulated PCC flocculation kinetics at condition "-+++"

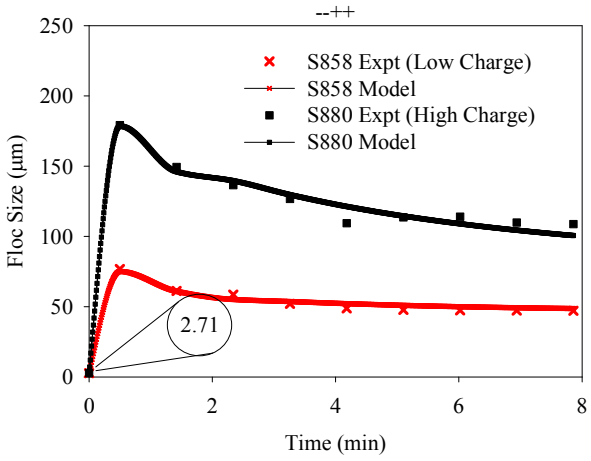

Fig. J6. Experimental and simulated PCC flocculation kinetics at condition "--++"

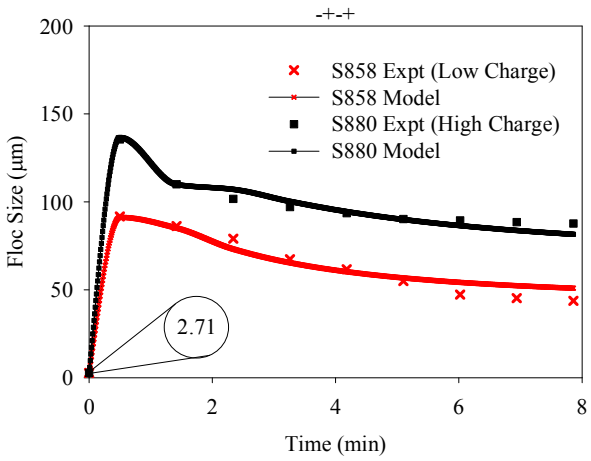

Fig. J7. Experimental and simulated PCC flocculation kinetics at condition "-+-+"

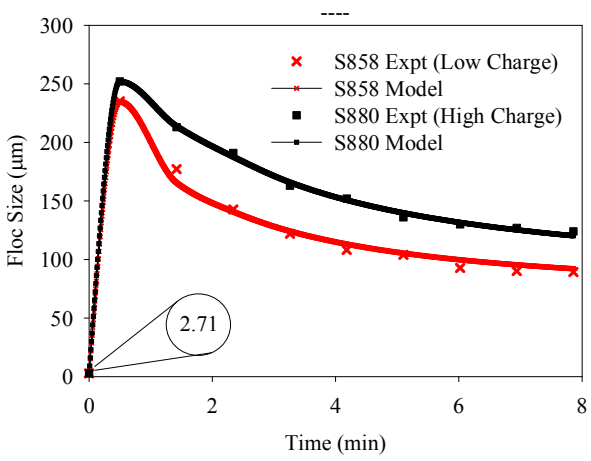

Fig. J8. Experimental and simulated PCC flocculation kinetics at condition "----"

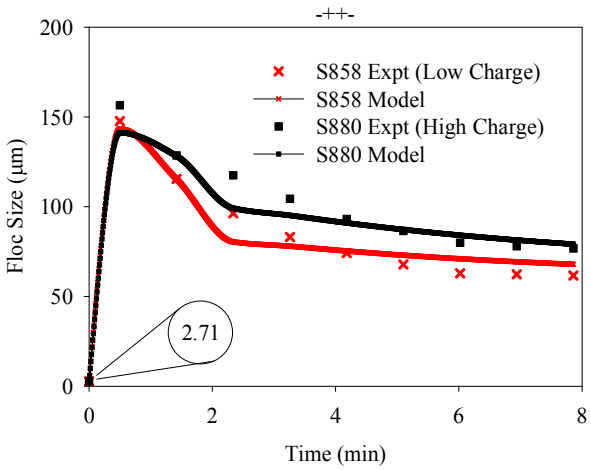

Fig. J9. Experimental and simulated PCC flocculation kinetics at condition "-++-"

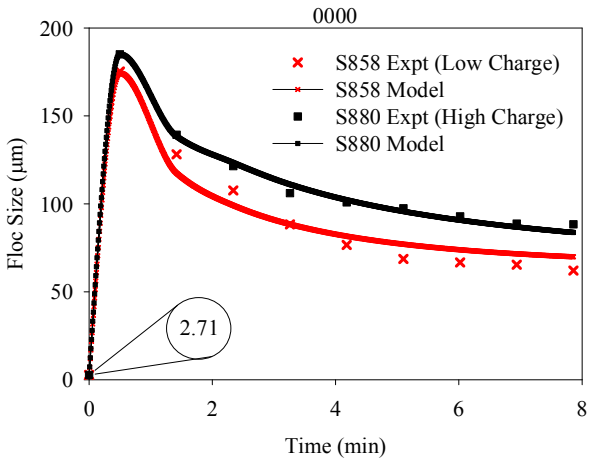

Fig. J10. Experimental and simulated PCC flocculation kinetics at condition "0000"

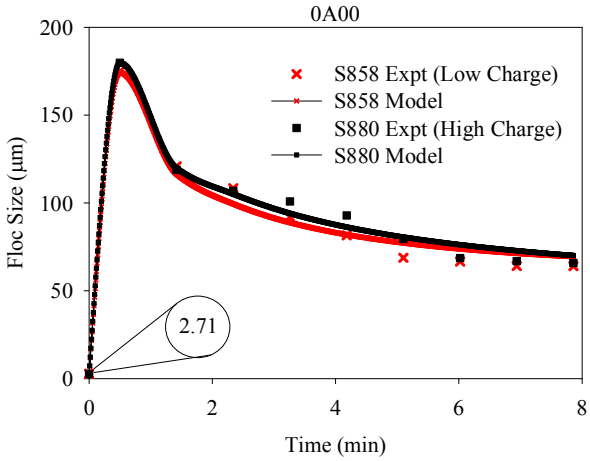

Fig. J11. Experimental and simulated PCC flocculation kinetics at condition "0A00"

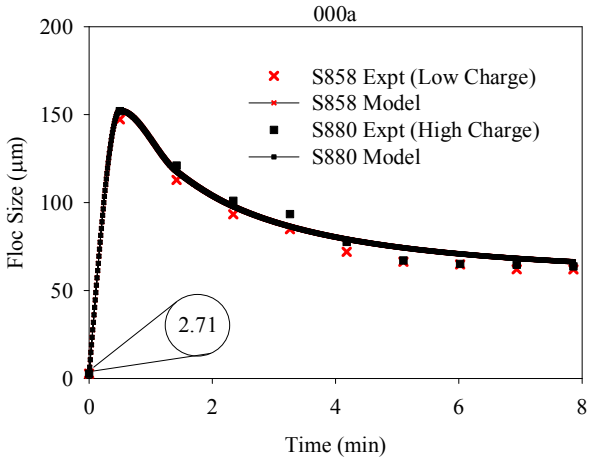

Fig. J12. Experimental and simulated PCC flocculation kinetics at condition "000a"

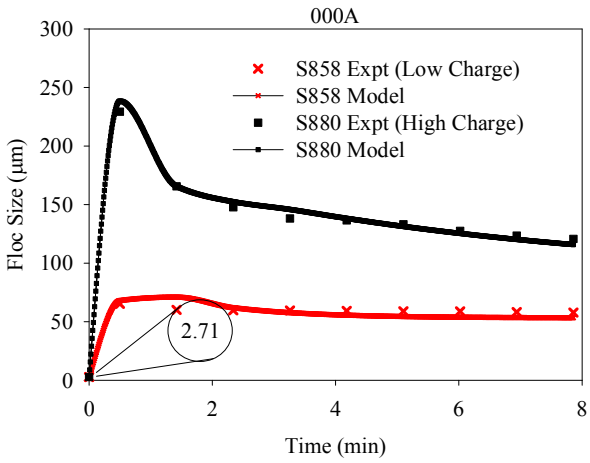

Fig. J13. Experimental and simulated PCC flocculation kinetics at condition "000A"

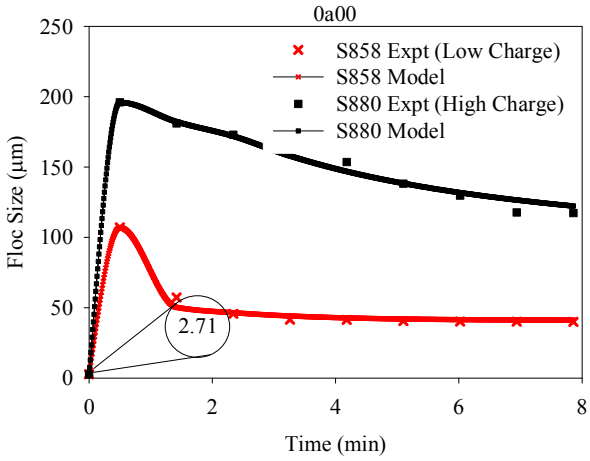

Fig. J14. Experimental and simulated PCC flocculation kinetics at condition "0a00"

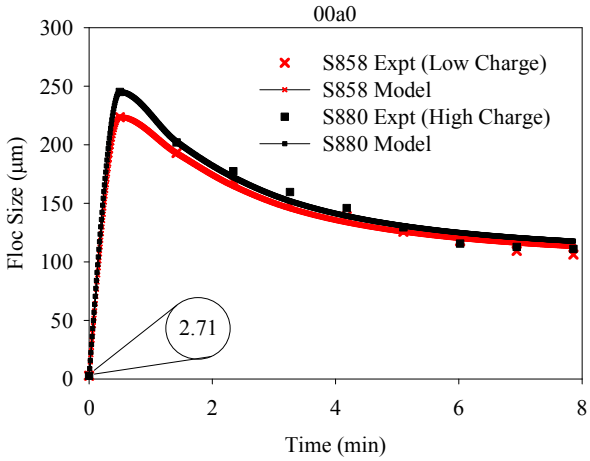

Fig. J15. Experimental and simulated PCC flocculation kinetics at condition "00a0"

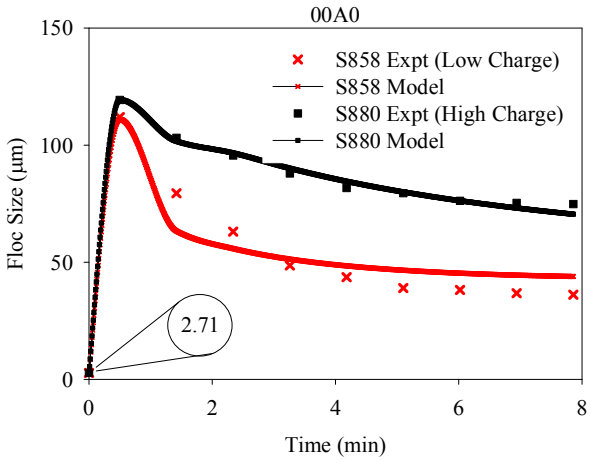

Fig. J16. Experimental and simulated PCC flocculation kinetics at condition "00A0"

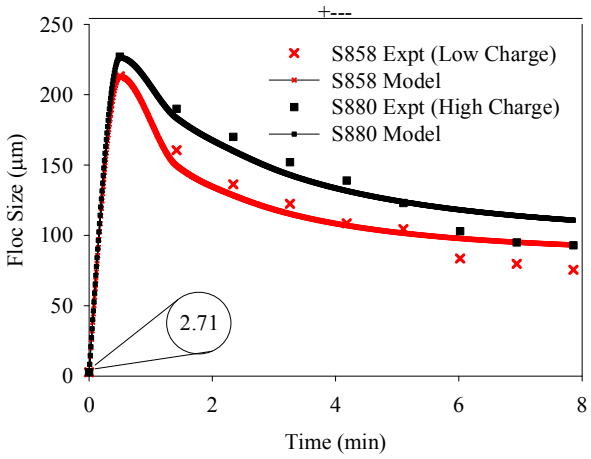

Fig. J17. Experimental and simulated PCC flocculation kinetics at condition "+---"

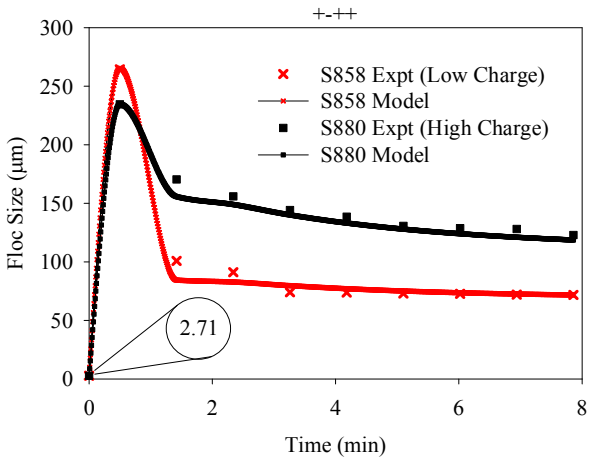

Fig. J18. Experimental and simulated PCC flocculation kinetics at condition "+-++"

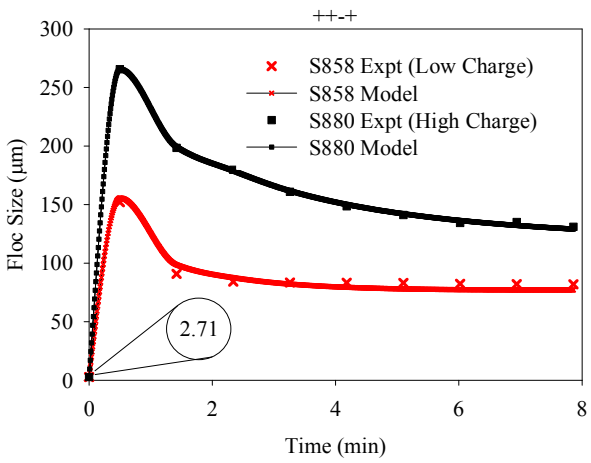

Fig. J19. Experimental and simulated PCC flocculation kinetics at condition "++-+"

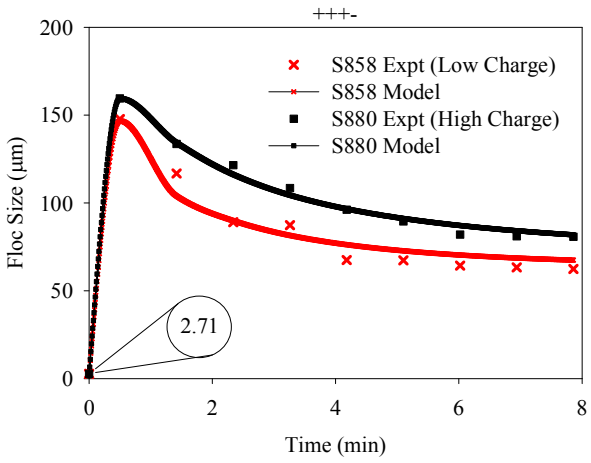

Fig. J20. Experimental and simulated PCC flocculation kinetics at condition "+++-"

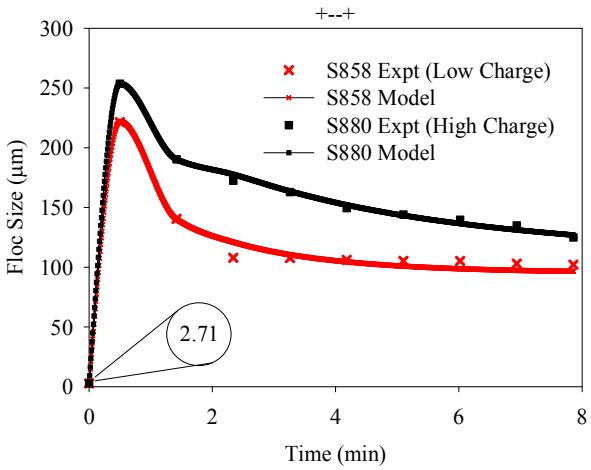

Fig. J21. Experimental and simulated PCC flocculation kinetics at condition "+--+"

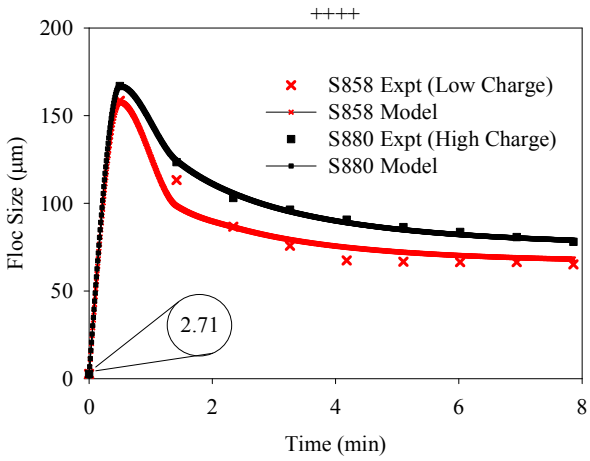

Fig. J22. Experimental and simulated PCC flocculation kinetics at condition "++++"

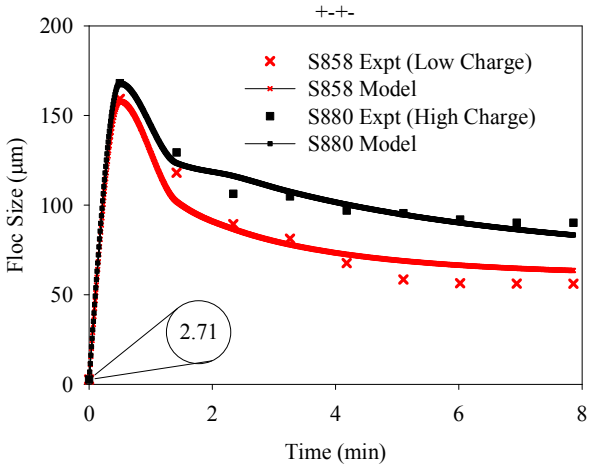

Fig. J23. Experimental and simulated PCC flocculation kinetics at condition "+-+-"

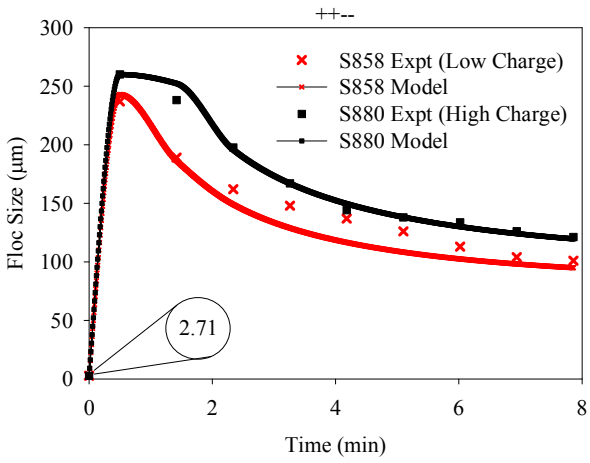

Fig. J24. Experimental and simulated PCC flocculation kinetics at condition "++--"

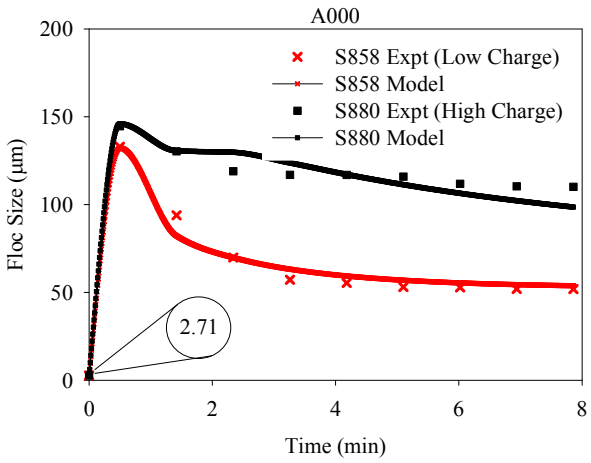

Fig. J25. Experimental and simulated PCC flocculation kinetics at condition “A000”